


RESEARCH ARTICLE

Integrated Radiolaria, benthic foraminifera and conodont biochronology of the pelagic Permian blocks/tectonic slices and geochemistry of associated volcanic rocks from the Mersin Mélange, southern Turkey: Implications for the Permian evolution of the northern Neotethys

Ugur Kagan Tekin¹ | Cengiz Okuyucu² | Kaan Sayit³  | Yavuz Bedi⁴ | Paula J. Noble⁵ | Leopold Krystyn⁶ | Mehmet Cemal Göncüoğlu³

¹Department of Geological Engineering, Hacettepe University, Beytepe, 06800, Ankara

²Department of Geological Engineering, Selcuk University, Konya, 42075, Turkey

³Department of Geological Engineering, Middle East Technical University, Ankara, 06800, Turkey

⁴Department of Geological Investigation, General Directorate of Mineral Research and Exploration, Ankara, 06800, Turkey

⁵Department of Geological Sciences and Engineering, MS 172, University of Nevada, Reno, Reno, Nevada, 89557-0138, USA

⁶Department of Palaeontology, Vienna University, Geozentrum Althanstraße 9, Vienna, 1090, Austria

Correspondence

Kaan Sayit.
Email: ksayit@metu.edu.tr

Funding information

TUBITAK, Grant/Award Number: 112Y370

Abstract

Blocks and tectonic slices within the Mersin Mélange (southern Turkey), which are of Northern Neotethyan origin (Izmir–Ankara–Erzincan Ocean (IAE)), were studied in detail by using radiolarian, conodont, and foraminiferal assemblages on six different stratigraphic sections with well-preserved Permian successions. The basal part of the Permian sequence, composed of alternating chert and mudstone with basic volcanics, is assigned to the late Asselian (Early Permian) based on radiolarians. The next basaltic interval in the sequence is dated as Kungurian. The highly alkaline basic volcanics in the sequence are extremely enriched, similar to kimberlitic/lamprophyric magmas generated at continental intraplate settings. Trace element systematics suggest that these lavas were generated in a continental margin involving a metasomatized subcontinental lithospheric mantle source (SCLM). The middle part of the Permian sequences, dated by benthic foraminifera and conodont assemblages, includes detrital limestones with chert interlayers and neptunian dykes of middle Wordian to earliest Wuchiapingian age. Higher in the sequence, detrital limestones are overlain by alternating chert and mudstone with intermittent microbrecciated beds of early Wuchiapingian to middle Changhsingian (Late Permian) age based on the radiolarians. A large negative shift at the base of the Lopingian at the upper part of section is correlated to negative shifts at the Guadalupian/Lopingian boundary associated with the end-Guadalupian mass extinction event. All these findings indicate that a continental rift system associated with a possible mantle plume existed during the late Early to Late Permian period. This event was responsible for the rupturing of the northern Gondwanan margin related to the opening of the IAE Ocean. When the deep basinal features of the Early Permian volcano-sedimentary sequence are considered, the proto IAE oceanic crust formed possibly before the end of the Permian. This, in turn, suggests that the opening of the IAE Ocean dates back to as early as the Permian.

KEYWORDS

biochronology, fossil assemblages, magmatic geochemistry, Permian, Tethyan evolution, Turkey

1 | INTRODUCTION

The 'Tethys' is one of the ancient oceanic realms believed to occupy the space between Laurasia and Gondwana during the Middle–Late

Paleozoic to Early Tertiary time interval (e.g. Robertson & Dixon, 1984; Sengör, 1979; Sengör, Altiner, Cin, Ustaomer, & Hsu, 1988; Stampfli & Borel, 2002). It is a collective term that has been used for a number of distinct oceanic domains that opened and closed within

This is an open access article under the terms of the Creative Commons Attribution-NonCommercial-NoDerivs License, which permits use and distribution in any medium, provided the original work is properly cited, the use is non-commercial and no modifications or adaptations are made.

© 2018 The Authors. *Island Arc* Published by John Wiley & Sons Australia, Ltd

this time interval (e.g. Sengör, Yilmaz, & Sungurlu, 1984; Stampfli & Borel, 2002). Although there is now no doubt that the beginning of the Tethyan evolution goes far back to the Middle–Late Paleozoic (e.g. Sengör et al., 1988), it still remains controversial how many Tethyan oceans came into existence and what their opening ages are. In the Tethyan context, it is common to regard the Palaeotethys as the older ocean, while the Neotethys is the younger one believed to have existed during the Late Paleozoic–Cenozoic (e.g. Sengör et al., 1984; Stampfli & Borel, 2002).

The Anatolian region is a complex tectonic entity, which has been mainly shaped by the Tethyan geodynamics (e.g. Sengör & Yilmaz, 1981). It includes a number of terranes that became welded during the Alpine orogeny, following the destruction of Neotethyan lithosphere (e.g. Göncüoğlu, Dirik, & Kozlu, 1997; Göncüoğlu et al., 2000). In the Anatolian region, the Neotethys is represented by two main branches; (i) a northern branch named the Izmir–Ankara–Erzincan (IAE) Ocean whose remnants are preserved within the IAE Suture Belt; and (ii) a southern branch whose remnants are found within the Bitlis–Zagros Suture Belt (Sengör & Yilmaz, 1981; Figure 1a). Of the two branches, the evolution of the northern domain is especially enigmatic, mostly regarding its opening history. For a long time, the IAE Ocean was believed to have opened during the Early Jurassic, following the closure of the Palaeotethys (Görür, Sengör, Akkök, & Yilmaz, 1983; Sengör & Yilmaz, 1981). This long-lived idea was contested by the finding of Carnian (Late Triassic) cherts within the IAE Suture Belt

in the Sakarya region (northern Turkey), which suggests that the rifting of the northern Gondwanan margin possibly occurred earlier than commonly assumed (Tekin, Göncüoğlu, & Turhan, 2002). This and many Triassic occurrences from the IAE Ocean showed that the Triassic ages are in fact not uncommon (e.g. Bragin & Tekin, 1996; Göncüoğlu, Tekin, & Turhan, 2001; Tekin & Göncüoğlu, 2002, 2007). While the age of rifting and oceanization of the IAE domain moved back into the Late Triassic (Göncüoğlu, Sayit, & Tekin, 2010; Tekin et al., 2002), the recent discovery of subduction-related basalts intercalated with Carnian cherts (Lycian nappes, southwest Turkey; Sayit, Göncüoğlu, & Tekin, 2015; Tekin & Göncüoğlu, 2002) has added another dimension to this issue.

To understand the evolution of the Tethyan Oceans, studies on mélanges would be very useful. According to Raymond (1984), a mélangé is defined as ‘the physical mixtures including diverse fragments assembled by tectonic and sedimentary processes’. Such mélanges were frequently formed during the Alpine closure of the Neotethyan branches in Anatolia. One of the best examples for such a case is related to the closure of the IAE Ocean of Neotethys, where mélanges, including oceanic material, together with blocks of marginal sedimentary successions, were emplaced onto the Tauride–Anatolide Platform (TAP) as huge gravity flows (e.g. Göncüoğlu et al., 2000; Göncüoğlu, Turhan, & Tekin, 2003; Robertson & Ustaömer, 2009; Figure 1a). By this process, a series of ‘flysch’ basins developed and then migrated for hundreds of kilometers on the TAP from north to south. In these basins, several kilometer-thick

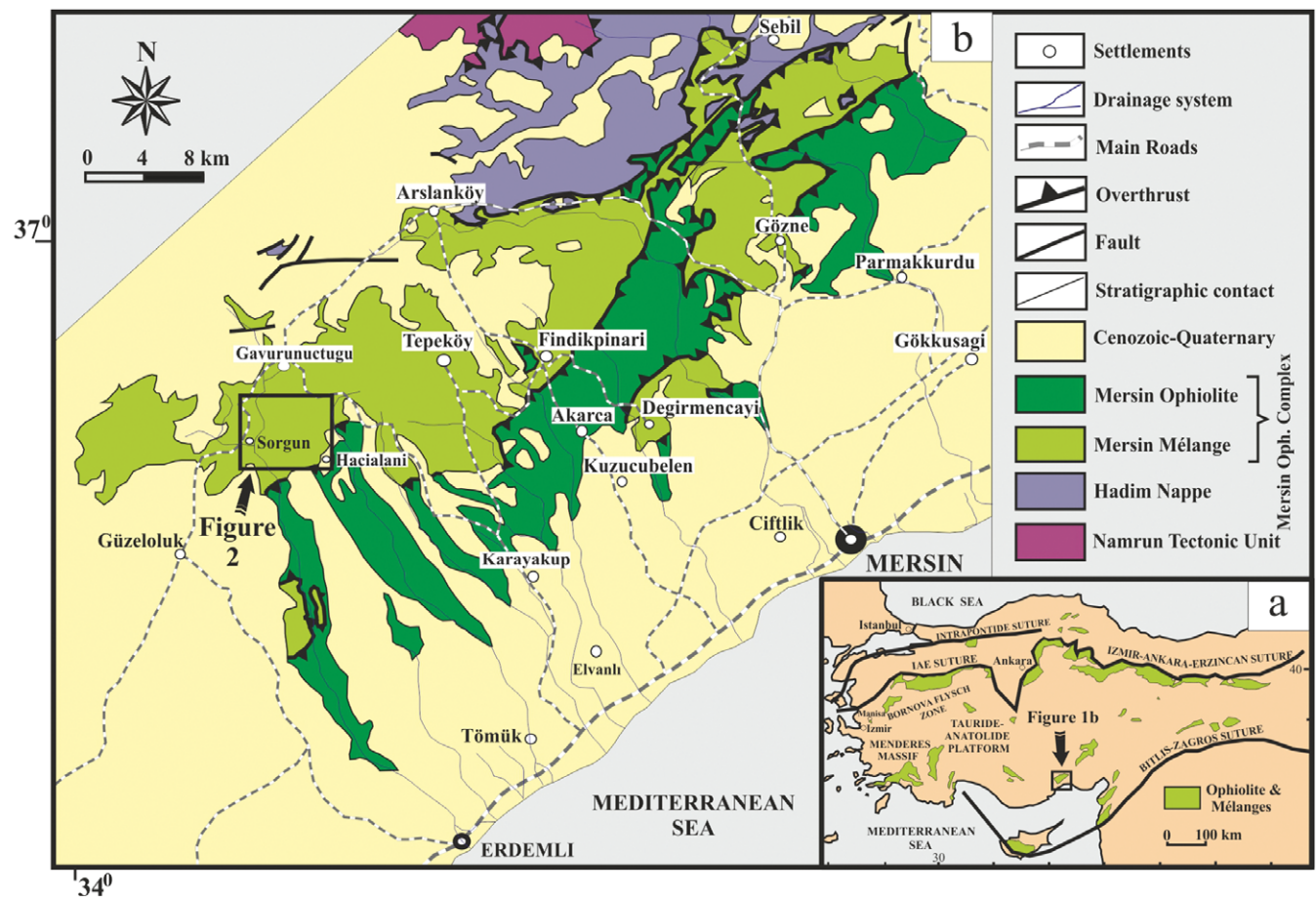


FIGURE 1 The geological map showing the distribution of the Mersin ophiolite complex in southern Turkey (revised after Alan et al., 2007; Senel, 2002). (a) The main ophiolite/mélangé units associated to suture zones in Turkey. (b) The location of the study area around Sorgun and Hacıalani towns

mélange complexes were formed (Andrew & Robertson, 2002; Özcan et al., 1988; Özgül, 1976, 1984, 1997; Tekin & Göncüoğlu, 2007).

The Mersin Ophiolitic Complex (Moix et al., 2011; Moix, Kozur, Stampfli, & Mostler, 2007; Pampal, 1984; Parlak & Robertson, 2004) comprises two units; the Mersin Mélange (MM) and the Mersin Ophiolite with its sub-ophiolitic metamorphic sole in southern Turkey (Figure 1b). According to Tekin, Bedi, Okuyucu, Göncüoğlu, and Sayit (2016), Tekin, Bedi, Okuyucu, Göncüoğlu, and Sayit et al. (2016), and Sayit, Bedi, Tekin, Göncüoğlu, and Okuyucu (2017), the Mersin Mélange is of sedimentary origin and contains mainly remnants of the Beyşehir–Hoyran nappes *sensu* Brunn et al. (1970, 1971) that originated from the IAE Ocean of the Neotethys (equals 'Bozkir Unit' by Özgül, 1976, 1984, 1997). Previously detailed studies performed on the Mersin Mélange revealed that it includes blocks/tectonic slices of Early Carboniferous to early Late Cretaceous ages (Moix et al., 2007, 2011; Tekin, Bedi, Okuyucu, Göncüoğlu, Sayit, et al., 2016). Tekin, Bedi, Okuyucu, Göncüoğlu and Sayit (2016) report the presence of blocks and tectonic slices of thick basaltic pillow and massive lava sequences of pre-late Anisian age and overlying pelagic-clastic sediment and radiolarian chert of middle to late Late Anisian age. A detailed geochemical study of the underlying pillow and massive lava sequences suggests that they were generated at an intra-oceanic back-arc basin (Sayit et al., 2017).

These findings suggest the possibility that a mature northern Neotethyan ocean already existed by the Middle Triassic; thus, the rifting of Gondwanan continental lithosphere may have occurred during the Early Triassic or earlier. This, in turn, implies that the opening of the northern and southern domains took place at almost the same time, since the opening of the southern branch of Neotethys is believed to have occurred during the Middle–Late Permian (e.g. Stampfli & Borel, 2002). In this regard, the Middle Permian basalts from Oman were interpreted to represent rifting of the Arabian continental margin leading to opening of Southern Neotethys (Lapierre et al., 2004). Therefore, an important problem that remains to be solved is whether any trace of continental magmatism exists in the northern realm (i.e. IAE domain), which would have occurred before Anisian (Middle Triassic).

The foremost aim of our study is to reconstruct the Permian geological evolution of the northern margin of the Tauride–Anatolide Platform, which is assumed to be the source area of the Permian blocks in the Mersin Mélange. For this, we studied the stratigraphy of the measured Permian sequences by using a multi-disciplinary approach (radiolarian, conodont, and foraminiferal biostratigraphy), and correlated our data with other Neotethyan successions worldwide, especially in China and Japan. In addition to these, we studied in detail the geochemistry and petrology of basic lavas from the basal part and organic-C $\delta^{13}\text{C}$ values of pelagic sediments from the upper part of these blocks/tectonic slices.

2 | GEOLOGICAL FRAMEWORK

The Mersin Ophiolitic Complex is an allochthonous body, tectonically overlying the Tauride Platform (Figure 1b). This complex includes two tectonic units; an ophiolitic series and a mélange (Pampal, 1984). Our study area is located in the latter entity, the mélange. The Mersin

Mélange (Parlak & Robertson, 2004) stretches for about 60 km in northeast–southwest direction and comprises blocks of diverse origin and ages. These blocks are embedded in a sandy-clayey clastic matrix whose composition remains mostly homogenous throughout the mélange (Tekin, Bedi, Okuyucu, Göncüoğlu, Sayit et al., 2016). In previous studies this mélange was referred to as the Tepeköy Mélange (Pampal, 1984) or the Findikpinari Mélange (Özer, Koc, & Özsayar, 2004) and is tectonically overlain by the ophiolitic unit (Figure 1).

The Mersin Mélange displays essentially a block-in-matrix character, with the size of blocks varying from tens of meters to kilometers in size. The block-in-matrix character is especially apparent on small-sized blocks, where elongated bodies of slide blocks with primary depositional relationships are observed (e.g. Moix et al., 2011) in an olistostromal matrix. By this evidence, Tekin, Bedi, Okuyucu, Göncüoğlu, and Sayit (2016), Tekin, Bedi, Okuyucu, Göncüoğlu, Sayit et al. (2016) and Sayit et al. (2017) ascribed the formation to a sedimentary mélange. The present relationship between the larger blocks and the matrix, on the other hand, appears to be sheared. However, this shearing is attributed to Tertiary (post-Lutetian) compression. The blocks within the mélange are characterized by diverse lithologies, including mudstone, sandstone, chert, limestone, quartzite, schist, and mafic volcanics. The Mersin Mélange was further subdivided into two units; Middle–Late Triassic Hacialani Mélange and Late Cretaceous Sorgun Ophiolitic Mélange (Moix et al., 2011). Recent studies by Tekin, Bedi, Okuyucu, Göncüoğlu, and Sayit (2016) and Tekin, Bedi, Okuyucu, Göncüoğlu, Sayit et al. (2016), however, showed that no such distinction occurs within the Mersin Mélange, and they regarded the mélange as a single mass-flow entity of Late Cretaceous age.

Previously, some researchers (e.g. Forel et al., *in press*; H. W. Kozur, Moix, & Ozsvart, 2007a, 2007b, 2007c, 2009; Moix et al., 2007, 2011; Ozsvart, Dumitrica, Hungerbühler, & Moix, 2017; Ozsvart, Dumitrica, & Moix, 2017; Ozsvart, Moix, & Kozur, 2015; Tekin, Bedi, Okuyucu, Göncüoğlu, & Sayit, 2016; Tekin, Bedi, Okuyucu, Göncüoğlu, Sayit et al., 2016) have carried out detailed paleontological studies on blocks/tectonic slices in the Mersin Mélange to clarify the radiolarian, foraminiferal and ostracod assemblages. Among these studies, Moix et al. (2011) investigated the limestone and chert blocks within the Mersin Mélange and report a chert-detrital limestone association ('Karinkali Block') near the Karincali–Southwest section in this study (Figure 2). A single sample (K5) taken from the middle part of the chert sequence was dated as Kungurian based on an unfigured radiolarian assemblage. This age assignment was applied to the complete succession (Moix et al., 2011, p. 76) in the block. Additionally, some isolated samples derived from different blocks in the mélange yielded Early Permian (Kungurian) to Middle Permian (Roadian to Capitanian) radiolarian assemblages. So far, those findings are the first indications for the presence of deep-marine Permian rocks and suggest a possibility that they originated from a basinal setting, yet almost completely destroyed. Recently, Tekin, Bedi, Okuyucu, Göncüoğlu, Sayit et al. (2016) re-mapped the central part of the Mersin Mélange and discovered a number of Permian blocks among other Paleozoic and Mesozoic ones.

To resolve the stratigraphic properties of Permian sequences in the Mersin Mélange, in this study samples for different purposes

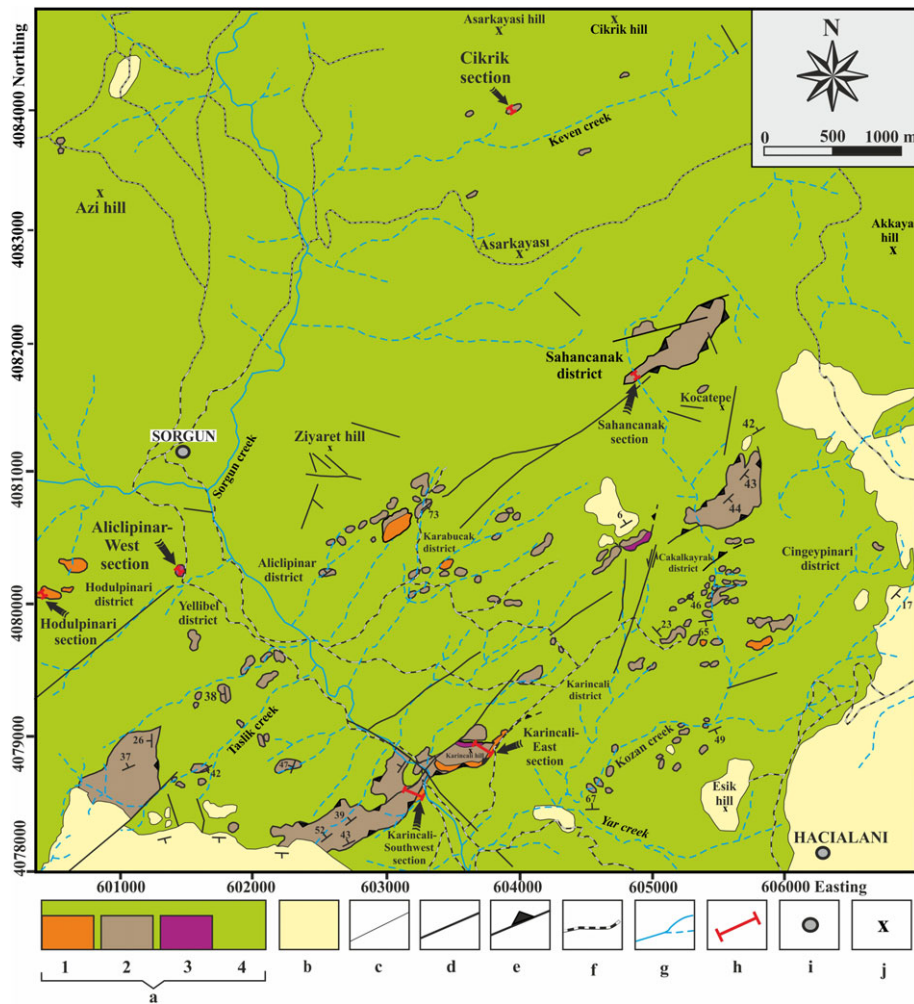


FIGURE 2 Detailed map showing the location of the stratigraphic sections and surrounding geology. Key: a, The Mersin Mélange: 1, Alternating chert, mudstone and basic volcanics of late Asselian to early Wordian age; 2, detrital limestone with rare chert interlayers of middle Wordian to earliest Wuchiapingian age; 3, alternating chert and mudstone with microbreccia breaks of Wuchiapingian to middle Changhsingian age; 4, undifferentiated mélangé (mainly matrix) of Late Cretaceous age; b, Cenozoic to Quaternary units; c, stratigraphic contact; d, fault; e, thrust; f, main roads; g, drainage system; h, section places; i, settlements; j, main peaks. Simplified after Tekin, Bedi, Okuyucu, Göncüoğlu, Sayit et al. (2016)

(micropaleontology, petrography, geochemistry, and isotope study) have been collected along six different stratigraphic sections (Cikrik, Sahancanak, Hodul, Karincali-Southwest, Karincali-East, and Aliclipinar-West; Figure 2).

3 | THE STUDIED STRATIGRAPHIC SECTIONS

The general features and lithological characteristics of the studied stratigraphic sections (Cikrik, Sahancanak, Hodul, Karincali-Southwest, Karincali-East and Aliclipinar-West) are described as follows;

3.1 | The Cikrik section

This section occurs in the northern part of the study area, situated on the northern bank of the Keven Creek (at Silifke O32a2 quadrangle sheet, between 40.83.850N/6.03.903E and 40.83.790N/6.03.942E UTM coordinates; Figure 2), and named after Cikrik Hill. The succession in this section is overturned and its total measured thickness is 25.6 m (Figure 3).

The basal part of the section is represented by alternation of green and red with minor gray colored, thin-bedded chert and mudstone (Figure 4a, labeled C-M). The contact between the base of the section and the underlying mélangé matrix is structural (Figure 4a). The basal part is followed by gray colored, thick-bedded, fine-grained carbonate breccia containing coarse pebbles and rare chert nodules (Figure 4a,b, labeled LB). Pebble size decreases towards the upper part of the section. A total of 17 samples (Cik-8 to Cik-24) were collected from the lower thin-bedded chert for radiolarian biostratigraphy. A single chert band with radiolarians was encountered in the center of the section (Figure 3). From the upper part of the section, two samples (Cik-6 and Cik-7) for conodonts, one sample (Cik-4) for radiolarians and four samples (Cik-1, to Cik-3, Cik-5) for benthic foraminiferal determinations were collected (Figure 3).

3.2 | The Sahancanak section

This section is located to the south of the Sahancanak district (at Silifke O32a2 quadrangle sheet, between 40.81.686N/6.04.836E and 40.81.748N/6.04.860E coordinates; Figure 2). The total thickness

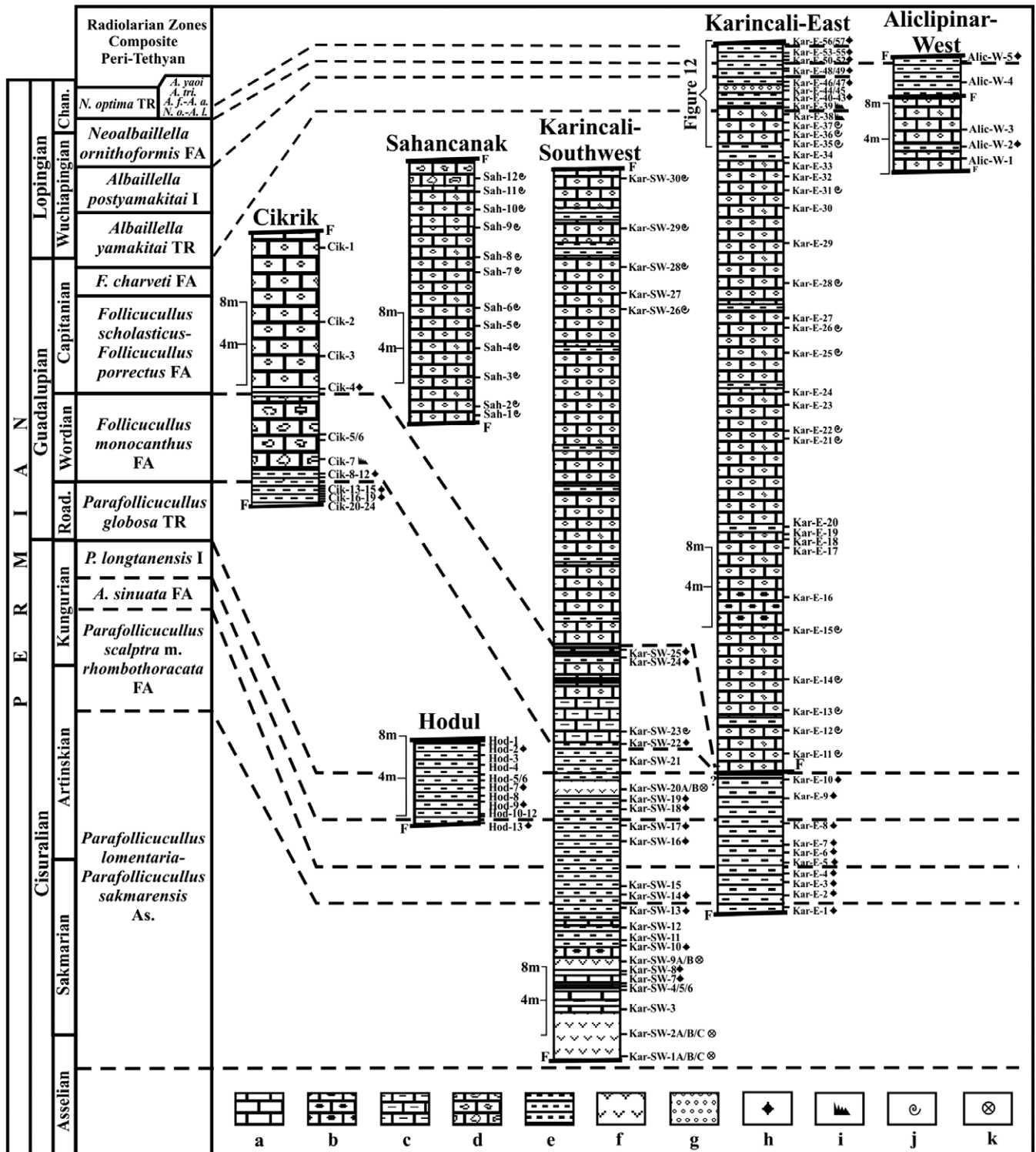


FIGURE 3 Correlation of stratigraphic sections in this study. Key: a, limestone; b, cherty limestone; c, clayey limestone; d, detrital limestone; e, alternating chert and mudstone; f, basic volcanic rock; g, microbreccia; h, radiolarian occurrence; i, conodont occurrence; j, benthic foraminifera occurrence; k, samples for geochemistry. Chan., Changhsingian. *N.o-A.I.*, *N. optima* - *A. lauta*; *A. f-a.*, *A. flexa*-*A. angusta*; *A. tri.*, *A. triangula*

of the section is about 33 m, and both the upper and lower contacts of the section are structural (Figure 3).

The Sahancanak section is mainly composed of carbonates, with the lower part of the section being composed of gray colored, thick-bedded detrital limestone (Figure 4c). The upper part of the section is characterized by gray to pink colored, medium- to thick-bedded detrital limestones. Neptunian dykes filled mainly by red pelagic mudrocks are commonly

observed features (Figure 4d). A total of 12 samples (Sah-1 to Sah-12) were collected along the section for benthonic foraminifera (Figure 3).

3.3 | The Hodul section

The location of this section is at the westernmost part of the study area (at Silifke O32a3 quadrangle sheet, between 40.80.021N/6.00.410E

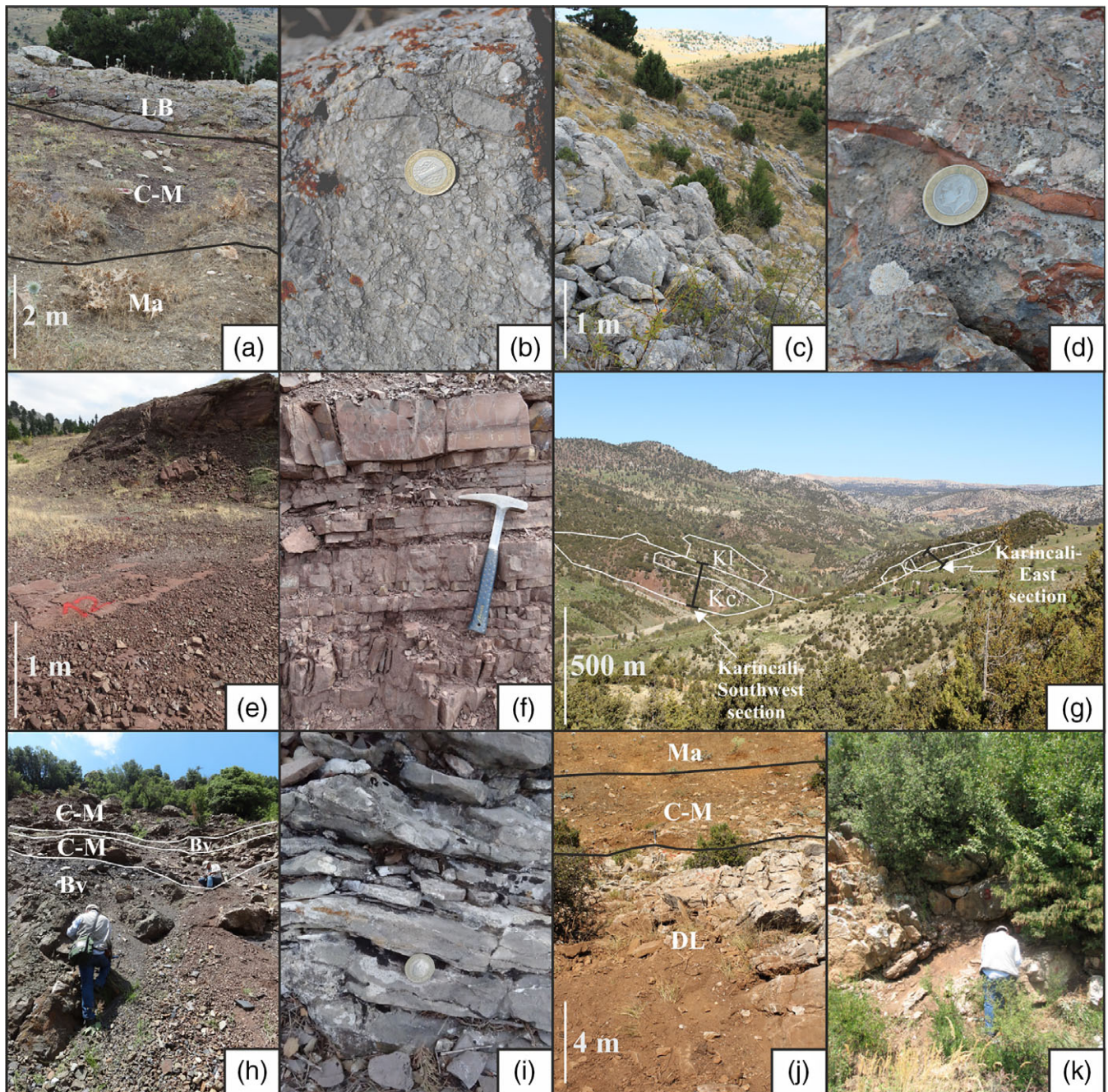


FIGURE 4 Field photographs from stratigraphic sections in this study. (a,b) the Cikrik section: (a) alternating red to gray colored chert-mudstone (C-M) at the basal part of the section of Roadian to Wordian age limited by mélangé matrix (Ma) followed by basal part of the coarse limestone breccia (LB) of Wordian age; (b) close-up of coarse limestone breccia in the central part of the section. (c,d) The Sahancanak section: (c) general view from the section; (d) Neptunian dyke with red-colored pelagic mudstone in the thick-bedded, gray colored detrital limestone of Capitanian age. (e,f) The Hodul section: (e) basal part of the section composed of red-colored alternating chert and mudstone of Kungurian age; (f) close-up of the red-colored, alternating thin to medium-bedded chert and mudstone of Kungurian–Roadian age. (g) Field photograph showing locations of Karincali-Southwest and Karincali-E sections measured along chert (Kc) and detrital limestone (Kl) at the east and west banks of the Sorgun creek, view from southeast to northwest. (h) The Karincali-Southwest section in a view from the basal part of section showing the basic volcanics (Bv) and alternating chert and mudstone (C-M) of late Asselian–middle Artinskian age. (i,j) The Karincali-East section: (i) basal part of the detrital limestone in the central part of the section of middle Wordian to Capitanian age; (j) view from the upper part of the section showing the detrital limestone (DL) of earliest Wuchiapingian age grading into alternating chert and mudstone (C-M) with microbreccia breaks of Wuchiapingian to middle Changhsingian age limited by mélangé matrix (Ma). (k) The Aliclipinar-West section, lower part of the section represented by detrital limestone of Capitanian age

and 40.80.045N/6.00.410E UTM coordinates; Figure 2). The section is named after the Hodulpinari district to the east of this locality (Figure 2). The succession in the section is overturned and its total thickness is about 8.3 m.

The Hodul section is composed of alternating red with lesser green colored, thin to medium-bedded chert and mudstone (Figure 4e,f). Both the upper and lower boundaries against the clastic matrix of the mélangé are sheared and embedded in the matrix of the mélangé. A total of

13 samples (Hod-1 to Hod-13) were taken along the section for radiolarian determinations, four of which (Hod-2, Hod-7, Hod-9, and Hod-13) yielded age-significant data (Figure 3).

3.4 | The Karincali-Southwest section

This is one of the more representative sections showing the typical features of the Permian rock sequence. It is located in the southwest of studied region (at Silifke O32a3 quadrangle sheet, between 40.78.502N/6.03.204E and 40.78.625N/6.03.010E UTM coordinates; Figure 2), and is named after Karincali hill. The total thickness of the section is about 108 m, and it is bounded by faults at both lower and upper contacts (Figures 2 and 3).

Based on its lithological characteristics, the Karincali-Southwest section can be subdivided into three main parts (Figure 3). The basal part of the section is dominated by alternating green colored, altered basic volcanics, laminated red to pink colored mudstone, green to red-colored, thin-bedded chert, and red to pink colored, thin-bedded limestone (Figures 3 and 4g,h). The middle part of the section is made up of alternating red to rarely green colored, thin to medium-bedded chert and mudstone with rare green colored altered basic volcanics, and yellow to brown-colored thin-bedded limestone intercalations (Figure 3). Towards the upper part of the section, gray to pink colored, thin to medium-bedded detrital limestone becomes dominant with rare chert levels (Figure 3). A total of 30 samples (eighteen samples from chert for radiolarian determinations, eight samples from limestone for benthic foraminiferal determinations and four samples from basic volcanics for geochemical analyses) were taken along the section (Figure 3).

3.5 | The Karincali-East section

This section is located in the southern part of the study area (at Silifke O32a3 quadrangle sheet, between 40.78.847N/6.03.759E and 40.78.920N/6.03.650E UTM coordinates; Figure 2) and very close to Karincali hill (Figure 2 and 4g). Both the upper and lower contacts are bounded by faults and the total thickness is about 89 m (Figure 3).

The lowermost part of the section is represented by alternating red-colored, thin to medium-bedded chert and mudstone (Figure 3). This part is overlain by medium to thick-bedded, gray colored detrital limestone with occasional red-colored chert bands (Figures 3 and 4i). Clasts in this detrital limestone are variable in size; most of them are 2–5 cm in diameters. Towards the upper part, alternating yellow to gray colored, thin-bedded chert and gray colored, thin to medium-bedded limestone are the dominant lithologies (Figures 3, and 4j). This part is overlain by alternating green to black-colored, thin-bedded chert and mudstone (Figures 3, and 4j). The sequence also contains medium-bedded, pink colored conglomerates towards the base of the limestone (Figure 3). Conglomerates include thin to coarse-grained materials originating from limestone, chert and basic volcanics (Figure 3).

A total of 57 samples were collected along the section for a variety of paleontological analyses (Figure 3). From the basal and

uppermost parts of the section, 27 samples (Kar-E-1 to Kar-E-10, Kar-E-34, Kar-E-40 to Kar-E-44, Kar-E-46 to Kar-E-57) were taken from chert for radiolarian analysis (Figure 3). Moreover, to check for benthic foraminifera and conodont contents in the detrital limestone and conglomerate, 30 samples were collected from the central part of the section (Figure 3).

3.6 | The Aliclipinar-West section

This is a very short section with 10.3 m total thickness, which is situated in west part of the study area (at Silifke O32a3 quadrangle sheet, between 40.80.171N/6.01.459E and 40.80.180N/6.01.465E UTM coordinates; Figure 2). The name of the section was derived from the Aliclipinar district (Figure 3).

The basal and central part of the section includes gray to beige-colored, medium-bedded detrital limestone with rare chert interbeds (Figure 4k). This part is overlain by red-colored chert and mudstone alternation at the top. This part is separated from the lower part by a structural contact (Figure 3). A total of five samples were collected along the section and only two of them (Alic-W-2 and Alic-W-5) collected from chert beds contains identifiable radiolarians (Figure 3).

4 | DATING OF PERMIAN SEQUENCES

Permian sequences within the Mersin Mélange have been dated by using radiolarians, benthonic foraminifera and conodonts. We used radiolarians to date the cherty parts of the sequences, chiefly in the basal and upper parts of the stratigraphic sequence. All chert samples from the stratigraphic sections have been processed with diluted hydrofluoric acid (5–10 % HF) following Dumitrica's (1970) and Pessagno and Newport's (1972) methods to obtain radiolarian assemblages.

The central part of the sequence was dated by benthonic foraminifera and conodonts which were recovered from detrital limestone with clasts of platform carbonate. Limestone materials were processed with diluted Acetic Acid (5–10 % CH₃COOH) or diluted Formic Acid (5–10 % HCOOH) to obtain Conodont assemblages. Subsequently, all residues underwent heavy liquid separation using SPT (Sodium Polytungstate) to concentrate conodonts. To study the benthic foraminifera and algae from the limestone materials, both oriented and random thin-sections were prepared.

The composite radiolarian biostratigraphic scheme employed is a synthesis based on data from southwest Japan (Ishiga, 1986, 1990; Kuwahara, Yao, & Yamakita, 1998; Shimakawa & Yao, 2006; A. Yao & Kuwahara, 2004), South China (Y. J. Wang, Cheng, & Yang, 1994; Y. J. Wang, Luo, & Yang, 2012; Y. J. Wang & Yang, 2011; Y. J. Wang, Yang, Cheng, & Li, 2006; N. Zhang, Henderson, Xia, Wang, & Shang, 2010; L. Zhang, Ito, Feng, Caridroit, & Danelian, 2014), Russia (e.g. Nazarov & Ormiston, 1985, 1993), Thailand, Malaysia (e.g. Jasin & Harun, 2011; Jasin, Said, & Rahman, 1995) and includes the most up to date chronostratigraphic correlation. In this study, we adopt the zonation presented in Aitchison, Suzuki, Caridroit, Danelian, and Noble (2017) with reference to some zones in

southwest Japan (i.e. *A. sinuata* zone; Figure 5) and follow the generic taxonomy of Noble et al. (2017).

4.1 | Radiolarian biostratigraphy

4.1.1 | Radiolarian biostratigraphy of lower and middle Permian sequences

The basal part of the Permian sequences is dominated by radiolarian chert containing moderately diverse but characteristic radiolarian assemblages that we are able to assign to existing radiolarian biozones established in the Paleotethyan realm of southeast Asia. The basal part of the Permian sequences within the Mersin Mélange contains rich and moderately diverse radiolarians of late Asselian (Early Permian) to early Wordian (Middle Permian) age (Figure 3). Radiolarian assemblages obtained in this study are illustrated in Figures 6–10. Details of these assemblages are summarized as follows:

The *Parafollicucullus lomentaria*–*Parafollicucullus sakmarensis* Assemblage Zone of Y. J. Wang and Yang (2011)

The *Parafollicucullus lomentaria* zone was first recognized in Japan (Ishiga, 1986, 1990; Ishiga & Imoto, 1980; Ishiga, Kito, & Imoto, 1982). It was characterized by an assemblage containing the nominal taxon along with *P. sakmarensis*, *P. longicornis*, *P. scalprata* and *P. ornata* and the top was defined by the first appearance of *P. scalprata m. rhombothoracata* (Ishiga et al., 1982). The assemblage is widely recognized in Asia, including South China (A. Yao & Kuwahara, 2004), Malaysia (Jasin & Harun, 2011), Thailand (Sashida & Salyapongse, 2002), North America (Blome & Reed, 1992; Cordey, 1998), and the southern Urals (H. Kozur & Mostler, 1989). Work in South China by Wang and others (Y. J. Wang et al., 1994; Y. J. Wang & Yang, 2011) recognize the *P. lomentaria*–*P. sakmarensis* Zone, which they indicate as correlative to the *P. lomentaria* Zone of Japan, but their stratigraphic range chart indicates an overlap between much of the range of *P. lomentaria* and *P. scalprata m. rhombothoracata* within the zone. Based on the ranges shown in Y. J. Wang and Yang (2011), the top of the *P. lomentaria* – *P. sakmarensis* Assemblage Zone is marked by the last appearance of the two nominal taxa of the zone (Figure 5).

Radiolarian assemblages belonging to this zone have been recognized in the Karincali-Southwest and Karincali-East sections (Figure 3). The basal part of the Karincali-Southwest section including basic volcanics, limestone, and chert and the basalmost part of the Karincali-East characterized by alternating chert and mudstone contain radiolarian assemblages most comparable to the *P. lomentaria*–*P. sakmarensis* Assemblage Zone described by Y. J. Wang and Yang (2011) (Figures 3, and 5; Tables 1 and 2).

The basal part of the Karincali-Southwest section (sample Kar-SW-7) contains *Parafollicucullus lomentaria* (Figure 7(16)), *Parafollicucullus longicornis* (Figure 7(19)), *Parafollicucullus triangularis* and *Latentifistularia* species (e.g. *Latentifistula hetroextrema* (Figure 8(29,30)) and *Quadricaulis flata*) that are characteristic of this zone and its correlatives (e.g. Ishiga, 1986, 1990; Jasin & Harun, 2011; Jasin, Harun, Said, & Saad, 2005; Y. J. Wang & Yang, 2011, Figure 5). This sample lacks *P. u-forma* and *P. elegans*, which are characteristic of the preceding zone (the *Parafollicucullus u-forma* Zone) and rule out an older age assignment (Figure 5). A similar assemblage has also been identified in the overlying sample Kar-SW-8. Kar-SW-10 (Table 1) has a similar assemblage as Kar-SW-8, with the

exception that *P. scalprata m. rhombothoracata* makes its first appearance. *P. sakmarensis* makes its first appearance in Kar-SW-13 (Figure 7 (23–25)), above the first appearance of *Parafollicucullus scalprata m. rhombothoracata*, and suggests that *P. sakmarensis* possibly has a higher first occurrence than it does in Japan, China, Malaysia, and the Urals where *P. lomentaria* and *P. sakmarensis* commonly overlap throughout most of the zone (Ishiga, 1990; Jasin & Harun, 2011; Y. J. Wang & Yang, 2011). Absence of *P. sakmarensis* in the older samples in the Karincali-Southwest section can also be a function of preservation and relative abundance of this taxon.

We assign these samples to the *P. lomentaria*–*P. sakmarensis* zone (Y. J. Wang & Yang, 2011) because the taxon occurrences are consistent with the Chinese succession with *P. scalprata m. rhombothoracata* co-occurring with both *P. sakmarensis* and *P. lomentaria*. This is in contrast to the *P. lomentaria* Zone by Ishiga (1990), whose top is defined by the first appearance of *P. scalprata m. rhombothoracata*.

The *Parafollicucullus scalprata m. rhombothoracata* Interval Zone of Y. J. Wang and Yang (2011)

The zone described in Y. J. Wang and Yang (2011) is a variant of the *Parafollicucullus rhombothoracata* Zone recognized in Japan (Ishiga, 1986, 1990; Ishiga & Imoto, 1980; Ishiga et al., 1982), and is recognized widely throughout Asia and North America (Caridroit in De Wever, Dumitrica, Caulet, Nigrini, & Caridroit, 2001). Whereas Ishiga studies (e.g. Ishiga, 1986, 1990; Ishiga & Imoto, 1980; Ishiga et al., 1982) defined the base as the first occurrence of the nominal taxon, Y. J. Wang and Yang (2011) defined an interval zone representing the partial range of the nominal taxon. Based on the range chart in Y. J. Wang and Yang (2011), the base is recognized by the last appearance of *P. sakmarensis* and the top as the first appearance of *Albaillella xiaodongensis*. We follow the definition in Y. J. Wang and Yang (2011), as it fits best with our occurrence data (Tables 1 and 2), and we assign samples Kar-SW-14 in the Karincali-Southwest section and Kar-E-2 to Kar-E-4 in the Karincali-East section (Tables 1 and 2) to this zone (Figures 3 and 5).

The chronostratigraphic calibration of the Cisuralian Tethyan radiolarian assemblages of southeast Asia is weak, and leaves a certain amount of uncertainty in the age of the assemblages we assign to the *P. lomentaria*–*P. sakmarensis* and *P. scalprata m. rhombothoracata* Zones. The age of the *P. lomentaria* and the correlative *P. lomentaria*–*P. sakmarensis* Zone is reported in different articles as follows: middle Wolfcampian (=Asselian) by Ishiga and others (Ishiga, 1986, 1990; Ishiga & Imoto, 1980; Jasin et al., 2005); middle–late Wolfcampian (Asselian–Artinskian) by Wang and others (Y. J. Wang et al., 1994, 2006; Y. J. Wang & Yang, 2011); late Asselian–middle Sakmarian (Caridroit in De Wever et al., 2001; Jasin & Harun, 2011; Sashida & Salyapongse, 2002); early to middle Sakmarian (Ito & Matsuoka, 2015); and late Artinskian–early Kungurian (H. Kozur & Mostler, 1989). Meanwhile, the age of the *P. scalprata m. rhombothoracata* Zone and its correlatives has been assigned to latest Wolfcampian (late Sakmarian to late Artinskian) in the body of work from from southeast Asia (e.g. Ishiga, 1986, 1990; Jasin & Harun, 2011; Spiller, 2002; Y. J. Wang et al., 1994, 2006, 2012; Y. J. Wang & Yang, 2011).

		Chronostratigraphy				Radiolarian Zones				Radiolarian datums constrained by conodonts
		Global	West Texas	China	Conodont Zones	Composite Peri-Tethyan	Southwest Japan	South China	Malaysia	
254 Ma	Lopingian	Chuan.	Wuchiapingian	Wuchiapingian	<i>H. praeparvus/H. changxingensis</i> <i>C. liangshanensis</i> <i>C. yini</i> <i>C. changxingensis</i> <i>C. subcarinata</i> <i>C. wangi</i>	<i>N. optima</i> TR <i>A. yaoi</i> <i>A. tri</i> <i>A. fa</i> <i>N. o-a.l.</i>	<i>N. optima</i> As. <i>N. ornithoformis</i>	<i>N. optima</i> As. <i>N. ornithoformis</i> As. <i>A. levis-A. excelsa</i> Ab <i>A. protolevis</i> I	<i>Neobaillella optima</i> As.	<ul style="list-style-type: none"> * FA <i>N. ornithoformis</i>, just below FA <i>C. wangi</i>² ▼ LA <i>A. cavitata, levis, protolevis</i> above FA <i>C. liangshanensis</i>¹ * FA <i>Neobaillella</i> sp. above FA <i>C. liangshanensis</i>¹ * FA <i>N. ornithoformis</i> with <i>C. guangyuanensis</i>⁵
					<i>C. orientalis/longicuspidata</i> <i>C. transcaucasica/liangshanensis</i> <i>C. guangyuanensis</i> <i>C. leveni</i> <i>C. asymmetrica</i> <i>C. dukouensis</i> <i>C. postbitteri postbitteri</i> <i>C. postbitteri hongshuiensis</i>	<i>A. postyamakitai</i> I <i>A. yamakitai</i> TR <i>F. charveti</i> FA	<i>F. charveti</i> - <i>A. yamakitai</i> As.	<i>F. bipartitus</i> - <i>F. charveti</i> - <i>F. orthogonus</i> As. <i>Foremanhelana triangula</i> Ab.	<i>Neobaillella ornithoformis</i> As.	
259 Ma	Guadalupian	Captanian	Maokaoan	<i>J. granti</i> <i>J. xuanhanensis</i> <i>J. altudaensis</i> <i>J. shannoni</i>	<i>F. charveti</i> FA	<i>Follicucullus scholasticus</i> - <i>Follicucullus ventricosus</i> - As.	<i>Follicucullus scholasticus</i> - <i>Follicucullus ventricosus</i> As.	<i>Follicucullus porrectus</i> As.	<ul style="list-style-type: none"> ▼ LA <i>A. yamakitai</i> with <i>C. dukouensis</i>¹ * FA <i>A. levis</i> (base FA <i>C. postbitteri</i>)^{1, 6} * FA <i>A. protolevis</i> (mid <i>C. hongshuiensis</i> Z.)¹ * FA <i>A. yamakitai, cavitata</i> (base <i>C. hongshuiensis</i> Z.)^{1, 6} * FA <i>A. charveti</i> (in <i>J. granti</i> Z.)⁶ 	
				<i>J. postserrata</i> Illawarra	<i>Follicucullus porrectus</i> FA					
265 Ma	Wordian	Guadalupian	Maokaoan	<i>J. postserrata</i> Illawarra	<i>Follicucullus monocanthus</i> FA	<i>Follicucullus monocanthus</i> TR	<i>Follicucullus monocanthus</i> I	<i>Follicucullus monocanthus</i> Ab.	<ul style="list-style-type: none"> * FA <i>F. porrectus, F. dilatatus</i> (base <i>J. postserrata</i> Z.)⁷ * FA <i>F. scholasticus</i> (above base <i>J. postserrata</i> Z.)³ 	
				<i>J. aserrata</i>						
269 Ma	Roadian	Kungurkian	Leonardian	<i>J. nankingensis</i>	<i>Parafollicucullus globosa</i> TR	<i>Parafollicucullus globosa</i> TR	<i>Parafollicucullus globosa</i> Ab	<i>Parafollicucullus globosa</i> Ab	* FA <i>F. monocanthus</i> ^{3, 7}	
273 Ma	Leonardian	Chihhsian	<i>Mesogondolella lamberti</i> <i>Neostreptognathus sulcaplicatus</i> <i>Mesogondolella idahoensis</i>	<i>Albaillella P. longi foremanae</i> I <i>A. sinuata</i>	<i>P. longtanensis</i> I <i>A. sinuata</i> FA	<i>P. ishigai</i> Ab. <i>A. sinuata</i> Ab.	<i>P. longtanensis</i> As. <i>A. sinuata</i> As.	* FA <i>P. globosa</i> base <i>J. nankingensis gracilis</i> Z. ^{4, 5, 7}		
			<i>Sweetognathus guizhouensis</i> <i>Neostreptognathus prayi</i> <i>Neostreptognathus pseudoctineii</i> <i>Neostreptognathus pequopensis</i>	<i>Parafollicucullus scalprata m. rhombothoracata</i> FA	<i>Parafollicucullus scalprata m. rhombothoracata</i> FA	<i>Albaillella xiadongensis</i> I				
283 Ma	Artinskian	Changmoan	<i>Sweetognathus clarki</i>			<i>Parafollicucullus rhombothoracata</i> I	<i>Parafollicucullus scalprata m. rhombothoracata</i> As.	<ul style="list-style-type: none"> ▼ Last appearance * First appearance 		
			<i>Sweetognathus whitei</i> <i>Sweetognathus anceps</i> <i>Mesogondolella bisselli</i> <i>Mesogondolella visibilis</i> <i>Mesogondolella lata</i> <i>Sweetognathus binodosus</i>	<i>Parafollicucullus lomentaria - Parafollicucullus sakmarensis</i> As.	<i>Parafollicucullus lomentaria</i> As.	<i>Parafollicucullus lomentaria - Parafollicucullus sakmarensis</i> As.	<i>Parafollicucullus lomentaria</i> As.			
290 Ma	Sakmarian	Wolfcampian	<i>Sw. merrilli M. uralensis</i>							
			<i>Streptognathodus postfusus</i> <i>Mesogondolella striata</i> <i>Streptognathodus fusus</i> <i>Streptognathodus constrictus</i> <i>Streptognathodus sigmoidalis</i> <i>Streptognathodus cristellaris</i> <i>Streptognathodus glenisteri</i> <i>Streptognathodus isolatus</i>		<i>Parafollicucullus u-forma m. II</i> FA <i>P. u-forma m. I</i> EA <i>P. bulbosa</i> (part)	<i>Parafollicucullus bulbosa</i> As. (part)				

FIGURE 5 Radiolarian zones for the Permian period and their chronostratigraphic correlation as presented by various authors in the Tethyan realm. Solid zonal boundary lines are constrained by conodont datums (on right). Global chronostratigraphic units are from Ogg, Ogg, and Gradstein (2016), West Texas stages (Gradstein, Ogg, Schmitz, & Ogg, 2012), Chinese stages (Jin, Shang, & Wang, 2003), and conodont zones are those currently recognized by the International Subcommission on Permian Stratigraphy (Shen et al., 2013). The composite Peri-Tethyan zonation, modified from Aitchison et al. (2017), also appears in Figure 3. Southwest Japan (Mino-Tamba belt) zonation (A. Yao, Kuwahara, Ezaki, Liu, & Hao, 2004) is based on Ishiga (1986, 1990), with modifications made by Kuwahara et al. (1998) and J. Yao, Yao, and Kuwahara (2001). The South China (Guangxi, Yunan, Guihzou regions) zonation in Y. J. Wang and Yang (2011) is adopted from Y. J. Wang et al. (1994, 2006), and the Peninsular Malaysia zonation is from Jasin and Harun (2011), with the addition of the *A. sinuata* Zone from Spiller (2002). Numbered references correspond to superscripts in radiolarian datums. Zone types: Ab, abundance or acme zone; As., assemblage zone; FA, first appearance zone (type of interval zone where base is defined by FA of nominal taxon and top by overlying zone); I, interval zone; TR, taxon range zone. Genus: *A*, *Albaillella*; *F*, *Follicucullus*; *N*, *Neobaillella*; *P*, *Parafollicucullus*. The following are abundance zones from Xia, Zhang, Wang, and Kakuwa (2004): *A. yaoi*, *A. tri* (*A. triangula*), *A. f-a* (*A. flexa*-*A. angusta*), *N. o-a.l.* (*N. optima*-*A. lauta*)

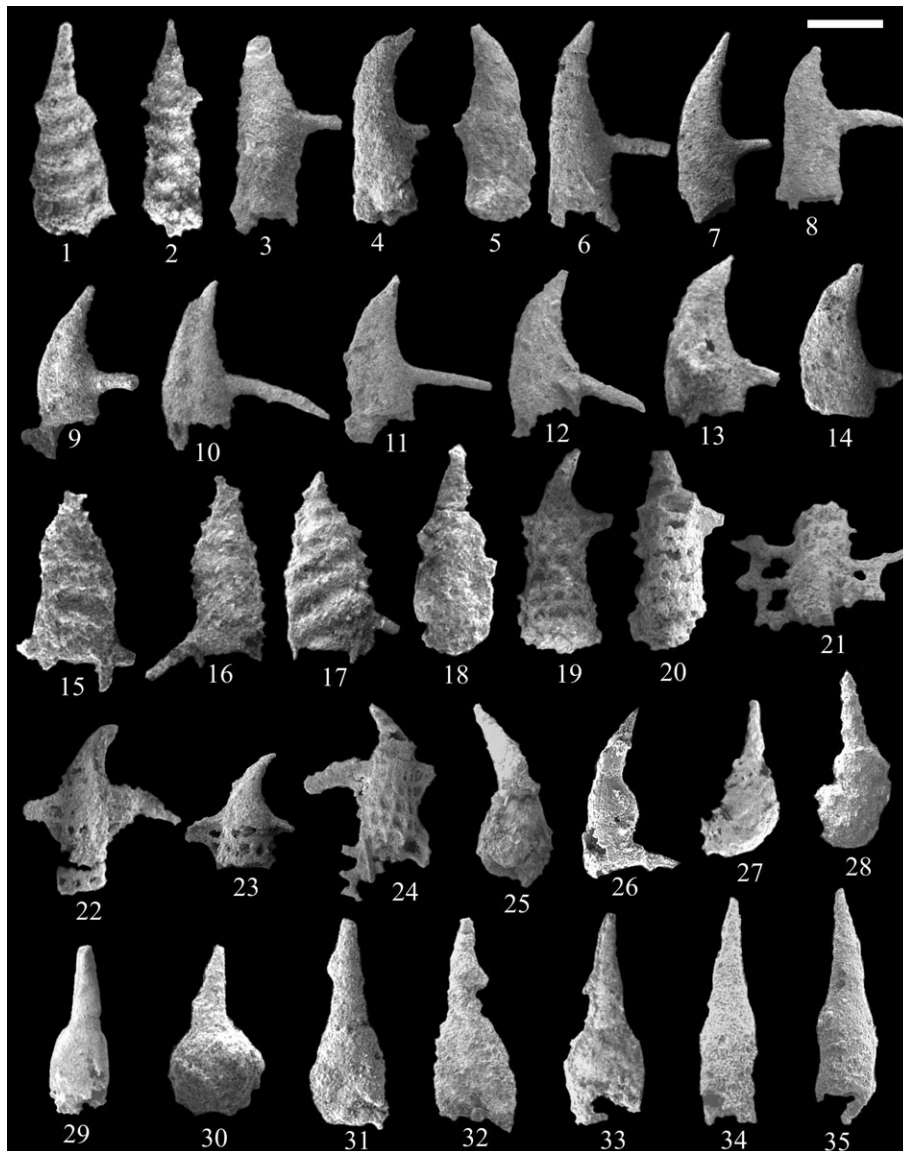


FIGURE 6 Permian radiolarians from the Mersin Mélange. (1,2) *Albaillella asymmetrica* Ishiga & Imoto: (1) Kar-SW-16; (2) Hod-7, scale bar = 80 μm . (3) *Albaillella excelsa* Ishiga, Kito & Imoto, Kar-E-56, scale bar = 85 μm . (4,5) *Albaillella flexa* Kuwahara: (4) Kar-E-56; (5) Kar-E-57, scale bar = 85 μm . (6–8) *Albaillella lauta* Kuwahara: (6) Kar-E-52; (7) Kar-E-54; (8) Kar-E-57, scale bar = 100 μm . (9–11) *Albaillella levis* Ishiga, Kito & Imoto: (9) Kar-E-50; (10) Kar-E-51; (11) Kar-E-53, scale bar = 90 μm . (12–14) *Albaillella protolevis* Kuwahara: (12) Kar-E-49; (13) Kar-E-52; (14) Kar-E-54, scale bar = 80 μm . (15–17) *Albaillella sinuata* Ishiga & Watase: (15) Kar-SW-17; (16) Kar-SW-18; (17) Hod-13, scale bar = 110 μm . (18) *Albaillella xiadongensis* Wang, Kar-SW-16, scale bar = 80 μm . (19,20) *Neoalbaillella gracilis* Takemura & Nakaseko: (19) Kar-E-49; (20) Kar-E-50, scale bar = 90 μm . (21) *Neoalbaillella optima* Ishiga, Kito & Imoto, Kar-E-50, scale bar = 100 μm . (22–24) *Neoalbaillella ornithoformis* Takemura & Nakaseko: (22) Kar-E-50; (23) Kar-E-54; (24) Kar-E-56, scale bar = 100 μm . (25) *Follicucullus charveti charveti* Caridroit & De Wever, Kar-E-41, scale bar = 110 μm . (26) *Follicucullus charveti falx* Caridroit & De Wever, Kar-E-41, scale bar = 150. (27,28) *Follicucullus charveti orthogonus* Caridroit & De Wever: (27) Kar-E-40; (28) Kar-E-41, scale bar = 130 and 160, respectively. (29) *Follicucullus dilatatus* Rudenko, Kar-E-47, scale bar = 120 μm . (30) *Follicucullus lagenarius* Rudenko, Cik-9, scale bar = 90 μm . (31–33) *Follicucullus monacanthus* Ishiga & Imoto: (31) Cik-9; (32) Kar-SW-24; (33) Kar-SW-25, scale bar = 120 μm . (34,35) *Follicucullus porrectus* Rudenko: (34) Kar-E-40; (35) Kar-E-46, scale bar = 120 and 150 μm , respectively

Based on their review of the radiolarian literature and updated calibration to the conodont biostratigraphy, Aitchison et al. (2017) consider the age of the *P. lomentaria* assemblage (minus *P. scalprata* and *P. scalprata m. rhombothoracata*) to be Sakmarian, but they further state that the first appearance of *P. scalprata* and *P. scalprata m. rhombothoracata* does not appear to predate the late Artinskian. If the first appearance of *P. scalprata m. rhombothoracata* is taken to be the most reliable datum then the age of these two zones can be considered to be late Artinskian–middle Kungurian. This implies that

age of the basal part of the Karincali-Southwest section dominated by basic volcanics can be of late Asselian–middle Artinskian age (Figure 3, Table 1).

The *Albaillella sinuata* Zone of Shimakawa and Yao (2006), or lower *Albaillella foremanae* Zone of N. Zhang et al. (2010)

The basal part of the Hodul section, central parts of the Karincali-Southwest and basal part of the Karincali-East sections, mainly

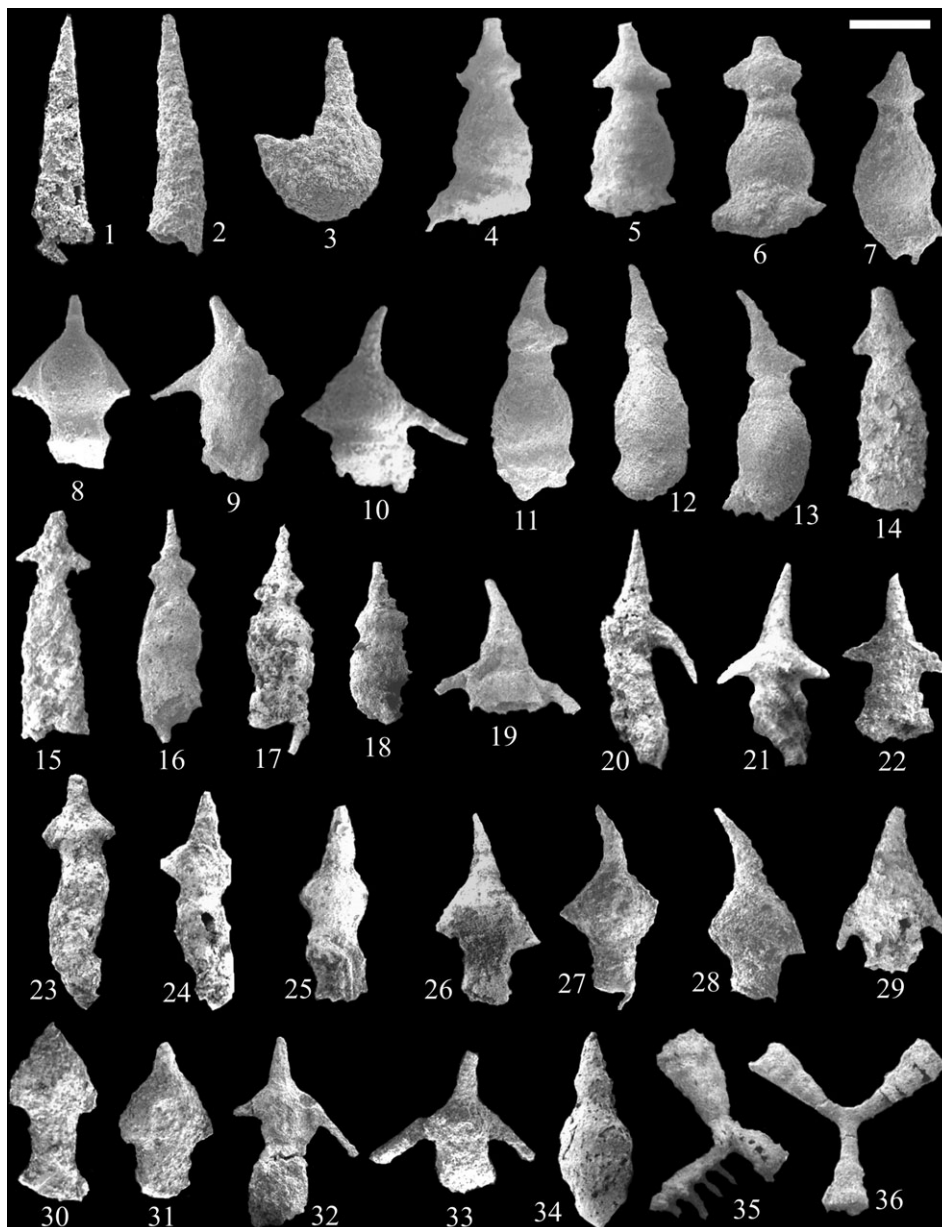


FIGURE 7 Permian radiolarians from the Mersin Mélange. (1,2) *Follicucullus scholasticus* Ormiston & Babcock: (1) Kar-E-41; (2) Kar-E-46, scale bar = 150 μm . (3) *Follicucullus sphaericus* Takemura, Kar-E-46, scale bar = 120 μm . (4–7) *Parafollicucullus fusiformis* Holdsworth & Jones: (4,5) Hod-2; (6) Cik-18; (7) Cik-11, scale bar = 120 μm . (8–10) *Parafollicucullus globosa* (Ishiga & Imoto): (8) Cik-19; (9) Cik-14; (10) Cik-11, scale bar = 120 μm . (11–13) *Parafollicucullus internata* (Wang): (11) Cik-15; (12) Cik-10; (13) Cik-10, scale bar = 120 μm . (14,15) *Parafollicucullus ishigai* (Wang): (14) Kar-SW-18; (15) Kar-E-10, scale bar = 130 μm . (16–18) *Parafollicucullus lomentaria* (Ishiga & Imoto): (16) Kar-SW-7; (17) Kar-SW-8; (18) Kar-SW-10, scale bar = 180 μm . (19) *Parafollicucullus longicornis* (Ishiga & Imoto), Kar-SW-7, scale bar = 120 μm . (20–22) *Parafollicucullus longtanensis* (Sheng & Wang): (20) Hod-2; (21) Hod-2; (22) Kar-E-9, scale bar = 110 μm . (23–25) *Parafollicucullus sakmarensis* Kozur, all from Kar-SW-13, scale bar = 120 μm . (26,27) *Parafollicucullus scalprata rhombothoracata* (Ishiga & Imoto): (26) Kar-SW-14; (27) Kar-E-3, scale bar = 130 μm . (28,29) *Parafollicucullus scalprata scalprata* (Holdsworth & Jones): (28) Kar-SW-17; (29) Kar-E-5, scale bar = 140 μm . (30,31) *Parafollicucullus triangularis* (Wang): (30) Kar-E-2; (31) Kar-E-4, scale bar = 160 μm . (32,33) *Parafollicucullus yanaharensis* (Nishimura & Ishiga): (32) Cik-18; (33) Cik-11, scale bar = 120 μm . (34) *Parafollicucullus zhengpanshanensis* (Sheng & Wang), Kar-SW-8, scale bar = 150 μm . (35,36) *Cauletella manica* (De Wever & Caridroit): (35) Kar-E-49; (36) Kar-E-56, scale bar = 150 μm

composed of alternating chert and mudstone, include characteristic assemblages of this zone (Figure 3). Sample Kar-SW-16 in the Karincali-Southwest section includes *Albaillella xiaodongensis* (Figure 6 (18)), *Albaillella asymmetrica* (Figure 6(1)) and *Parafollicucullus scalprata scalprata*, and sample Kar-SW-17 includes the first appearance of *Albaillella sinuata* (Figure 6(15)). This part of section appears to be correlative to the the *Albaillella sinuata* Zone of Ishiga (1990) in Japan,

either the *Albaillella xiaodongensis* Zone or the *Albaillella sinuata* Zone of Y. J. Wang et al. (1994, 2006, 2012), Y. J. Wang and Yang (2011) (Figure 5) in China, and the *A. sinuata* Zone in Malaysia (Spiller, 2002). In China, alternative zonations for this interval have also been proposed. The *Albaillella sinuata* Zone is a first appearance zone proposed from the Qinzhou area in South China by Shimakawa and Yao (2006), and the *A. foremanae* Zone, a first appearance zone proposed by

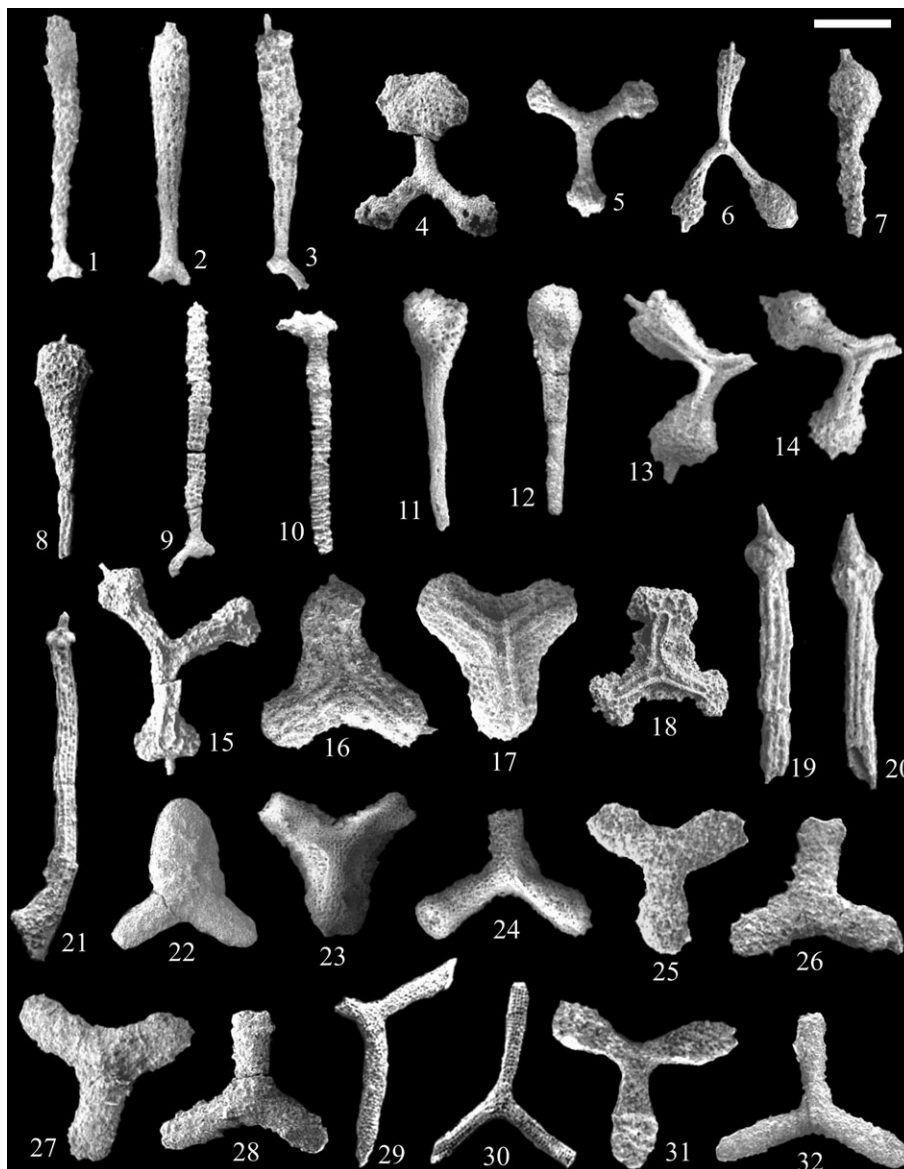


FIGURE 8 Permian radiolarians from the Mersin Mélange. (1–3) *Ishigaum craticula* Shang et al.: (1) Kar-E-50; (2) Kar-E-56; (3) Kar-E-56, scale bar = 130 μm . (4) *Ishigaum obesum* De Wever & Caridroit, Kar-E-52, scale bar = 120 μm . (5,6) *Ishigaum trifustus* De Wever & Caridroit: (5) Kar-E-49; (6) Kar-E-53, scale bar = 140 μm . (7,8) *Ishigaum tristylum* Feng: (7) Kar-E-48; (8) Alic W-5, scale bar = 150 μm . (9,10) *Pseudotormentus kamigoriensis* De Wever & Caridroit: (9) Hod-2; (10) Kar-SW-24, scale bar = 330 and 290 μm , respectively. (11,12) *Shangella longa* Feng: (11) Kar-E-54; (12) Kar-E-55, scale bar = 170 μm . (13–15) *Triplanospongus angustus* (Noble & Renne); (13) Kar-E-54; (14) Kar-E-55; (15) Alic-W-5, scale bar = 130 μm . (16–18) *Triplanospongus musashiensis* Sashida & Tonishi: (16) Kar-E-55; (17,18) Alic-W-5, scale bar = 110 μm . (19–21) *Areolicaudatus semiglobosa* Feng: (19) Kar-E-53; (20) Kar-E-54; (21) Alic-W-5, scale bar = 130 μm , 130 μm , 200 μm , respectively. (22–24) *Latentifistula aspersongiosa* Sashida & Tonishi: (22) Cik-4; (23) Kar-E-54; (24) Kar-E-55, scale bar = 220 μm . (25) *Latentifistula banchengensis* Wang, Kar-SW-17, scale bar = 150 μm . (26–28) *Latentifistula crux* Nazarov & Ormiston: (26) Kar-SW-18; (27) Kar-SW-19; (28) Kar-E-1, scale bar = 150 μm . (29,30) *Latentifistula hetroextrema* Nazarov, both from Kar-SW-7, scale bar = 300 μm . (31,32) *Latentifistula patagilateralis* Nazarov & Ormiston: (31) Kar-SW-25; (32) Kar-E-8, scale bar = 200 μm

N. Zhang et al. (2010) from the Dachongling section, also in South China. According to Y. J. Wang and Yang (2011), *Albaillella sinuata* is rare in its lower range and becomes abundant in the middle of its range, causing them to establish the *Albaillella sinuata* Acme Zone. In contrast, Shimakawa and Yao (2006), also working in South China, show an overlap in the range of both *A. sinuata* and *A. xiaodongensis* but with no notable acme, and occurring below the first appearance of *P. longtanensis*, leading them to redefine the *A. sinuata* zone as a first occurrence zone, more in line with that of Ishiga (1990). The *A. sinuata* Zone by Shimakawa and Yao (2006), like that of Ishiga

(1990), encompasses both the *A. xiaodongensis* and *A. sinuata* zones by Y. J. Wang and Yang (2011), and the *A. foremanae* Zone by N. Zhang et al. (2010) appears to encompass both the *A. sinuata* and overlying *P. longtanensis* zones by Ishiga (1990). Herein, we follow the zonal definition of Shimakawa and Yao (2006) from South China, as it best fits the faunal succession seen in our material.

In the Karincali-East section, the lowest samples assigned to this zone, samples Kar-E-5 and Kar-E-6 lack *Albaillella sinuata* but contain *Parafollicucullus scalprata scalprata* (Figure 7(29)), and *A. sinuata* occurs in both Kar-E-7 and Kar-E-8. Ishiga (1990) shows a more attenuated

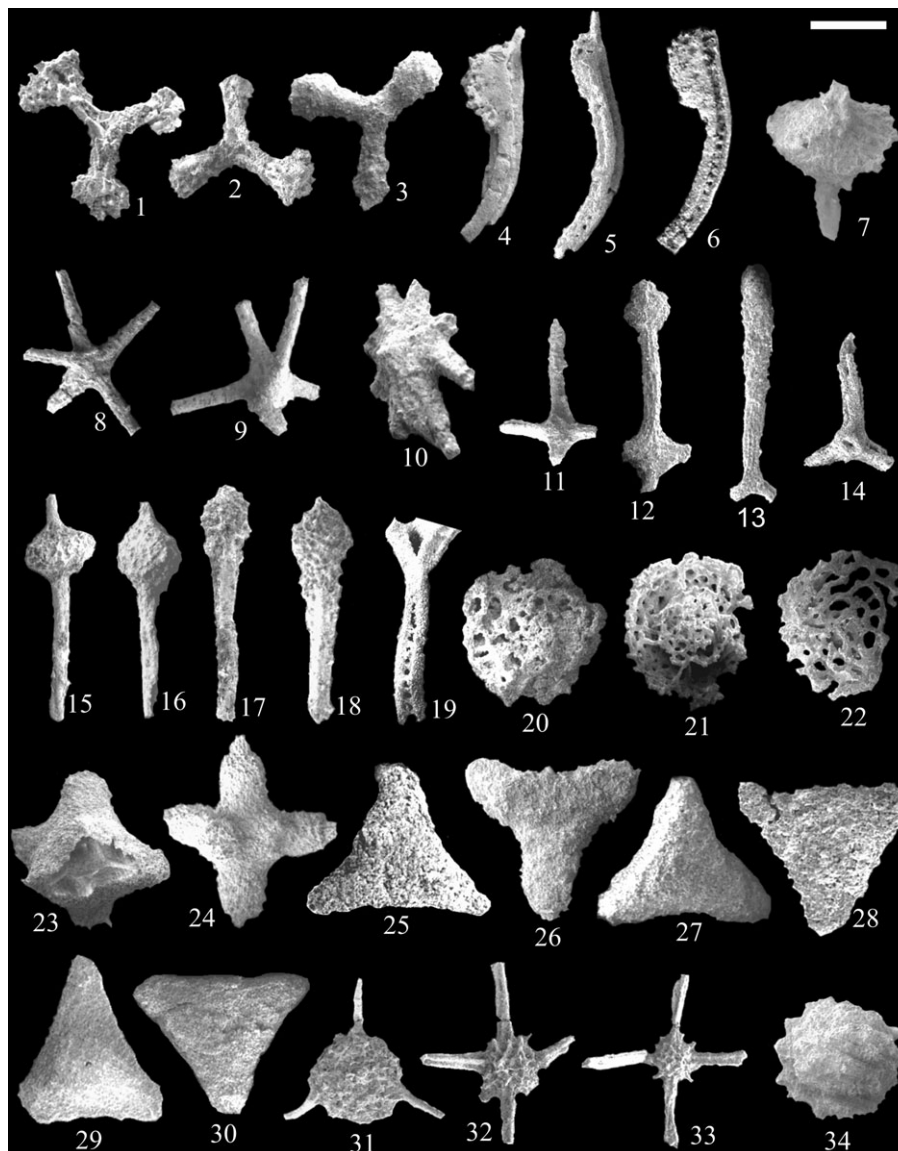


FIGURE 9 Permian radiolarians from the Mersin Mélange. (1,2) *Latentifistula similicutis* Caridroit & De Wever: (1) Kar-E-40; (2) Kar-E-41, scale bar = 140 μm . (3) *Latentifistula texana* Nazarov & Ormiston, Hod-9, scale bar = 150 μm . (4–6) *Ormistonella adhaerens* Feng: (4) Kar-E-48; (5) Kar-E-54; (6) Alic-W-5, scale bar = 140 μm . (7) *Ormistonella elegans* (Feng), Kar-E-50, scale bar = 100 μm . (8,9) *Polyfistula hexalobota* Nazarov & Ormiston, both from Hod-2, scale bar = 200 μm . (10) *Polyfistula regularis* Feng, Kar-E-48, scale bar = 140 μm . (11,12) *Quadricaulis flata* (Wang): (11) Hod-9; (12) Kar-SW-16, scale bar = 250 μm . (13) *Quadricaulis inflata* (Sashida & Tonishi), Kar-SW-16, scale bar = 290 μm . (14–16) *Quadricaulis gracilis* (De Wever & Caridroit): (14) Kar-E-52; (15) Kar-E-54; (16) Alic-W-5, scale bar = 200 μm . (17,18) *Quadricaulis phlogides* (Wang & Li): (17) Kar-SW-14; (18) Kar-E-2, scale bar = 130 μm . (19) *Quadricaulis scalae* (De Wever & Caridroit), Kar-E-56, scale bar = 130 μm . (20–22) *Grandetortura nipponica* Sashida & Tonishi: (20) Cik-4; (21) Kar-E-2, (22) Kar-E-6, scale bar = 220 μm . (23) *Octatormentum? floriferum* Sashida & Tonishi, Kar-E-56, scale bar = 160 μm . (24) *Octatormentum yaoi* Wu & Feng, Kar-E-56, scale bar = 200 μm . (25–27) *Ruzhencevispongius triradiatus* Wang: (25) Cik-4; (26) Kar-SW-17; (27) Kar-SW-17, scale bar = 180 μm . (28–30) *Ruzhencevispongius uralicus* Kozur: (28) Cik-4; (29) Kar-E-1; (30) Kar-E-2, scale bar = 180 μm . (31) *Tetragregnon nitidus* Nazarov & Ormiston, Kar-SW-7, scale bar = 210 μm . (32,33) *Stigmosphaerostylus parapycnoclada* (Nazarov & Ormiston), both from Kar-SW-7, scale bar = 150 μm . (34) *Hegleria mammilla* (Sheng & Wang), Kar-E-8, scale bar = 140 μm

stratigraphic range of *P. scalprata* in Japan, making its last occurrence below the *A. sinuata* Zone but subsequent work in Japan and China show that *P. scalprata* ranges well above the *A. sinuata* Zone (Shimakawa & Yao, 2006). Based on the presence of *Albaillella sinuata*, it can be suggested that at least the level above Kar-E-6 should correspond to the *Albaillella sinuata* Zone (Table 2). Sample Hod-13 in the Hodul section includes both *Parafollicucullus scalprata scalprata* and *Albaillella sinuata* (Figure 6(17)), similar to China, and is also assigned to the *Albaillella sinuata* Zone (Figures 3 and 5; Table 3).

In terms of age assignment, the *A. sinuata* assemblage in Malaysia was assigned to the Leonardian (Spiller, 2002), revised to Kungurian–Roadian in Metcalfe (2000). In China, the *A. xiaodongensis* Zone and *A. sinuata* Zones in Y. J. Wang and Yang (2011) are assigned to the the lower and middle Leonardian, respectively, which is roughly equivalent to the Kungurian. The *Parafollicucullus scalprata* Zone in A. Yao and Kuwahara (2004) and Shimakawa and Yao (2006) do not contain independent biostratigraphic control from the Migong section in Qinzhou but instead adopt the age assignments from the zonation

established in southwest Japan. Ishiga's zonation was calibrated with fusulinaceans and conodonts, although age revisions to his assignments have been discussed in many papers (see Aitchison et al., 2017). The best age calibration from conodonts appears in N. Zhang

et al. (2010) for the top of the *A. foremanae* zone, which ends at the Kungurian–Roadian boundary, at the base of the *J. nankingensis gracilis* conodont zone, and supports an age of a middle Kungurian time interval for our material (Figure 5).

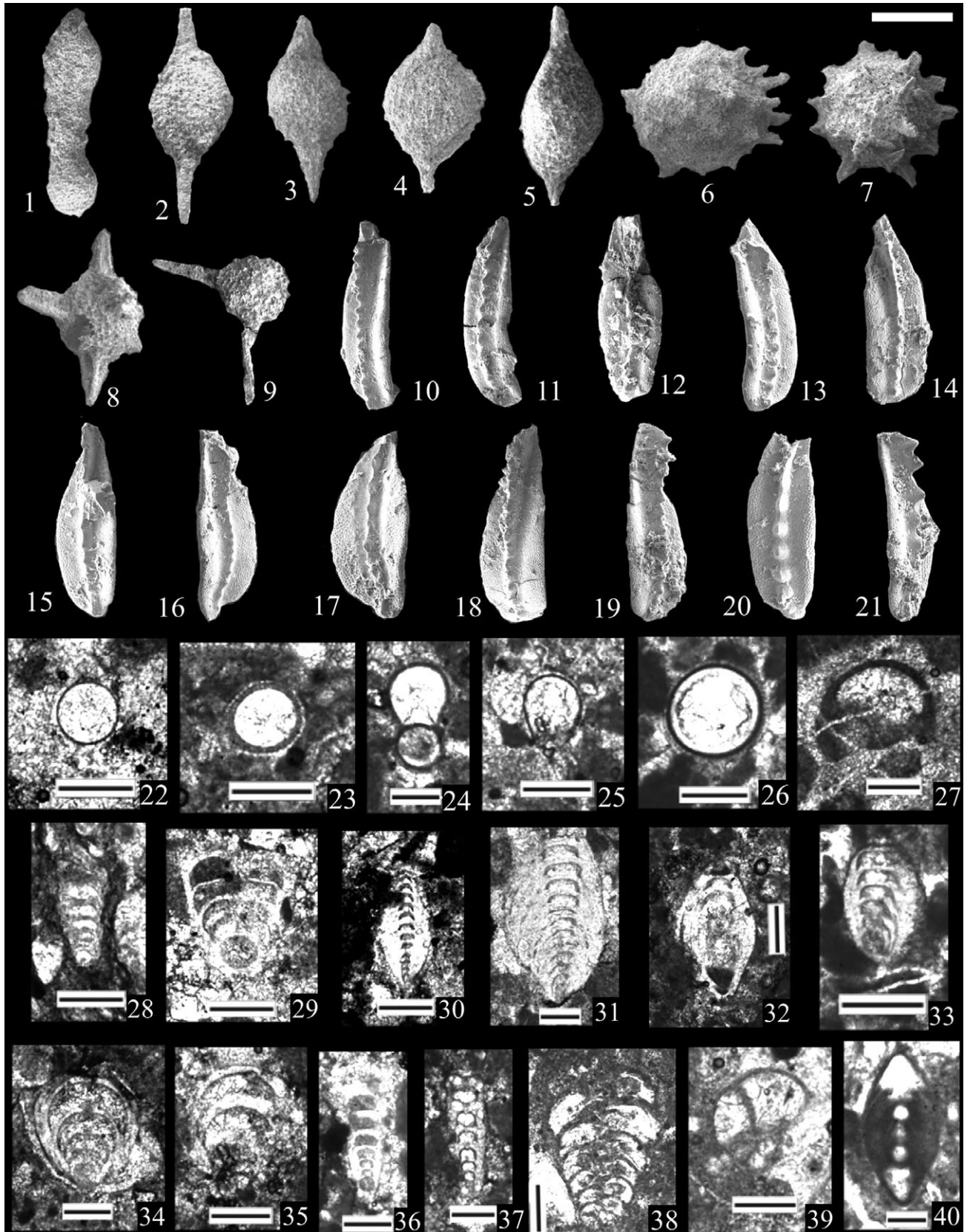


FIGURE 10 Legend on next page.

The *Parafollicucullus longtanensis* Zone of Ishiga (1990), or upper *Albaillella foremanae* Zone of N. Zhang et al. (2010)

Similar to the assemblage of the *Albaillella sinuata* Zone, the radiolarian assemblage of this zone has been identified in the Hodul, Karincali-Southwest and Karincali-East sections (Figure 3). Radiolarians in these sections are derived from chert levels in alternating chert and mudstone and the Karincali-Southwest section contains a basic volcanic interlayer within this lithology.

Ishiga (1986, 1990) proposed the *Parafollicucullus longtanensis* Zone, for the upper part of the Kungurian in Japan, Malaysia (Jasin & Harun, 2011; Metcalfe, 2000), and in South China (Shimakawa & Yao, 2006), whereas the *Parafollicucullus ishigai* Zone (Y. J. Wang et al., 1994) and the upper part of the *A. foremanae* Zone (N. Zhang et al., 2010) covers the same interval (Figure 5). Both *P. longtanensis* and *P. ishigai* co-occur in sample Kar-SW-18 (Figure 7(14)) in the Karincali-Southwest section (Table 1), sample Kar-E-9 (Figure 7(22)) in the Karincali-East section (Table 2) and sample Hod-9 in the Hodul section (Table 3). Similar assemblages have also been obtained from Kar-SW-19 in the Karincali-Southwest section (Table 1), sample Kar-E-10 in the Karincali-East section (Table 2) and sample Hod-7 in the Hodul section (Table 3) and included into the same zone. In this study, the interval between the first co-occurrence of *Parafollicucullus ishigai* (= *Pseudoalbaillella* sp. C in earlier literature) and *Parafollicucullus longtanensis* to the first appearance of *Parafollicucullus globosa* is accepted as *Parafollicucullus longtanensis* Zone based on the studies of Ishiga (1990), A. Yao and Kuwahara (2004), Y. J. Wang et al. (1994, 2006, 2012) and Y. J. Wang and Yang (2011). The age of this zone is reported as late Kungurian by Ishiga (1990), Shimakawa and Yao (2006), Spiller (2002), A. Yao and Kuwahara (2004), and also late Kungurian (based on the zonal age of *P. ishigai*) by Y. J. Wang et al. (1994, 2006, 2012) and Y. J. Wang and Yang (2011) (Figure 5).

The *Parafollicucullus globosa* Zone of N. Zhang et al. (2010)

The basal part of the Cikrik section and the upper part of the Hodul section composed of alternating chert and mudstone contain typical assemblages of the *Parafollicucullus globosa* Zone (Figure 3). No sample contains characteristic fauna of this zone in the Karincali-Southwest section, but this could be explained by the poor preservation of the radiolarian assemblage. Due to tectonic attenuation, the interval corresponding to this zone is also absent in the Karincali-East section (Figure 3).

According to Ishiga (1986), the base of this zone is marked by the presence of *Parafollicucullus globosa*, while top of this zone marked by the first occurrence of *F. monacanthus*. *Parafollicucullus fusiformis*, *P. internata* and *P. yanaharensis* are also common taxa associated with the zone (Y. J. Wang et al., 2012). These indicative taxa are present in the sample Hod-2 in the Hodul section and samples Cik-13, Cik-14, Cik-15, Cik-18, and Cik-19 in the Cikrik section (*P. fusiformis* at Figure 7(4–6), *P. globosa* at Figure 7(8,9), *P. internata* at Figure 7(11) and *P. yanaharensis* at Figure 7(32)). At the basal part of the zone (sample Hod-2 in the Hodul section in Figure 7(21,22) and Cik-19 in Cikrik section), *P. longtanensis* also appears associated to the characteristic taxa of this zone (Tables 3 and 4).

The age of this zone is reported as Roadian (Middle Permian) by different researchers (e.g. Ishiga, 1986, 1990; Ito & Matsuoka, 2015; Jasin & Harun, 2011; Kuwahara et al., 1998; Y. J. Wang et al., 1994, 2006, 2012; Y. J. Wang & Yang, 2011; Xia, Ning, Kakuwa, & Lil, 2005; A. Yao & Kuwahara, 2004; Figure 5). We applied this assignment to this study.

The *Follicucullus monacanthus* Zone of L. Zhang et al. (2014)

Two sections (the Cikrik and Karincali-Southwest) bear radiolarian assemblages of this zone (Figure 3). The uppermost part of the alternating chert and mudstone at the base in the Cikrik section, and limestone with chert interlayers in the central part of the Karincali-Southwest section include this assemblage (Figure 3).

According to Ishiga (1986), the interval of this zone is marked by the presence of *Follicucullus monacanthus* (interval zone). The end of this zone is marked by the absence of *F. monacanthus* and the presence of *Follicucullus scholasticus*/*Follicucullus porrectus* (e.g. Ishiga, 1986; Ito, Feng, & Matsuoka, 2015; Y. J. Wang & Yang, 2011; Xia et al., 2005; Figure 5). Samples Cik-9 to Cik-12 in the Cikrik section contain *F. monacanthus* (Figure 6(31)) associated with *P. globosa* (Figure 7(8,9)), *P. fusiformis* (Figure 7(7)) and *P. internata* (Figure 7(12,13); Table 4). Similar to this assemblage, sample Kar-SW-22, Kar-SW-24, and Kar-SW-25 in the Karincali-Southwest section (Table 1) contains some Latentifistularia in addition to *F. monacanthus* (Figure 6(32,33)). These assemblages are best correlative to the *Follicucullus monacanthus* Zone indicating roughly middle Guadalupian age (Ishiga, 1986, 1990; Ito, Feng, & Matsuoka, 2013; Ito et al., 2015; Kuwahara et al., 1998; Y. J. Wang et al., 1994, 2006, 2012; A. Yao & Kuwahara, 2004). Recent work (Ma, Feng, Caridroit,

FIGURE 10 Permian radiolarians, conodonts, benthonic foraminifera from the Mersin Mélange. (1–9) Radiolarians. (1) *Bistarkum martiali* Feng, Kar-E-54, scale bar = 170 μm . (2,3) *Archaeospongoprimum chiangdaoensis* (Sashida); (2) Kar-E-53; (3) Kar-E-56, scale bar = 90 μm . (4,5) *Paroertlispongia fontainei* (Sashida); (4) Kar-E-49; (5) Kar-E-54, scale bar = 100 μm . (6,7) *Paracopycnra akikawaensis* (Sashida & Tonishi); (6) Kar-E-51; (7) Kar-E-54, scale bar = 110 μm . (8) *Tetraspongodiscus stauracanthus* Feng, Kar-E-56, scale bar = 120 μm . (9) *Yujingella triacantha* Feng, Alic-W-5, scale bar = 200 μm . (10–21) Conodonts. (10–12) *Mesogondolella siciliensis* (Kozur), all from Cik-7, scale bar = 530 μm . (13–15) *Clarkina hongshuiensis* Henderson et al., all from Kar-E-38, scale bar = 400 μm . (16,17) *Jinogondolella? cf. altudaensis* (Kozur), both from Kar-E-38, scale bar = 340 μm and 220 μm , respectively. (18,19) *Clarkina hongshuiensis* Henderson et al., both from Kar-E-39, scale bar = 400 μm . (20,21) *Clarkina postbitteri* Mei & Wardlaw, both from Kar-E-39, scale bar = 320 μm . Twenty-two to forty are benthic foraminifera, scale bar for all figures is 200 μm . (22) *Eotuberitina bulla* Conil & Lys, Kar-SW-26, axial section. (23–25) *Eotuberitina reitlingerea* Miklukho-Maklay: (23) Kar-SW-28; (24) Kar-E-26; (25) Kar-E-32, axial sections. (26,27) *Eotuberitina* spp.: (26) Kar-E-12; (27) Sah-5, axial sections. (28,29) *Geinitzina* spp.: (28) Kar-SW-29; (29) Kar-E-11, axial sections. (30) *Pachyphloia cf. ovata* Lange, Kar-E-31, axial section. (31) *Pachyphloia pedicula* Lange, Kar-E-22, axial section. (32,33) *Pachyphloia* spp.: (32) Kar-SW-28, transversal section; (33) Kar-E-12, oblique section. (34) *Cryptoseptida? sp.*, Kar-E-36, axial section. (35) *Langella? sp.*, Kar-SW-26, subaxial section. (36) *Nodosinelloides cf. pinardae* Groves & Wahlman, Kar-E-15, axial section. (37) *Nodosinelloides sp.*, Kar-E-14, axial section. (38) *Palaeotextularia sp.*, Kar-E-35, axial section. (39) *Globivalvulina sp.*, Kar-SW-28, axial section. (40) *Neoendothyrha permica* (Lin), Sah-10, axial section

TABLE 1 Distribution of radiolarians in the Karincali-Southwest section

AGE	Cisuralian										Guadalupian		
	Late Asselian-late Kungurian										Wordian		
	P. lomentaria/P. sakmariensis			P. s. r.			Albaillella sinuata				P. longtanensis		
SAMPLES	Kar-SW-7	Kar-SW-8	Kar-SW-10	Kar-SW-13	Kar-SW-14	Kar-SW-16	Kar-SW-17	Kar-SW-18	Kar-SW-19	Kar-SW-22	Kar-SW-24	Kar-SW-25	
<i>Parafollicuculus longicornis</i>	X												
<i>Latentifistula hetroextrema</i>	X												
<i>Tetrogregon nitidus</i>	X												
<i>Stigmosphaerostylus parapyrocyclada</i>	X												
<i>Parafollicuculus lomentaria</i>	X	X	X										
<i>Parafollicuculus triangularis</i>	X	?	X	X									
<i>Quadricaulis flata</i>	X	?	?	?	?	X	X						
<i>Ishigaum trifustus</i>	X	?	?	?	?	?	?	?	?	X	X	X	
<i>Parafollicuculus zhengpanshanensis</i>	X												
<i>Parafollicuculus s. rhombothoracata</i>		X	X	X	X								
<i>Latentifistula crux</i>		X	X	?	?	?	?	X	X				
<i>Parafollicuculus sakmariensis</i>				X									
<i>Quadricaulis phlogides</i>			X	X	X								
<i>Albaillella asymmetrica</i>						X							
<i>Albaillella xiadongensis</i>						X							
<i>Parafollicuculus s. scalprata</i>					X	X							
<i>Quadricaulis inflata</i>					X	X							
<i>Latentifistula banchengensis</i>						X							
<i>Ruzhencevispongus triradiatus</i>						X		?	X				
<i>Albaillella sinuata</i>						X		X	X				
<i>Parafollicuculus longtanensis</i>							X						
<i>Parafollicuculus ishigai</i>								X					
<i>Follicuculus monacanthus</i>										X	X	X	
<i>Parafollicuculus yanaharensis</i>											X		
<i>Pseudotormentus kamigoriensis</i>											X		
<i>Latentifistula patagilaterala</i>												X	

P. lomentaria/P. sakmariensis, Parafollicuculus lomentaria/Parafollicuculus sakmariensis; P. s. r., Parafollicuculus scalprata rhombothoracata; P. longtanensis, Parafollicuculus longtanensis. X, occurrence; ?, possible occurrence.

TABLE 2 Distribution of radiolarians at the base of the Karincali-East section

AGE	Cisuralian									
	Late Asselian – Kungurian									
RADIOLARIAN ZONES	<i>P. l. – P. s.</i>	<i>Parafollicucullus s. rhombothoracata</i>			<i>Albaillella sinuata</i>				<i>Parafollicucullus longtanensis</i>	
SAMPLES	Kar-E-1	Kar-E-2	Kar-E-3	Kar-E-4	Kar-E-5	Kar-E-6	Kar-E-7	Kar-E-8	Kar-E-9	Kar-E-10
<i>Parafollicucullus sakmarensis</i>	X									
<i>Ruzhencevispongos uralicus</i>	X	X								
<i>Ruzhencevispongos triradiatus</i>	X	X	X							
<i>Parafollicucullus s. rhombothoracata</i>	X	X	X	X						
<i>Latentifistula crux</i>	X	?	?	X	X					
<i>Parafollicucullus triangularis</i>		X	X	X						
<i>Quadricaulis inflata</i>		X	?	X						
<i>Grandetortura nipponica</i>		X	?	?	?	X				
<i>Quadricaulis phlogides</i>		X	?	?	?	?	?	X		
<i>Parafollicucullus longicomis</i>			X							
<i>Quadricaulis flata</i>			X	?	?	X	?	?	?	X
<i>Parafollicucullus s. scalprata</i>					X	X	X	X	X	
<i>Latentifistula patagilaterala</i>					X	?	?	X	X	
<i>Parafollicucullus ishigai</i>						X	X	X	X	X
<i>Albaillella sinuata</i>							X	X	X	
<i>Hegleria mammilla</i>								X		
<i>Parafollicucullus longtanensis</i>									X	X

P. l. – P. s., *Parafollicucullus lomentaria*–*Parafollicucullus sakmarensis*. X, occurrence; ?, possible occurrence.

TABLE 3 Distribution of radiolarians in the Hodul section

AGE	Cisuralian			Guadalupian
	Kungurian			Roadian
RADIOLARIAN ZONES	<i>Albaillella sinuata</i>	<i>Parafollicucullus longtanensis</i>		<i>Parafollicucullus globosa</i>
SAMPLES	Hod-13	Hod-9	Hod-7	Hod-2
<i>Albaillella sinuate</i>	X			
<i>Parafollicucullus scalprata scalprata</i>	X			
<i>Albaillella asymmetrica</i>	X	?	X	
<i>Quadricaulis flata</i>	X	X	X	X
<i>Parafollicucullus ishigai</i>		X		
<i>Latentifistula crux</i>		X		
<i>Latentifistula texana</i>		X		
<i>Parafollicucullus longtanensis</i>		X	X	X
<i>Parafollicucullus yanaharensis</i>			X	
<i>Ishigaum trifustis</i>			X	
<i>Latentifistula patagilaterala</i>			X	
<i>Parafollicucullus fusiformis</i>				X
<i>Parafollicucullus globosa</i>				X
<i>Parafollicucullus internata</i>				X
<i>Polyfistula hexalobota</i>				X
<i>Pseudotormentus kamigoriensis</i>				X

X, occurrence; ?, possible occurrence.

Danelian, & Zhang, 2016; Xia et al., 2005; L. Zhang et al., 2014) from southern China reports that the age of this zone is Wordian based on the correlation of radiolarian assemblages to the conodont assemblages (Figure 5). This age assignment is applied to this study. Conodont materials obtained from the Cikrik section are also well-correlated to the radiolarian ages (see chapter 4.2.1).

The *Follicucullus scholasticus*/*Follicucullus porrectus* Zone of L. Zhang et al. (2014) and D. Sun and Xia (2006)

Based on studies of Ito et al. (2015), Xia et al. (2005), and L. Zhang et al. (2014), the basal part of this zone is marked by the absence of *Follicucullus monacanthus* and the presence of *Follicucullus scholasticus*/*Follicucullus porrectus*. Sample Cik-4 in the Cikrik section consists

TABLE 4 Distribution of radiolarians in the Cikrik section

AGE RADIOLARIAN ZONES SAMPLES	Guadalupian									
	Roadian					Wordian				Capitanian
	<i>Parafollicucullus globosa</i>					<i>Follicucullus monacanthus</i>				<i>F. scholasticus</i> - <i>F. porrectus</i>
	Cik-19	Cik-18	Cik-15	Cik-14	Cik-13	Cik-12	Cik-11	Cik-10	Cik-9	Cik-4
<i>Parafollicucullus longtanensis</i>	X									
<i>Parafollicucullus globosa</i>	X	X	X	X	X	?	X	X		
<i>Parafollicucullus fusiformis</i>	X	X	X	X	X	X	X	X	X	
<i>Parafollicucullus internata</i>		X	X	X	X	X	X	X	X	
<i>Parafollicucullus yanaharensis</i>		X	?	?	?	?	X			
<i>Parafollicucullus banchengensis</i>			X							
<i>Follicucullus monacanthus</i>						X	X	X	X	
<i>Follicucullus lagenarius</i>									X	
<i>Follicucullus scholasticus</i>										X
<i>Latentifistula aspersongiosa</i>										X
<i>Latentifistula crux</i>										X
<i>Ruzhencevispongos triradiatus</i>										X
<i>Ruzhencevispongos uralicus</i>										X
<i>Grandetortura nipponica</i>										X

X, occurrence; ?, possible occurrence.

of *Follicucullus scholasticus* in addition to *Latentifistularia* (Table 4) and is assigned to this zone. Similar to this assemblage, sample Alic-W-2 in the Aliclipinar-West section includes taxa (Table 5) also typically found within this zone. These two samples (Cik-4 in the Cikrik section and Alic-W-2 in the Aliclipinar-West section) were retrieved from chert interlayers within the detrital limestone. The age of this zone is reported as Capitanian based on the correlation of radiolarian assemblages to the conodont assemblages (Ma et al., 2016; L. Zhang et al., 2014; Figure 5) and we follow the same age assignment.

Based on radiolarian and conodont biostratigraphy in the Cikrik and Karincali-Southwest sections, it can be concluded that carbonate accumulation in the basin started in the middle Wordian and terminated in the earliest Wuchiapingian (Figure 3). Benthic foraminifera, algae, and conodont assemblages obtained from these detrital limestones will be discussed in later sections (see section 4.2).

4.1.2 | Radiolarian biostratigraphy of upper Permian sequences

The upper part of the Permian sequence is of pelagic origin, composed of alternating chert and mudstone. From this lithology, rather diverse and abundant radiolarian assemblages have been obtained from the Karincali-East and the Aliclipinar-West sections (Figure 3).

Radiolarian zonations for the Late Permian were initially established in southwest Japan (Ishiga, 1986, 1990; Kuwahara, Yao, & An, 1997; Kuwahara et al., 1998) and South China (Kuwahara et al., 2007; Y. J. Wang et al., 1994), and refinements have continued through calibration with conodont biostratigraphy (Nishikane, Kaiho, Henderson, Takahashi, & Suzuki, 2014; Nishikane et al., 2011; D. Sun & Xia, 2006; Xia et al., 2004, 2005; J. Yao et al., 2001). A summary of these zones and their age control is found in Aitchison et al. (2017) and is adopted herein. Radiolarian assemblages belonging to the following radiolarian zones of early Wuchiapingian to middle Changhsingian age are encountered in this study (Figure 5).

The *Albaillella yamakitai* Zone of Nishikane et al. (2011) and L. Zhang et al. (2014)

Overlying detrital limestone beds in the Karincali-East section, alternating green to black-colored, thin-bedded chert and mudstone is the dominant lithology with medium-bedded, pink colored conglomeratic interlayers occurring between samples Kar-E-40 to Kar-E-47 (Figure 3). Within this interval, four samples (Kar-E-40, Kar-E-41, Kar-E-46, and Kar-E-47) are rich in species of *Follicucullidae* (e. g. *Follicucullus charveti charveti* in Figure 6(25), *F. charveti falx* in Figure 6(26), *F. charveti orthogonus* in Figure 6(27,28), *F. dilatatus* in Figure 6(29), *F. lagenarius*, *F. porrectus* in Figure 6(34,35), *F. scholasticus* in Figure 7 (1,2) and *F. sphaericus* in Figure 7(3)) and also contain *Latentifistularia* (e.g. *Latentifistula similicutis* in Figure 9(1,2); Table 6)

Based strictly on the radiolarian assemblage, these samples could be assigned to either the latest Guadalupian (late Capitanian) *Albaillella charveti* Zone as defined by L. Zhang et al. (2014), or the overlying *A. yamakitai* Zone of earliest Lopingian (early Wuchiapingian) age (Nishikane et al., 2011) because all of these taxa range through the Guadalupian/Lopingian boundary. The zonal markers for the *Albaillella yamakitai* Zone (i.e. *A. yamakitai* and *A. cavitata*) are absent in these samples, but their absence can be a function of low diversity or preservation. Given the age control from conodonts in the underlying limestones discussed earlier, as well as the carbon isotope results (discussed later), these samples are assigned to the *A. yamakitai* Zone. It is significant to note that the *A. yamakitai* Zone has only recently been broken out from the underlying zone, as earlier iterations of the upper Permian biostratigraphy combine these zones, such as the *F. charveti*-*A. yamakitai* Zone of Kuwahara et al. (1998), and the *F. bipartitus*-*F. charveti*-*F. orthogonus* zone (Y. J. Wang et al., 2006).

The *A. yamakitai* Zone (Figure 5) is a taxon range zone, based on the total range of the nominal species, but also includes the taxa observed in the Karincali-East section. Nishikane et al. (2011, 2014) provides critical age control showing that the first occurrence of

TABLE 5 Distribution of radiolarians in the Aliclipinar-West section

AGE	Guadalupian Capitanian <i>F. scholasticus</i> - <i>F. porrectus</i>	Lopingian Changhsingian <i>Neobaillella optima</i> <i>N. optima</i> - <i>A. lauta</i>
RADIOLARIAN ZONES		
RADIOLARIAN SUBZONES		
SAMPLES	Alic-W-2	Alic-W-5
<i>Follicucullus porrectus</i>	X	
<i>Follicucullus scholasticus</i>	X	
<i>Albaillella lauta</i>		X
<i>Neobaillella gracilis</i>		X
<i>Neobaillella ornithoformis</i>		X
<i>Ishigaum trifustis</i>		X
<i>Ishigaum tristylum</i>		X
<i>Shangella longa</i>		X
<i>Triplanospongos angustus</i>		X
<i>Triplanospongos musashiensis</i>		X
<i>Areolicaudatus semiglobosa</i>		X
<i>Latentifistula aspersongiosa</i>		X
<i>Ormistonella adhaerens</i>		X
<i>Quadricaulis gracilis</i>		X
<i>Quadricaulis inflata</i>		X
<i>Ruzhencevispongos triradiatus</i>		X
<i>Yujingella triacantha</i>		X

X, occurrence.

A. yamakitai is within the uppermost beds of the Guadalupian (Capitanian) at the base of the *Clarkina hongshuiensis* Zone, and the last occurrence is within the Wuchiapingian with *Clarkina dukouensis* (Figure 5).

The *Neobaillella ornithoformis* Zone of Xia et al. (2004, 2005) and Nishikane et al. (2011)

This is the second zone for Late Permian time interval according to Kuwahara (1999) and Xia et al. (2004, 2005), and its lower limit is defined by the first occurrence of *Neobaillella ornithoformis* (Figure 6 (22–24)), whereas the upper limit is defined by the first occurrence of *Neobaillella optima*. Various subzones have been recognized within the *N. ornithoformis* Zone, including acme zones by Kuwahara et al. (1998), with variations adopted by Xia et al. (2004, 2005). Y. J. Wang et al. (2006) recognized a different zonal sequence in South China (Figure 5) and relies on assemblages or acmes in defining the zones. It is important to note that the total range of certain key taxa defining the acme zones of Kuwahara et al. (1998) and Xia et al. (2004, 2005) such as *A. levis* and *A. protolevis* overlap almost entirely spanning most of the Wuchiapingian (Nishikane et al., 2011; Figure 5). This makes it difficult to apply these subzones to the Mersin faunas because of sparse radiolarian recovery and only fair preservation.

Samples Kar-E-48 and Kar-E-49 are assigned to this zone. Both *Neobaillella ornithoformis* (Figure 6(22–24)) and *Albaillella protolevis* (Figure 6(12–14)) first appear in sample Kar-E-48 in the Karincali-East section (Table 6). *Albaillella levis* (Figure 6(9–11)) appears for the first time in sample Kar-E-49 in the Karincali-East section which is slightly after the appearance of *Albaillella protolevis* (Table 6).

The age of the base of the *N. ornithoformis* Zone was assigned to early to middle Wuchiapingian by Xia et al. (2004, 2005). Nishikane et al. (2011) provide further refinement from southwest Japan, showing that the first occurrence of *N. ornithoformis* occurs with *Clarkina guangyuanensis* in the middle Lopingian. The top of the *N. ornithoformis* Zone is dated as earliest Changhsingian (Aitchison et al., 2017).

The *Neobaillella optima* Zone

Based on the zonal scheme of Xia et al. (2004), it is a total range zone of the nominal taxon corresponding to late Wuchiapingian to early Changhsingian time interval, but as discussed in Aitchison et al. (2017), the age is adjusted to be entirely in the Changhsingian (Figure 5). Four subzones have been proposed within the *N. optima* Zone, and assemblages of the basal two subzones appear to be present in the Karincali-East and Aliclipinar-West sections (Figures 3 and 5; Tables 5 and 6).

The *Neobaillella optima*-*Albaillella lauta* Subzone of Xia et al. (2004)

The base of this subzone is recognized by the co-occurrence of *Neobaillella optima* and *Albaillella lauta* and the top by the first appearance datum of *Albaillella flexa*-*Albaillella angusta* according to Xia et al. (2004). In the Karincali-East section, *Neobaillella optima* is rare and only present in sample Kar-E-50 (Figure 6(21); Table 6). Very close to this interval, *Albaillella lauta* first appears in sample Kar-E-51 and persists until the top of the section (Figure 6(6–8)) together with *Albaillella levis* (Figure 6(9–11)), *Neobaillella ornithoformis* (Figure 6 (22–24)), and abundant *Latentifistularia* and *Spumellaria* mainly defined by Feng (1992), Feng and Liu (1993), Feng, Meng, He, and Gu (2006), and Shang, Caridroit, and Wang (2001) (Figures 8–10; Table 6). Radiolarian assemblages in samples Kar-E-50 to Kar-E-55 are typical for this zone (Table 6). Similarly sample Alic-W-5 in the Aliclipinar-West section includes *Albaillella lauta*, *Albaillella levis*, *Neobaillella ornithoformis* and taxa belonging to *Latentifistularia* and *Spumellaria* (Table 5). Age of this zone is assigned to the Changhsingian based on the discussion provided in Aitchison et al. (2017) (Figures 3 and 5).

The *Albaillella flexa*-*Albaillella angusta* subzone of Xia et al. (2004)

Based on the definition of Xia et al. (2004), the base is defined by the co-occurrence of *Albaillella flexa*-*Albaillella angusta* and the top by the presence of *Albaillella triangularis*. In the top of the Karincali-East section, substantial changes in the radiolarian assemblage occur beginning in sample Kar-E-56, and a very different fauna including *Albaillella excelsa* (Figure 6(3)), *Albaillella flexa* (Figure 6(4,5)), *Octatormentum ? floriferum* (Figure 9(23)) and *Octatormentum yaoi* (Figure 9 (24)) appears for the first time. Although *Albaillella angusta* was not recognized in samples Kar-E-56 and Kar-E-57, there are sufficient taxa reported from the *Albaillella flexa*-*Albaillella angusta* subzone to warrant its assignment to this subzone (Table 6). The age of this zone is reported as early Changhsingian by Xia et al. (2004), adjusted slightly upwards to the middle Changhsingian (Aitchison et al., 2017).

TABLE 6 (Continued)

AGE	Changhsingian														
	Lopingian					Wuchiapingian									
RADIOLARIAN ZONES RADIOLARIAN SUBZONES	Albaillella yamakitai					Neobaillella ornithoformis					Neobaillella optima				
	Kar-E-40	Kar-E-41	Kar-E-46	Kar-E-47	Kar-E-48	Kar-E-49	Kar-E-50	Kar-E-51	Kar-E-52	Kar-E-53	Kar-E-54	Kar-E-55	Kar-E-56	Kar-E-57	
<i>Ishigium obesum</i>									X						
<i>Areolicaudatus semiglobosa</i>									X	X	X				
<i>Quadracaulis scalae</i>									X	?	?		X		
<i>A. chiangdaoensis</i>									X	?	?		X		
<i>Bistarkum martiali</i>										X					
<i>Shangella longa</i>										X					
<i>Albaillella excelsa</i>														X	
<i>Octatormentum yaoi</i>														X	
<i>Octatormentum ? floriferum</i>														X	
<i>T. stauracanthus</i>														X	
<i>Grandetortura nipponica</i>														X	
<i>Albaillella flexa</i>														X	

X, occurrence; ?, possible occurrence.

and this latter age assignment is applied to this study (Figures 3, and 5).

4.2 | Benthic foraminifera, algae and conodont datings of the middle Middle to basalmost upper Permian detrital carbonates in the central part of the Permian sequences

To understand the detailed characteristics of benthic foraminifera, algae and conodont assemblages of middle Guadalupian to earliest Lopingian detrital carbonates, samples from three stratigraphic sections (Sahancanak, Karincali-Southwest, and Karincali-East) were analyzed (Figure 3). Conodont, foraminiferal, and algal assemblages from these sections are illustrated at Figures 10 and 11. Details of these assemblages are as follows.

4.2.1 | Conodont assemblages from the Cikrik section

Conodont assemblage (*Mesogondolella siciliensis* (Kozur) in Figure 10 (10–12) and *Mesogondolella* sp.) obtained from stratigraphically younger strata (sample Cik-7) in the Cikrik section reveals the Roadian to Wordian age (H. W. Kozur & Wardlaw, 2010). Conodont data supports the age obtained from radiolarian assemblages of older strata where samples Cik-8 to Cik-12 were collected (Figure 3).

4.3 | Benthic foraminifera and algae assemblages from the Sahancanak section

Twelve samples were collected from carbonate-rich levels in the section for determination of foraminiferal/algal assemblages. They are mainly detrital limestone and are very similar to those of late Middle Capitanian carbonates observed in the Mersin Mélange. Foraminiferal fauna in detrital limestone are transported and reworked material. Evidence of this process is the presence of broken and abraded foraminiferal shells (e.g. Figures 10(27) and 11(6,24,27)). Because of the reworking and redeposition, Middle Permian (middle Wordian–Capitanian) carbonate strata include older clasts of fusulinids of Early Permian (mainly Asselian) age.

Although many samples from the Sahancanak section include different algal and foraminiferal assemblages, they are not highly diverse. The lowest sample (Sah-1) from the basal part of the section yielded *Tubiphytes* sp. and an undetermined endothyroid specimen (Figure 3; Table 7). The genus *Tubiphytes* is cosmopolitan and known from Moscovian to Cretaceous strata and it is not a good tool for precise age determination. Above the barren sample Sah-2, a transverse section of *Yangchienia* sp. with very typical wall and septa features was encountered in sample Sah-3. The first appearance datum (FAD) of *Yangchienia* in Tethyan sections is in the Roadian and it persists until the end of the Capitanian (e.g. Leven, 2001, 2003; Leven & Bogoslovskaya, 2006; Leven & Gorgij, 2011). The overlying sample (Sah-4) includes similar taxa compared to the underlying one (Table 7).

A relatively rich foraminiferal assemblage (*Hemigordius* ? sp. at Figure 11(27), *Nankinella* sp., *Yangchienia* ? sp. and *Eotuberitina* sp. at Figure 10(27)) has been identified in sample Sah-5 (Table 7). The genus *Nankinella* ranges from Pennsylvanian to Permian, and thus it is not possible to provide a more precise age constraint for this sample.

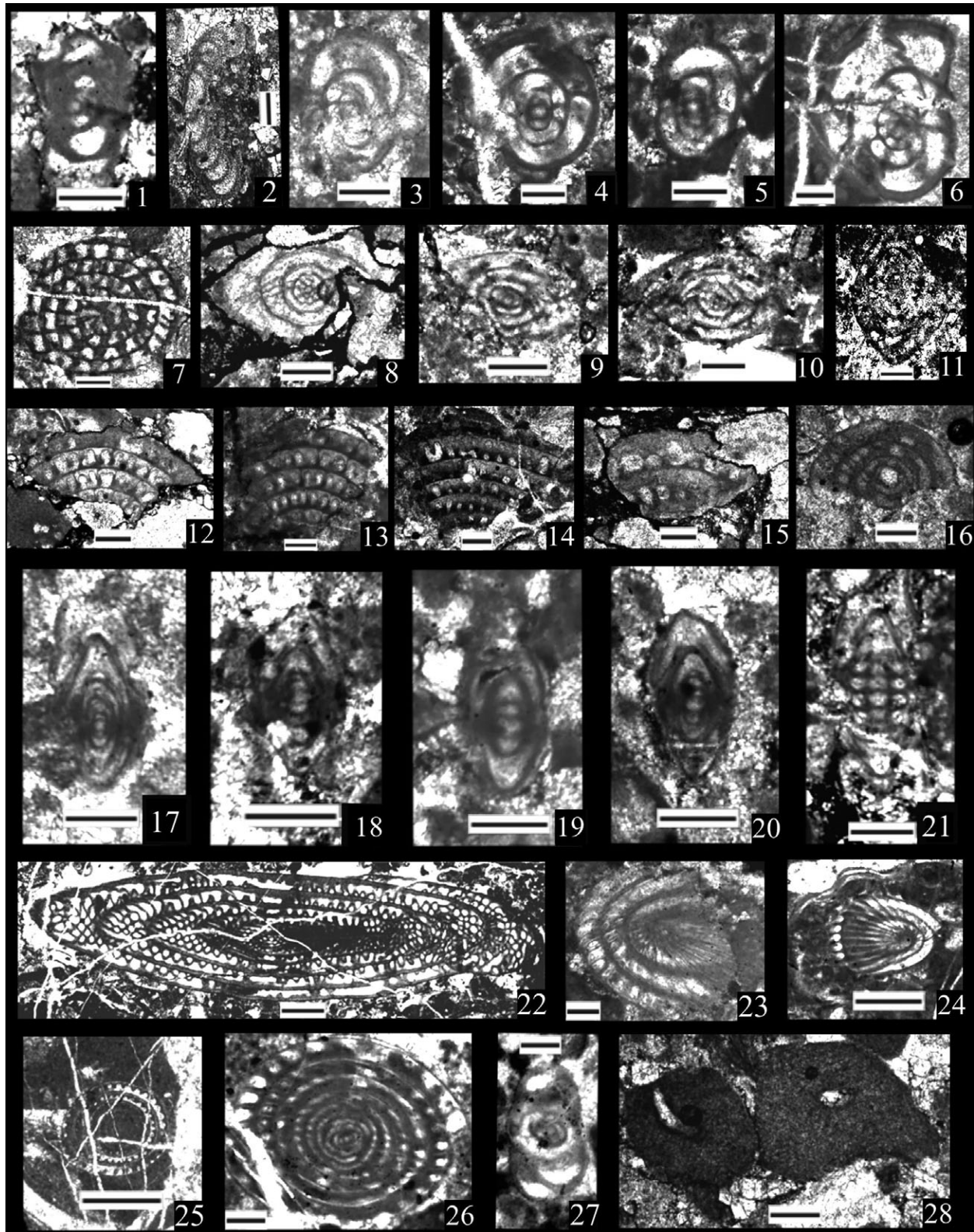


FIGURE 11 Permian benthonic foraminifera and algae from the Mersin Mélange. Scale bar is 200 μm except 22, 24, 25 (1 mm). (1) *Neoendothyra* ex gr. *reicheli* Reitlinger, Kar-SW-30, oblique section. (2) *Tetrataxis* sp., Kar-SW-30, subaxial section. (3–6) *Pseudokahlerina* spp.: (3) Kar-SW-26; (4) Kar-E-11; (5) Kar-E-12, axial sections; (6) Sah-9, equatorial section. (7) *Pseudodoliolina* ? sp., Kar-E-13, subequatorial section. (8–10) *Dunbarula* spp.: (8) Kar-SW-23; (9) Kar-SW-26; (10) Kar-SW-27, axial sections. (11) *Nankinella* sp., Kar-E-36, axial section. (12–15) *Neoschwagerina* spp.: (12) Kar-SW-30, oblique section with *Tubiphytes*; (13) Kar-E-15; (14) Kar-E-31; (15) Kar-E-35, oblique sections. (16) *Profusulinella* ? sp., Kar-E-37, axial section. (17–20) *Reichelina* cf. *minuta* Erk: (17) Kar-E-26; (18) Kar-E-28; (19) Kar-E-28; (20) Kar-E-31, axial sections. (21) *Reichelina* sp., Kar-E-21, subaxial section. (22) *Ruzhenevites subcylindricus* (Bensch), Sah-7, subaxial section. (23–26) *Yangchienia* spp.: (23) Kar-E-15, tangential section; (24) Sah-4, tangential section; (25) Sah-8, subequatorial section; (26) Sah-9, central oblique section. (27) *Hemigordius* ? sp., Sah-5, axial section. (28) *Tubiphytes* sp., Kar-E-11

TABLE 7 Distribution of benthic foraminifera in the Sahancanak section

AGE	Guadalupian											
	Capitanian											
SAMPLES	Sah-1	Sah-2	Sah-3	Sah-4	Sah-5	Sah-6	Sah-7	Sah-8	Sah-9	Sah-10	Sah-11	Sah-12
<i>Tubiphytes</i> sp.	X	?	?	X	?	X	?	X	?	X	?	X
<i>Yangchienia</i> sp.			X	X	?	?	?	X	X	X		
<i>Yangchienia</i> ? sp.				X	X	X	?	X	?	?	X	
<i>Nankinella</i> sp.					X							
<i>Hemigordius</i> ? sp.					X							
<i>Eotuberitina</i> sp.					X	?	X	?	?	X	?	X
<i>Globivalvulina</i> ? sp.						X						
<i>Pachyphloia</i> ? sp.							X					
<i>Ruzhenzevites subcylindricus</i>							X					
<i>Geinitzina</i> sp.							X	?	X	X		
<i>Pseudokahlerina</i> sp.									X			
<i>Neoendothyra permica</i>										X		

X, occurrence; ?, possible occurrence.

Sample Sah-7 includes an assemblage composed of two tentatively identified foraminiferal taxa (*Yangchienia* ? sp. and *Globivalvulina* ? sp.), plus a specimen of *Ruzhenzevites subcylindricus* (Figure 11(22)) of Early Permian (mainly Asselian) age. The *Ruzhenzevites subcylindricus* specimen is very typical with its subcylindrical test, septal fluting and type of coiling (Table 7). This association was determined for the first time by Bensch (1972) in Fergana (Uzbekistan) from the Lower Permian strata and subsequently has been determined in Asselian strata of Iran and other regions (e.g. Leven & Gorgij, 2006, 2011; Leven & Taheri, 2003).

The upper part of the Sahancanak section (samples Sah-8 to Sah-12) yielded mainly Middle to Upper Permian foraminiferal assemblages including *Neoendothyra permica* (Figure 10(40)), *Yangchienia* sp. (Figure 11(25,26)), *Pseudokahlerina* sp. (Figure 11(6)), *Eotuberitina* sp. and *Geinitzina* sp. (Table 7). One age diagnostic taxon from this interval is *Pseudokahlerina* sp. which is a characteristic taxon of the Capitanian (Middle Permian) time interval (Angiolini et al., 2008; Leven & Gorgij, 2011; Leven & Okay, 1996; Turhan, Okuyucu, & Göncüoğlu, 2004). On the other hand, the other taxon, *Neoendothyra permica*, was described from the Upper Permian strata of China, but is known also from Middle to Upper Permian (Capitanian to Changhsingian) strata of Japan (Kobayashi, 1997; Kobayashi, Shiino, & Suzuki, 2009). Based on the evaluation of the foraminiferal assemblage in the Sahancanak section, it can be suggested that the unit is Roadian to Capitanian in age, and in particular, the youngest assemblage is Capitanian in age (Figure 3; Table 7).

4.4 | Benthic foraminifera and algae assemblages from the the Karincali-Southwest section

A total of eight samples (Kar-SW-23 to Kar-SW-30) were collected from this section (Figure 3) for foraminiferal and algal determinations. Similar to those recovered from the Sahancanak section, these assemblages occur in detrital limestones and the foraminiferal specimens are largely abraded or broken (Figures 10(28,32,35,39), and 11(1-3,6,8,9,12)). The lower part of the section (samples Kar-SW-23 to Kar-

SW-27) yielded an assemblage including *Eotuberitina bulla* (Figure 10(22)), *Geinitzina* sp., *Langella* ? sp. (Figure 10(35)), *Neoschwagerina*? sp., *Pseudokahlerina* sp. (Figure 11(3)), *Dunbarula* sp. (Figure 11(8-10)) and *Tubiphytes* sp. (Table 8). Although, the genus *Dunbarula* first appears in upper Roadian-lower Wordian strata in Japan (Kobayashi, 2006a, 2006b) and upper Wordian strata in Iran (Leven & Gorgij, 2011), its age is reported to be as young as Capitanian (e.g. Angiolini et al., 2008; Kobayashi, 2006c; Kobayashi & Altiner, 2011; Leven & Gorgij, 2011). The co-occurrence of *Neoschwagerina*? sp. and *Pseudokahlerina* sp. further indicates that the age of the upper part of this section is Capitanian based on previous studies (e.g. Angiolini et al., 2008; Leven & Gorgij, 2011; Leven & Okay, 1996; Turhan et al., 2004; Figure 3; Table 8).

The uppermost part of this section (Kar-SW-28 to Kar-SW-30) includes *Eotuberitina reitlingerea* (Figure 10(23)), *Geinitzina* sp. (Figure 10(28)), *Pachyphloia* sp. (Figure 10(32)), *Globivalvulina* sp. (Figure 10(39)), *Neoendothyra* ex gr. *reicheli* (Figure 11(1)), *Tetrataxis* sp. (Figure 11(2)), *Neoschwagerina* sp. (Figure 11(12)), and *Tubiphytes* sp. These are mainly long-ranging taxa except for *Neoschwagerina* sp. which is very common in Wordian to Capitanian strata based on previous studies (e.g. Leven, 1981; Leven & Gorgij, 2011; Leven & Okay, 1996; Turhan et al., 2004). *Neoendothyra* ex gr. *reicheli* is reported from Wordian to Changhsingian strata in Turkey, Iran (Elburz, Zagros), Afghanistan and *Transcaucasia* (Gaillot & Vachard, 2007; Ghasemi-Nejad, 2002; Mohtat-Aghai & Vachard, 2005; Turhan et al., 2004; Vaziri, Yao, & Kuwahara, 2005). According to the previous studies (Table 8) the age of this assemblage is Middle Permian (Wordian to Capitanian). Based on foraminiferal determinations, the age of samples in the Karincali-Southwest section is Capitanian (Figure 3; Table 8).

4.5 | Benthic foraminifera, algae and conodont assemblages from the the Karincali-East section

A total of 27 samples (Kar-E-11 to Kar-E-37) were collected along the Karincali-East section for foraminiferal and algal determinations (Figure 3; Table 9). Like both the Sahancanak and the Karincali-

TABLE 8 Distribution of benthic foraminifera in the Karincali-Southwest section

AGE	Guadalupian					
	Capitanian					
SAMPLES	Kar-SW-23	Kar-SW-26	Kar-SW-27	Kar-SW-28	Kar-SW-29	Kar-SW-30
<i>Neoschwagerina</i> ? sp.	X					
<i>Dunbarula</i> sp.	X	X	X			
<i>Geinitzina</i> sp.	X	X	?	?	X	
<i>Tubiphytes</i> sp.	X	?	?	X	?	X
<i>Eotuberitina bulla</i>		X				
<i>Pseudokahlerina</i> sp.		X				
<i>Langella</i> ? sp.		X				
<i>Eotuberitina reitlingerea</i>				X		
<i>Pachyphloia</i> sp.				X		
<i>Globivalvulina</i> sp.				X		
<i>Neoendothyra</i> ex gr. <i>reicheli</i>						X
<i>Tetrataxis</i> sp.						X
<i>Neoschwagerina</i> sp.						X

X, occurrence; ?, possible occurrence.

Southwest sections, the foraminiferal assemblages are largely corroded or broken related to extensive reworking (Figures 10(30,36), and 11(13–16,23)).

A rich benthic foraminiferal and algal association (*Eotuberitina* sp. at Figure 10(26), *Geinitzina* aff. *postcarbonica*, *Geinitzina* sp. at Figure 10(29), *Pachyphloia* sp. at Figure 10(33), *Nodosinelloides* cf. *pinardae* at Figure 10(36), *Nodosinelloides* sp. at Figure 10(37), *Pseudokahlerina* sp. at Figure 11(4,5), *Pseudodoliolina* ? sp. at Figure 11(7), *Neoschwagerina* sp. at Figure 11(13), *Yangchienia* sp. at Figure 11(23) and *Tubiphytes* sp. at Figure 11(28)) has been identified from the central part of the Karincali-East section (Table 9). *Pseudokahlerina* sp., *Pseudodoliolina* ? sp. and *Neoschwagerina* sp. are characteristic taxa of the Middle Permian (Roadian to Capitanian) strata in Tethyan localities, whereas *Pseudokahlerina* sp. is the diagnostic taxon for the Capitanian stage (Angiolini et al., 2008; Leven, 1981, 1993, 2003; Leven & Gorgij, 2011; Leven & Okay, 1996; Turhan et al., 2004). *Geinitzina* aff. *postcarbonica* is one of the long-ranging taxa in the studied material and is known to range throughout the entire Permian (central America by Spandel, 1901; Groves & Boardman, 1999; Iran by Bozorgnia, 1973; southern China by E. Wang, 1982; Japan by Ueno, 1989; Mexico by Vachard et al., 1993; Bolivia by Mamet, 1996). *Nodosinelloides* cf. *pinardae* is another taxon identified from the central part of the section and has a range from latest Gzhelian (latest Carboniferous) to Artinskian (Early Permian) in the Russian Platform (Baryshnikov, Zolotova, & Koscheleva, 1982; Gerke & Sosipatrova, 1975), Serbia (Filipovic, 1995), Japan (Adachi, 1985), America and Canada (Groves & Wahlman, 1997; Pinard & Mamet, 1998). This part of the section also yielded a foraminiferal assemblage containing *Pachyphloia pedicula* (Figure 10(31)), and *Reichelina* cf. *minuta* (Figure 11(17–20)) and *Reichelina* sp. (Figure 11(21)). This association is characteristic and well-known from Middle–Upper Permian (e.g. Erk, 1942; Filimonova, 2010; Gaillot & Vachard, 2007; Kotlyar, Nestell, Zakharov, & Nestell, 1999) strata, and *Reichelina* cf. *minuta* was determined for the first time from the *Parafusulina*–*Polydiexodina* zone (probably the base of the Capitanian) in the Bursa region, western Turkey by Erk (1942).

A rich fusulinid and algal association (*Pachyphloia* cf. *ovata* (Figure 10(30)), *Cryptoseptida* ? sp. (Figure 10(34)), *Palaeotextularia* sp. (Figure 10(38)), *Nankinella* sp. (Figure 11(11)), *Neoschwagerina* sp. (Figure 11(14,15)), *Profusulinella* ? sp. (Figure 11(16)), *Reichelina* cf. *minuta* (Figure 11(20)) and *Tubiphytes* sp.) was obtained from the upper part of detrital limestone of Karincali-East section. Except for the presence of *Profusulinella* ? sp., this association indicates a Middle to Late Permian age. *Profusulinella* ? sp. is represented only by one and a half specimens in the studied material and due to its wall structure, septa and shape of the test, it was only tentatively included in the genus *Profusulinella*, which is characteristic taxon of the lower Bashkirian-lower Moscovian (Middle Carboniferous) strata in southern Urals, Russian Platform, Donbass in Russia and North America (see details in Groves, Kulagine, & Villa, 2007). The recovered assemblage indicates that age of the upper part of the detrital limestone in Karincali-East section is Capitanian and many taxa found in the assemblage are reworked material of Middle Carboniferous and Early Permian age (Figure 3; Table 9).

Two samples (Kar-E-38 and Kar-E-39) collected from close to the uppermost part of the limestone unit of the Karincali-East section contain diverse conodont assemblages (Figure 3). While *Clarkina hongshuiensis* (Figure 10(13–15)) and *Jinogondolella* ? cf. *altudaensis* (Figure 10(16,17)) have been obtained from sample Kar-E-38, sample Kar-E-39 yielded *Clarkina hongshuiensis* (Figure 10(18,19)), *Clarkina postbitteri* (Figure 10(20,21)), Gondolellid indet. and *Sweetognathus* sp. The conodont assemblage from Kar-E-38 indicates a late Guadalupian age when compared to occurrences in Texas (Lambert, Wardlaw, Nestell, & Nestell, 2002) and China (Jin et al., 2006).

This age is in good agreement with the appearance of *Clarkina postbitteri* in the next higher sample Kar-E-39 which is the zonal index of the first conodont zone of the Wuchiapingian GSSP section in China (Jin et al., 2006). Following Jin et al. (2006) the co-occurrence of *C. hongshuiensis* and *C. postbitteri* in the basal Wuchiapingian is unexpected. In the sense of those authors it could only be explained by either reworking or condensation due to a low sedimentation rate.

TABLE 9 Distribution of benthic foraminifera from the central part of the Karincali-East section

AGE	Guadalupian																											
	Capitanian																											
	Kar- E-11	Kar- E-12	Kar- E-13	Kar- E-14	Kar- E-15	Kar- E-16	Kar- E-17	Kar- E-18	Kar- E-19	Kar- E-21	Kar- E-22	Kar- E-23	Kar- E-24	Kar- E-25	Kar- E-26	Kar- E-28	Kar- E-29	Kar- E-30	Kar- E-31	Kar- E-32	Kar- E-33	Kar- E-35	Kar- E-36	Kar- E-37				
<i>Geinitzina</i> aff. <i>postcarbonica</i>	X																											
<i>Pseudokahlerina</i> sp.	X	X																										
<i>Neoschwagerina</i> sp.	X	?	?	?	X	?	?	?	?	?	?	?	?	?	?	?	?	?	?	?	?	?	?	?	?	X		
<i>Eotubertina</i> sp.	X	X	?	?	?	X	X	?	?	?	X	X	?	?	?	X	X	X	?	?	?	?	?	?	?	X		
<i>Tubiphytes</i> sp.	X	?	X	X	X	?	X	?	?	X	?	X	?	?	?	?	?	?	?	?	?	?	?	?	?	X		
<i>Pachyphloia</i> sp.	X																											
<i>Pseudodololima</i> ? sp.										X																		
<i>Nodosinelloides</i> sp.				X	?	?	?	?	?	?	?	?	?	?	?	?	?	?	?	?	?	?	?	?	?			
<i>Nodosinelloides</i> cf. <i>pinardae</i>										X																		
<i>Yangchienia</i> sp.										X																		
<i>Geinitzina</i> sp.					X	?	?	?	?	X	?	?	?	?	?	?	?	X	X									
<i>Reichelina</i> sp.										X																		
<i>Pachyphloia pedicula</i>													X															
<i>Globivalvulina</i> sp.										X	?	?	?	?	?	?	?	?	?	?	?	?	?	?	?	X		
<i>Tubertina</i> sp.													X															
<i>Reichelina</i> cf. <i>pulchra</i>														X	X	X	?	?	?	?	?	?	?	?	?	X		
<i>Reichelina</i> cf. <i>minuta</i>														X	X	X	?	?	?	?	?	?	?	?	?	X		
<i>Eotubertina reitlingera</i>														X	X	?	?	?	?	?	?	?	?	?	?	X		
<i>Pachyphloia</i> cf. <i>ovata</i>																										X		
<i>Palaeotextularia</i> sp.																										X		
<i>Nankinella</i> sp.																										X		
<i>Cryptoseptida</i> ? sp.																										X		
<i>Profusulinella</i> ? sp.																										X		

X, occurrence; ?, possible occurrence.

But conversely it may simply be the result of a longer range of *C. hongshuiensis* as documented by Xia et al. (2005) in the Dachonling section in South China, a record not discussed by Jin et al. (2006).

Collectively taking into consideration the radiolarian ages from the interbedded chert and mudstone to the base of detrital limestone, the benthic foraminiferal and algal ages from detrital limestone and the conodont ages from the top of this limestone, a middle Wordian (middle Guadalupian) to earliest Wuchiapingian (earliest Lopingian) age is assigned to the detrital limestone part of the Permian sequence (Figure 3).

5 | ORGANIC-C δ¹³C VALUES FROM THE UPPER PART OF THE KARINCALI-EAST SECTION

5.1 | Laboratory methods

Although carbon isotope stratigraphy was not an initial objective of this study, a limited number of analyses were conducted when the initial age results indicated that the Karincali-East section encompassed the Guadalupian–Lopingian boundary, an interval from which a negative δ¹³C excursion is widely reported (Bond, Hilton, Wignall, Ali, & Stevens, 2010). As funds were limited, and given that the top of the section is siliceous mudstone and chert, the choice was made to run only δ¹³C_{org}. Samples were powdered and fumigated in an HCl

chamber for a period of three weeks to remove the carbonate phase following the method of Yamamuro and Kayanne (1995). Residues were dried at 50 °C, homogenized, and run for δ¹³C_{org} using a Micro-mass IsoPrime stable isotope ratio mass spectrometer following the method described in Werner, Bruch, and Brand (1999). All stable isotope values are reported in units of ‰ relative to the standard Vienna Pee Dee Belemnite (VPDB), with an uncertainty of 0.1 ‰.

5.2 | Results

The values of the bulk δ¹³C_{org} from the samples retrieved from upper part of the Karincali-East section are depleted, ranging from −22.5 ‰ to −39.8 ‰ (Figure 12; Table S1). Two samples run from the detrital limestone yielded the least depleted values (−22.5 ‰ and −27.4 ‰) and fall within the range of marine organic matter (MOM), with a least depleted terrestrial organic matter (TOM) component. Paleozoic MOM typically ranges between −25 ‰ and −30.5 ‰ (Simoneit et al., 1993), whereas TOM values reported from the Guadalupian range from −20 ‰ to −26 ‰ (Peters-Kottig, Strauss, & Kerp, 2006). A large negative shift of 8.8 ‰ occurs at the top of the limestone, in sample Kar-E-38A, at approximately the Guadalupian–Lopingian boundary (GLB), and highly depleted values persist in the Lopingian above the limestone for the remainder of the section. All Lopingian values are substantially more depleted than the Guadalupian values, and, in fact, exceed the values for typical Paleozoic MOM (above) and Lopingian TOM (−21 ‰ to −31 ‰) as reported in Peters-Kottig et al. (2006).

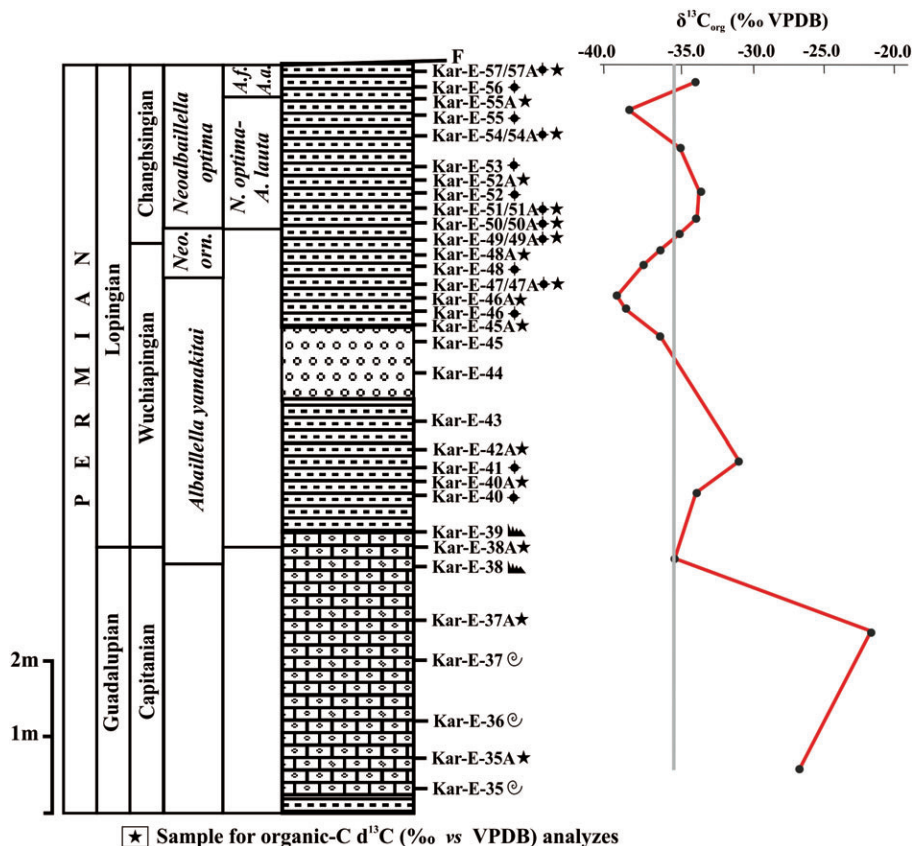


FIGURE 12 Detailed log of the upper part of the Karincali-East section with a plot of δ¹³C_{org} (‰ vs VPDB) values. Mean Lopingian value of 36 ‰ is plotted as gray reference line. *Neo. orn.*, *Neoalibaillella ornithiformis* Zone, *A.f.-A.a.*, *Alibaillella flexa*- *Alibaillella angusta*. For a key to the lithological symbols, see Figure 3

The mean for all 14 Lopingian samples is 36.1 ‰ with a variance of 4.2 (Figure 12; Table S1). Since the negative shift occurs below a lithology change within the limestone, it is unlikely to reflect local facies controls, and an additional source or mechanism is required to explain the large negative excursion at the GLB aside from simply varying TOM and MOM source material.

Previous works on the GLB, largely on $^{13}\text{C}_{\text{carb}}$, interpreted isotopic excursions to be caused by perturbations in the carbon cycle in association with the end-Guadalupian extinction event, with causes ranging from eustatic regression (e.g. W. Wang, Cao, & Wang, 2004), ocean cooling and widespread anoxia (Isozaki, Kawahata, & Minoshima, 2007; Isozaki, Kawahata, & Ota, 2007), to volcanism (Wei, Chen, Yu, & Wang, 2012; Wignall, Kershaw, Collin, & Crasquin-Soleau, 2009) that may have been accompanied by methane gas release (Retallack & Jahren, 2008). Although many sections report a negative excursion, a positive excursion is also reported (Wei, Baima, Qiu, & Dai, 2018). The exact position, duration and magnitude of these excursions vary between localities (Jost et al., 2014; Shen et al., 2013), and in some cases the $^{13}\text{C}_{\text{carb}}$ is best attributed to diagenesis, or post-depositional alteration rather than an indication of a global biotic crisis (Jost et al., 2014; Wei et al., 2018).

Like $^{13}\text{C}_{\text{carb}}$, negative excursions in $\delta^{13}\text{C}_{\text{org}}$ are reported from some marine GLB sections (Kaiho et al., 2005; Nishikane et al., 2014) as well as from terrestrial sections from around the world (Retallack et al., 2006). Highly depleted values (−28 ‰) comparable to some of the Karincali-East section, as well as a modest 1 ‰ negative excursion at the GLB, are reported from the Gujo-hachiman section, Gifu Prefecture, Japan (Nishikane et al., 2014) an oceanic radiolarite. Isotopic values more negative than −31 ‰ occur in a few GLB sections, most notably the nonmarine Permian–Triassic section at Graphite Peak, Australia where values as depleted as −46 ‰ (Krull & Retallack, 2000; Retallack et al., 2006) and were previously explained by the release of methane (Krull, Retallack, Campbell, & Lyon, 2000; Retallack & Jahren, 2008).

Organic matter degradation during burial and early diagenesis provides an additional mechanism for attaining highly depleted $\delta^{13}\text{C}_{\text{org}}$ values. The process of anaerobic degradation by bacteria, a process taking place during deposition and early burial or organic matter, tends to favor the metabolizable carbohydrates and proteins which are isotopically heavier (Tyson, 1995). This selective degradation can deplete the isotopic values by as much as 6 ‰ (Spiker & Hatcher, 1984; Walsh, 1983). Based on the data we have collected, we cannot rule out organic matter (OM) degradation as a contributing factor to the depleted values in the Lopingian, but given that the first depleted value occurs in limestone, below the more organic rich shales, it is not purely a function of OM content and facies, but a result of environmental conditions prevailing in the Lopingian. It is reasonable to conclude that the observed negative shift in Lopingian values is linked to end-Guadalupian negative excursions reported elsewhere, yet at this point, a specific cause cannot be attributed. Either more extensive OM degradation or introduction of depleted carbon from methane release or through anoxia can be contributory factors.

6 | PETROGRAPHY, GEOCHEMISTRY, AND PETROGENESIS OF THE MAFIC VOLCANIC ROCKS FROM THE BASAL PART OF THE KARINCALI-SOUTHWEST SECTION

6.1 | Petrography of the mafic volcanics

Lavas from the basal part of the Karincali-Southwest section petrographically display lamprophyric features, though the presence of low-grade alteration makes it difficult to give a proper name to these mafic igneous rocks. These lavas are characterized by aphanitic and porphyritic textures, with phenocrysts set in a fine-grained groundmass. The groundmass is altered to chlorite, sericite and zeolite. The primary phenocryst phases that survive alteration are mostly clinopyroxene, apatite and to a lesser extent biotite. Clinopyroxene is Ti-rich augite. Apatite generally occurs as needle-like crystals, though hexagonal basal sections are also encountered. Biotite is generally found replacing clinopyroxene and in some cases it is being replaced by green amphibole. In addition to these mineral phases, olivine also occurs, but as pseudomorphs of calcite and chlorite.

6.1.1 | Analytical method and alteration

A total of seven samples were analyzed for major and trace elements in the ACME Labs (Canada) to assess the petrogenesis of the Early Permian (late Asselian–Kungurian) lavas from the basal part of the Karincali-Southwest section (Table S2). The analyses of major elements and Sc were analyzed by fusion inductively coupled plasma–emission spectrometry (ICP–ES), whereas the remaining trace elements were measured by fusion inductively coupled plasma–mass spectrometry ICP–MS, except Ni and Pb on which aqua regia digestion was applied. The precision was better than 5 % for most of the major and trace elements based on replicate sample runs and standards.

All samples display signs of low-grade alteration as revealed by petrography. Although the loss on ignition (LOI) values would be increased due to volatile-rich mineralogy of such rocks, the observed LOI values are too high to entirely result from original mineralogy, and consistent with the alteration. Therefore, mobilization of elements with low ionic potential (e.g. Ba, Rb, and K) is expected to occur under such conditions (e.g. Humphris & Thompson, 1978). The highly depleted K and Rb contents of some samples can indicate leaching of these elements due to post-magmatic effects. The high-field strength elements (HFSE) and rare-earth elements (REE), however, are known to be largely immobile during low-grade alteration (e.g. Staudigel, Plank, White, & Schmincke, 1996), and their abundances can be regarded to reflect the pristine, unaltered geochemistry. We therefore use mainly HFSE and REE to make our petrogenetic interpretations.

6.1.2 | Results

Lava samples from the basal part of the Karincali-Southwest section display highly alkaline characteristics and are chemically classified as nephelinite/basanite on the basis of immobile element systematics (Figure 13). They have low silica contents between 40.3 wt% and 42.7 wt% (all major oxide values have been recalculated to 100 % on a volatile-free basis). Although some silica loss is possible to occur during the alteration, such low contents are consistent with the silica-

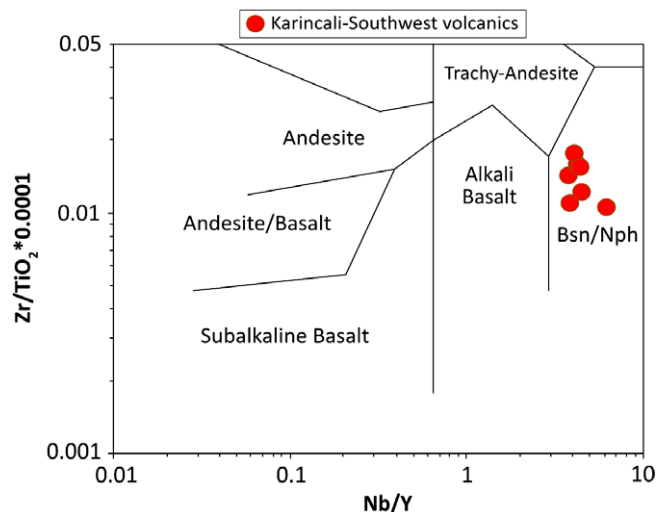


FIGURE 13 Chemical classification of the Permian volcanic rocks from Mersin Mélange (after Winchester & Floyd, 1977). Bsn/Nph, basanite/nephelinite

undersaturated mineralogy of these rocks. MgO shows a relatively wide range between 5.4 wt% and 14.0 wt%, indicating that not all samples are primary and reflect evolved compositions modified by fractional crystallization. The TiO_2 contents of Karincali lavas are noticeably high, with values between 3.5 wt% and 6.2 wt%. Likewise, the P_2O_5 attains very high values between 1.2 wt% and 3.0 wt%, which is consistent with the apatite-rich mineralogy of these lavas.

Samples from the basal part of the Karincali-Southwest section are extremely rich in incompatible trace elements. Th, for example, ranges between 15.6 ppm and 22.6 ppm, exhibiting values up to ~ 200 times that of normal mid-ocean ridge basalt (N-MORB) (Average Th value for N-MORB = 0.12; S. S. Sun & McDonough, 1989). Nb displays values between 124.4 ppm and 272.3 ppm, reaching up to values ~ 117 times that of N-MORB (Average Nb value for N-MORB = 2.33; S. S. Sun & McDonough, 1989). Immobile trace elements exhibit steeply sloping patterns characterized by decreasing enrichment from most incompatible elements towards compatible elements (Figure 14). Some samples are slightly more depleted in Nb, resulting in higher Th/Nb and La/Nb values than the rest of samples. The same samples also show depletion in Zr and Hf. The REE patterns of Karincali lavas are characterized by strong enrichment in LREE over HREE ($[\text{La}/\text{Yb}]_N = 28.2\text{--}48.0$; where subscript N denotes chondrite-normalized) (Figure 14). HREE are also highly fractionated, displaying high $(\text{Dy}/\text{Yb})_N$ values (1.9–2.1).

6.2 | Petrogenesis

The lavas from the Karincali-Southwest section are characterized by extreme enrichment in highly incompatible elements (e.g. Nb) with very low ratios of Zr/Nb. Since both Zr and Nb are immobile during low-grade alteration, the very high values for Nb and Zr/Nb are not an artifact of post-magmatic processes, but appear to be related to the mantle source and magmatic processes (e.g. melting). Nb behaves more incompatibly than Zr in the upper mantle (e.g. Salters, Longhi, & Bizimis, 2002; S. S. Sun & McDonough, 1989). During crust-forming events, this compatibility difference has resulted in mantle domains

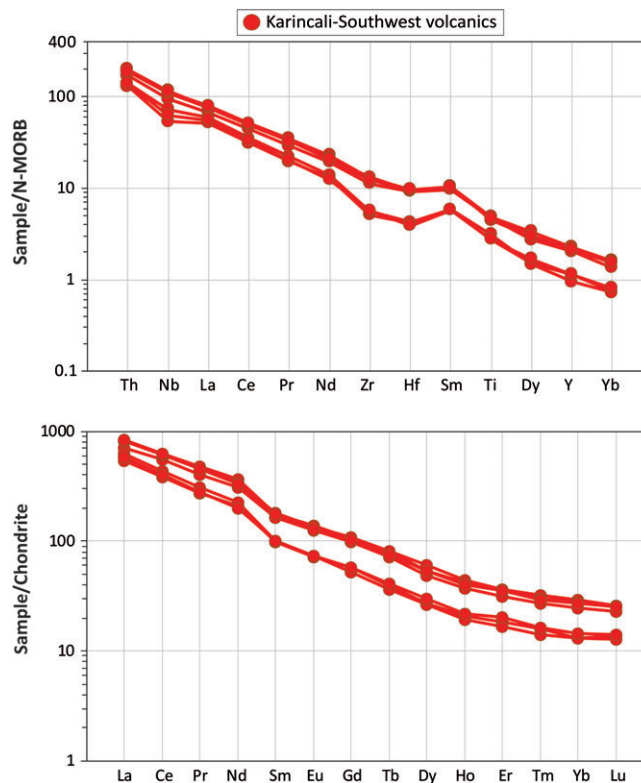


FIGURE 14 Trace element and REE patterns of the Permian volcanic rocks from the Mersin Mélange (N-MORB and chondrite normalization values from S. S. Sun & McDonough, 1989)

that are depleted in Nb relative to Zr. Therefore, while the depleted mantle is characterized by high Zr/Nb (34.2, depleted MORB mantle (DMM); Workman & Hart, 2005), the relatively undepleted or enriched mantle domains would have lower Zr/Nb ratios (e.g. 16.0 for the bulk silicate Earth (BSE); McDonough & Sun, 1995). Based on this, the very low Zr/Nb ratios of Karincali lavas can be explained by a strong contribution from enriched mantle domains. In addition, low degrees of melting can also have been effective in lowering the Zr/Nb ratio observed in these lavas.

The idea above is also supported by Zr/Yb and Nb/Yb ratios. Since lava samples from the basal part of the Karincali-Southwest section are mafic in composition, these ratios (also including Zr/Nb) are not expected to have been significantly altered by the fractional crystallization process. Therefore, such elemental ratios should reflect the nature of mantle source and partial melting. Yb is also an immobile element, but it is more compatible relative to Nb and Zr during upper mantle melting (e.g. S. S. Sun & McDonough, 1989). Therefore, the effect of derivation from a depleted source coupled with moderate/high degrees of melting would tend to create low Zr/Yb and Nb/Yb ratios like that of N-MORBs (which are assumed to be derived from a DMM-type source; N-MORB Zr/Yb = 24.3, Nb/Yb = 0.76; S. S. Sun & McDonough, 1989). In contrast, contribution from enriched sources and/or low degrees of partial melting would lead to high values of Zr/Yb and Nb/Yb. The ratios observed in the Karincali samples are consistent with the latter case, in which the studied lavas display actually very high Zr/Yb and Nb/Yb ratios (168.9–205.8 and 53.4–77.0, respectively). This suggests, therefore, that the enriched sources, possibly coupled with low degrees of melting, made a significant

contribution to the petrogenesis of the lava samples from the basal part of the Karincali-Southwest section.

The Th–Nb–La systematics of the lava samples from the basal part of the Karincali–Southwest section indicates no relative significant enrichment of Th and La over Nb. Since these elements all behave incompatibly during the upper mantle melting, the relative depletion of Nb relative to Th and La can be linked to the processes operating on a subducted slab (e.g. McCulloch & Gamble, 1991). During dehydration and melting of the oceanic crust, Th and La display incompatible behavior (e.g. Pearce & Peate, 1995). In contrast, Nb is commonly believed to be retained in the slab by residual Ti phases (like rutile) (e.g. Ayers & Watson, 1993). The net result is that Th and La are transferred to the mantle wedge largely via sediment melt, whereas Nb is left behind (on the slab), therefore making no contribution to the elemental budget of the mantle wedge. Since the Karincali lavas do not display apparent negative anomalies in Nb (Figure 14), a major role for the slab-derived fluids/melts can be excluded for the petrogenesis of the Karincali lavas.

This idea is strengthened further by the distribution of Karincali samples on Nb/Yb–Th/Yb plot (Pearce & Peate, 1995). In this plot (Figure 15), Nb and Yb are subduction-immobile elements, whereas Th is subduction-mobile. Magmas generated in non-subduction settings (like MORBs) define a linear trend that is governed by the source depletion/enrichment and partial melting. In subduction-related settings, however, Th becomes decoupled from Nb and Yb due slab-induced processes, which causes magma compositions displaced from the MORB array. The fact that the samples plot on the MORB array, thus suggest that the source region of these lavas has not been modified by a subduction component.

The extrusives from the basal part of the Karincali–Southwest section display extreme enrichment in the most incompatible element fractionation of LREE–HREE as mentioned before. The significant enrichment of the highly incompatible elements (e.g. Th, Nb, and

LREE) can be attributed to low-degrees of partial melting. It must be noted, however, that the enrichment levels are so high that it would be difficult to derive such elemental compositions only via low-degree melting (e.g. Le Roex, Bell, & Davis, 2003). A possible cause for this anomalous enrichment can be a metasomatized source region modified by fluids and/or low-degree partial melts (e.g. McKenzie & O'Nions, 1995). The depletion in HREE relative to LREE and fractionated HREE patterns (high Dy/Yb), on the other hand, suggests the role of residual garnet, since garnet can effectively retain HREE elements (e.g. Johnson, 1998; McKenzie & O'Nions, 1991). The residual garnet was possibly involved either in the mantle source or the source region itself was already fractionated in terms of LREE/HREE due to metasomatism by small degree garnet-facies melts.

6.3 | Tectonomagmatic constraints

The trace element systematics of these lavas indicate extreme incompatible element enrichment and suggests no role for involvement of subduction-related metasomatism. The magmas generated at mid-ocean ridges are commonly of depleted nature (N-MORBs), though enriched magma compositions also exist (E-MORB) (e.g. Hoernle et al., 2011; Niu & Batiza, 1997; Zindler, Staudigel, & Batiza, 1984). Even when the extreme end of E-MORBs is considered, the enrichment levels observed in the lavas from Karincali–Southwest section remains considerably higher (Figure 15), thus eliminating the possibility of generation of these lavas in a mid-ocean ridge setting. The enrichment levels shown by the Karincali samples are even more enriched than oceanic island basalts (OIBs) (Figure 15), which exclude an ocean island origin for the genesis of these extrusives. Furthermore, since Th–Nb–La and Th–Nb–Yb systematics indicates no (or insignificant) involvement of the subduction component, the generation of Karincali lavas at a subduction zone (either continental or oceanic) does not seem likely.

The unusual enrichment level with no subduction input eliminates mid-ocean ridge, oceanic island and subduction zone tectonic settings. The best alternative for generation of magmas consistent with such trace element systematics, therefore, appears to be a continental within-plate setting. In these tectonic environments, the mantle part of the continental lithosphere (i.e. subcontinental lithospheric mantle (SCLM)) is an ideal place to create such enriched signatures. The SCLM can be fluxed and metasomatized by the fluids and/or melts derived from asthenospheric mantle, including MORB source mantle, mantle plumes and subducted slabs (e.g. Gibson et al., 1993; McKenzie & O'Nions, 1995). The SCLM has been commonly suggested as a source component involved in the petrogenesis of highly alkaline, potassic/ultrapotassic magmas (e.g. kimberlites, lamproites, melilitites) (e.g. Carlson, Esperanca, & Svisero, 1996; Janney et al., 2002; Le Roex et al., 2003; Figure 15). Although SCLM contributes to the genesis of these magmas, the role of other components, including asthenospheric MORB mantle, mantle plumes and subducted slabs also deserves some discussion.

Since SCLM can store the metasomatic inputs (for several million years), the enrichment events do not necessarily occur during the period of magmatism or recent melting events; they can be inherited from an ancient melt extraction (from underlying asthenospheric

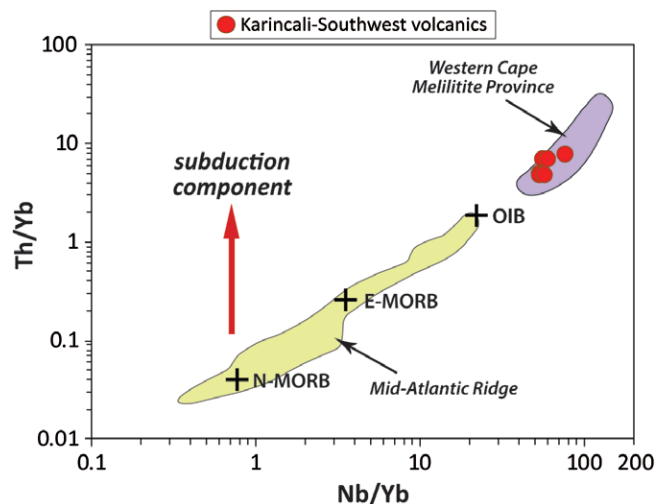


FIGURE 15 Nb/Yb–Th/Yb plot of the Permian volcanic rocks from the Mersin Mélange (after Pearce & Peate, 1995). N-MORB, E-MORB, and OIB compositions from S. S. Sun and McDonough (1989). Mid-Atlantic Ridge 33°–35° data from Niu, Bideau, Hékinian, and Batiza (2001), Western Cape Melilitite Province data from Janney, Le Roex, Carlson, and Viljoen (2002)

mantle) or subduction events. Since the lavas from the Karincali-Southwest section do not display a significant trace of subduction component, this suggests either that these lavas have not been generated in a subduction zone (as explained above) or that the metasomatizing agents are not slab-derived fluids/melts. Therefore, this places the origin of metasomatic materials in the asthenospheric mantle (MORB source mantle or a mantle plume) in the Karincali case. The melting of metasomatized SCLM can be triggered by heat derived from the asthenospheric mantle or melts. In the case of a mantle plume, it can act solely as a heat source or can actively be involved by introducing its melts.

7 | DISCUSSION

One of the debated issues in recent years regarding the evolution of the IAE Ocean was about its opening. The greatest complexity perhaps came from the assumption that this branch of Neotethys is a Mesozoic ocean that opened following the destruction of the Palaeotethys. In this context, the rifting of northern Gondwana occurred during the Lower Jurassic (Sengör & Yilmaz, 1981). Thus, the idea of Lower Jurassic rifting highly restricted the life spans of the Palaeotethys and IAE Oceans. Such separation required the pre-Lower Jurassic remnants to be regarded as 'Palaeotethyan', and Lower Jurassic or younger Mesozoic remnants to be 'Neotethyan'. The Triassic remnants along the IAE Suture Belt, thus, were excluded from the definition of Neotethys. Instead, such fragments were considered to be tectonically intercalated Palaeotethyan pieces. The discovery of Triassic chert located away from the IAE Suture Belt (Bornova Flysch Zone, western Turkey; Tekin & Göncüoğlu, 2007), however, indicates that the age of northern Neotethyan relicts can be indeed pre-Lower Jurassic.

The Carnian finding mentioned above was the oldest age from the northern realm until that time. This is not the only Triassic finding away from the IAE Suture Belt, strengthening the idea that Triassic sequences are not uncommon within the northern branch of Neotethys. One such sequence was the Carnian (Upper Triassic) pelagic limestone from the Lycian Nappes (Southwest Turkey; Tekin & Göncüoğlu, 2002). Another and the most recent one, which includes Anisian chert, came from the Mersin Mélange (southern Turkey; Tekin, Bedi, Okuyucu, Göncüoğlu, & Sayit, 2016). Although both localities are situated in southern Turkey, they are shown to be of northerly origin (Collins & Robertson, 1999; Parlak & Robertson, 2004; Tekin, Bedi, Okuyucu, Göncüoğlu, & Sayit, 2016). The finding from the Mersin Mélange was a significant one, since the Anisian age extracted from the pelagic sediments became the oldest age acquired from the IAE Ocean until now.

The paleontological evidence alone bears some important implications and can suggest either the existence of the IAE Ocean already in the Middle Triassic or the existence of a deep basin that was yet to evolve to become the IAE Ocean. Geochemical data, where they are associated with precise ages (paleontological or radiometric), can additionally help to provide geodynamic constraints with respect to tectonic setting and time. E-MORB and OIB-type signatures were found in the ophiolitic mélanges along the IAE Suture Belt. OIB-type

signatures were interpreted by Rojay, Yaliniz, and Altiner (2001) and Rojay et al. (2004) as seamounts formed on the IAE oceanic crust. These authors, on the basis of this finding, defended the idea of Lower Jurassic rifting. However, E-MORB type basalts associated with Carnian chert from the Sakarya region along the IAE Suture Belt indicated the existence of a deep basin already by the Late Triassic, suggesting that the rifting occurred well before the Lower Jurassic (Göncüoğlu et al., 2003). There are also subduction-related lithologies encountered within the northern realm. The plagiogranite dykes from the Ankara Ophiolitic Mélange yielded supra-subduction zone (SSZ) type signatures with U–Pb ages of 179 Ma (Dilek & Thy, 2006). Another Early Jurassic age with SSZ-type characteristics was found in the Refahiye region (Topuz et al., 2013). These findings suggest the existence of a mature ocean in that time period. Subduction-related characteristics were also found in the Triassic, which make the picture even more interesting. In the Lycian Nappes, arc-type basalts were found associated with Carnian chert (Sayit et al., 2015), while oceanic back-arc basin characteristics were found in the basalts associated with Anisian chert (Sayit et al., 2017). Therefore, such data indicate the existence of a mature IAE ocean even during the Middle Triassic.

Recent findings (in terms of both paleontology and geochemistry) appear to have added new perspectives on the evolution of the IAE Ocean. The discovery of Anisian lavas from the Mersin Mélange immediately brings the question whether oceanic sequences older than the Anisian do exist within the northern domain. As mentioned above the Mersin Mélange contains the fragments transported from the IAE Ocean (Beyşehir–Hoyran nappes sensu Brunn et al., 1970, 1971) according to Tekin et al. (Tekin, Bedi, Okuyucu, Göncüoğlu, & Sayit, 2016; Tekin, Bedi, Okuyucu, Göncüoğlu, Sayit et al., 2016). Therefore, if Anisian lavas indeed represent an oceanic back-arc basin as suggested by Sayit et al. (2017), then some older (pre-Anisian) continental/oceanic fragments should exist within the Mersin Mélange or any other part that preserves the remnants of the IAE Ocean.

8 | CONCLUSIONS

Some important results from this study are as follows:

1. The basal part of the sequence, represented by alternations of basic volcanics, limestone, chert, and mudstone, ranges from late Asselian (early Cisuralian) to Wordian (middle Guadalupian) age based on a sequence of five radiolarian assemblages tied into existing global biostratigraphic schemes (Figure 3). These assemblages provide critical age control for interpreting the provenance and tectonic significance of this sequence.
2. Two levels of basic volcanics have been encountered and their age has been assigned to the late Asselian and Kungurian (Early Permian), respectively. The age obtained from these lavas makes them the first discovery of Early Permian magmatism from this domain. Such an age also suggests that the IAE domain followed a similar evolutionary path as the southern Neotethys, because the rifting event that ended up with the formation of the latter domain is believed to have occurred during the Late Permian (Lapierre et al., 2004).

3. The geology and geochemistry of the Early Permian lavas suggest that they formed in a continental within-plate setting undergoing extension, i.e. a continental rift setting. The association of basalts with pelagic radiolarian-rich sediments suggests that the basin was deep, though the underlying continental lithosphere was still thick as displayed by the ultra-alkaline, lamprophyric nature of the lavas.
4. The existence of a continental rift setting during the Early Permian is also important in terms of the rupturing of the northern Gondwanan margin at this time period. Considering the fact that the Early Permian (296–270 Ma) volcano-sedimentary sequence represents a deep basin environment, the formation of proto IAE oceanic crust would probably have occurred before the end of Permian. This, in turn, implies that the IAE Ocean can no longer be considered as an ocean that began forming in the Mesozoic, since its appearance extends back to the Permian. The existence of an oceanic back-arc basin during the Anisian (Sayit et al., 2017) also supports mature Neotethyan oceanic crust of pre-Anisian age.
5. Trace element systematics of the Early Permian lavas suggests involvement of an asthenospheric mantle source, which was either a MORB mantle source or a mantle plume. The latter alternative is more likely, considering that the supercontinent Pangea was underlain by large low-velocity regions during the Permian, which is considered to be source of mantle plumes (Burke & Torsvik, 2004).
6. The central part of the sequence is well-characterized by detrital limestone with some chert bands and neptunian dykes. The age of this part of the sequence ranges from middle Wordian through earliest Wuchiapingian based on radiolarian, foraminiferal, and conodont biostratigraphy. Foraminiferal assemblages in the detrital limestone were mainly transported or reworked from Lower Permian (mainly Asselian) strata. It appears that these limestones may have accumulated during the breaking up of unstable platform that formed in the Early to Middle Permian, possibly as old as Late Carboniferous, and material from the rim of the basin was transported to a newly originated rift system.
7. The uppermost part of the sequence is composed of detrital limestone at the base, progressing to alternating chert and mudstone intercalated with microbreccia beds. Its age is assigned to early Wuchiapingian-middle Changhsingian (Late Permian) based on radiolarian and conodont biostratigraphy.
8. A large negative shift in $\delta^{13}\text{C}_{\text{org}}$ of 8.8 ‰ occurs in the highest limestone beds at the base of the Lopingian in the upper part of the Karincali-Southwest section, and is correlated to negative shifts reported in other sections at the Guadalupian–Lopingian boundary in association with the end-Guadalupian mass extinction event. The Lopingian values of $\delta^{13}\text{C}_{\text{org}}$ are highly depleted (mean -36.1 ‰) and cannot be explained through common marine processes of changes in OM source nor increased productivity. The introduction of highly negative methanogenic OM through methane gas release, or anoxic microbial processes can in part explain these values, as can increased degradation of nonrefractory OM in the Lopingian. The microbreccia occurrence in the chert and mudstone sequence of the Karincali-Southwest

section could be related to sudden subsidence of the basin or due to rapid transgression during the Lopingian.

ACKNOWLEDGEMENTS

We are grateful to TUBITAK (Project No: 112Y370) for providing financial support to this research. The authors wish to thank Batuhan Esen for his kind contributions to the preparation of text. Nikita Bragin and Taniel Danelian are thanked for their constructive comments on the manuscript and Keisuke Ishida for the editorial handling.

ORCID

Kaan Sayit  <https://orcid.org/0000-0001-6859-4536>

REFERENCES

- Adachi, S. (1985). Smaller foraminifers of the Ichinotani Formation (Carboniferous-Permian), Hida Massif, central Japan. *Science Reports of the Institute of Geoscience, University of Tsukuba, Section B, Geological Sciences*, 6, 59–139.
- Aitchison, J. C., Suzuki, N., Caridroit, M., Danelian, T., & Noble, P. (2017). Paleozoic radiolarian biostratigraphy. In T. Danelian, M. Caridroit, P. Noble, & J. C. Aitchison (Eds.), *Catalogue of Paleozoic radiolarian genera Geodiversitas* (Vol. 39, pp. 503–531). Paris: Scientific Publications of the Muséum national d'Histoire naturelle.
- Alan, I., Sahin, S., Keskin, H., Altun, I., Bakirhan, B., Balci, V., ..., Celik, Ö. F. (2007). *Geodynamic evolution of central Tauride-Eregli (Konya)-Ulukisla (Nigde)-Karsanti (Adana)-Namrun (Icel) region* (Report No: 245). Ankara: General Directorate of Mineral Research and Exploration, Department of Geological Investigation (in Turkish).
- Andrew, T., & Robertson, A. H. F. (2002). The Beyşehir-Hoyran-Hadim Nappes: Genesis and emplacement of Mesozoic marginal and oceanic units of the northern Neotethys in southern Turkey. *Journal of the Geological Society*, 159, 529–543.
- Angiolini, L., Chaouachi, C., Soussi, M., Andrina, V., Davydov, V. I., Henderson, C. M., ... Carabelli, L. (2008). New fossil findings and disconcordy of conodonts in the Guadalupian of Jebel Tebaga de Medenine: Biostratigraphic implications. *Permophiles*, 51, 10–22.
- Ayers, J. C., & Watson, B. (1993). Rutile solubility and mobility in supercritical aqueous fluids. *Contributions to Mineralogy and Petrology*, 114, 321–330.
- Baryshnikov, V. V., Zolotova, V. P., & Koscheleva, V. F. (1982). New species of foraminifers from the Artinskian Stage of the Perm pre-Urals. *Akademiya Nauk SSSR, Ural'skii Nauchnyi Tsentri, Institut Geologii i Geokhimii, Sverdlovsk*, 3–54 (in Russian).
- Bensh, F. R. (1972). *Upper Paleozoic stratigraphy and Fusulinids of southern Fergana*. Izdatelstvo FAN, Akademiya Nauk Uzbekistan SSR (in Russian).
- Blome, C. D., & Reed, K. M. (1992). Permian and Early (?) Triassic radiolarian faunas from the Grindstone terrane, Central Oregon. *Journal of Paleontology*, 66, 351–383.
- Bond, D. P. G., Hilton, J., Wignall, P. B., Ali, J. R., & Stevens, L. G. (2010). The Middle Permian (Capitanian) mass extinction on land and in the oceans. *Earth Science Reviews*, 102, 100–116.
- Bozorgnia, F. (1973). *Paleozoic foraminiferal biostratigraphy of central and east Albroz Mountains, Iran Geological Laboratories, Publication* (Vol. 4). Tehran: National Iranian Oil Company.
- Bragin, N. Y., & Tekin, U. K. (1996). Age of radiolarian-chert blocks from the Senonian Ophiolitic Melange (Ankara, Turkey). *Island Arc*, 5, 114–122.
- Brunn, J. H., De Graciansky, P. C., Gutnic, M., Juteau, T., Lefèvre, R., Marcoux, J., ... Poisson, A. (1970). Structures majeures et corrélations stratigraphiques dans les Taurides occidentales. *Bulletin de la Société Géologique de France*, 12, 515–556.
- Brunn, J. H., Dumont, J. F., Graciansky, P. C., Gutnic, M., Juteau, T., Marcoux, J., ... Poisson, A. (1971). Outline of the geology of the

- western Taurids. In A. S. Campbell (Ed.), *Geology and history of Turkey* (pp. 225–255). Tripoli: Petroleum Exploration Society of Libya.
- Burke, K., & Torsvik, T. H. (2004). Derivation of large igneous provinces of the past 200 million years from long-term heterogeneities in the deep mantle. *Earth and Planetary Science Letters*, 227, 531–538.
- Carlson, R. W., Esperanca, S., & Svisero, D. P. (1996). Chemical and Os isotopic study of Cretaceous potassic rocks from Southern Brazil. *Contributions to Mineralogy and Petrology*, 125, 393–405.
- Collins, A. S., & Robertson, A. H. F. (1999). Evolution of the Lycian allochthon, western Turkey, as a north-facing late Palaeozoic to Mesozoic rift and passive continental margin. *Geological Journal*, 34, 107–138.
- Cordey, F. (1998). Radiolaires des complexes d'accrétion de la Cordillère Canadienne (Colombie-Britannique). *Commission Géologique du Canada Bulletin*, 509, 1–209.
- De Wever, P., Dumitrica, P., Caulet, J. P., Nigrini, C., & Caridroit, M. (2001). *Radiolarians in the sedimentary record*. London, England: Gordon and Breach Science Publishing.
- Dilek, Y., & Thy, P. (2006). Age and petrogenesis of plagiogranite intrusions in the Ankara mélange, central Turkey. *Island Arc*, 15, 44–57.
- Dumitrica, P. (1970). Cryptocephalic and Cryptothoracic Nasselleria in some Mesozoic deposits of Romania. *Revue Roumaine de Géologie, Géophysique et Géographie (Série Géologie)*, 14, 45–124.
- Erk, A. S. (1942). Sur la présence du genre *Codonofusiella* Dunbar et Skinner dans le Permien de Bursa (Turquie). *Eclogae Geologicae Helvetiae*, 34(dated 1941), 243–253.
- Feng, Q. (1992). Permian and Triassic radiolarian biostratigraphy in south and southwest China. *Earth Science, Journal of China University of Geoscience*, 3, 51–62.
- Feng, Q., & Liu, B. (1993). Permian radiolarians on southwestern Yunnan. *Earth Science, Journal of China University of Geoscience*, 18, 553–563.
- Feng, Q., Meng, Y., He, W., & Gu, S. (2006). Taxonomy of Order Latentifusularia (Radiolaria) from the Latest Permian in southern Guangxi, China. *Journal of Paleontology*, 80, 826–848.
- Filimonova, T. V. (2010). Smaller foraminifers of the Lower Permian from western Tethys. *Stratigraphy and Geological Correlation*, 18, 687–811.
- Filipovic, I. (1995). The Carboniferous of northwestern Serbia. *Rasprave Geološkog Zavoda Gemini, Belgrade, Tome*, XXV, 1–104. (in Serbian and English).
- Forel, M. B., Tekin, U. K., Okuyucu, C., Bedi, Y., Tuncer, A., & Crasquin, S. (in press). Discovery of a long-term refuge for ostracods (Crustacea) after the end-Permian extinction: A unique Carnian (Late Triassic) fauna from the Mersin Mélange, southern Turkey. *Journal of Systematic Palaeontology*. <https://doi.org/10.1080/14772019.2017.1391342>
- Gaillot, J., & Vachard, D. (2007). The Khuff Formation (Middle East) and time-equivalents in Turkey and South China: Biostratigraphy from Capitanian to Changhsingian times (Permian), new foraminiferal taxa, and palaeogeographical implications. *Coloquios de Paleontologia*, 57, 37–223.
- Gerke, A. A., & Sosipatrova, A. G. P. (1975). Stratigraphic significance of Late Paleozoic foraminifers in the northeastern USSR. In V. I. Ustritskii (Ed.), *Upper Paleozoic of the northeastern USSR* (pp. 26–41). Leningrad, Russia: Nauchno-Issledovatel'skii Institut Geologii Arktiki, Ministerstva Geologii SSSR, Sbornik Statei (in Russian).
- Ghasemi-Nejad, E. (2002). Biostratigraphy and depositional history of the Paleozoic deposits in the south of Central Alborz Basin, based on foraminifera. *Iranian International Journal of Science*, 3, 93–114.
- Gibson, S. A., Thompson, R. N., Leat, P. T., Morrison, M. A., Hendry, G. L., Dickinson, A. P., & Mitchell, J. G. (1993). Ultrapotassic Magmas along the flanks of the Oligo-Miocene Rio Grande Rift, USA: Monitors of the zone of lithospheric mantle extension and thinning beneath a continental rift. *Journal of Petrology*, 34, 187–228.
- Göncüoğlu, M. C., Dirik, K., & Kozlu, H. (1997). General characteristics of pre-Alpine and Alpine Terranes in Turkey: Explanatory notes to the terrane map of Turkey. *Annales Geologique de Pays Hellenique*, 37, 515–536.
- Göncüoğlu, M. C., Sayit, K., & Tekin, U. K. (2010). Oceanization of the northern neotethys: Geochemical evidence from ophiolitic mélange basalts within the Izmir-Ankara suture belt, NW Turkey. *Lithos*, 116, 175–187.
- Göncüoğlu, M. C., Tekin, U. K., & Turhan, N. (2001). Late Carnian radiolarite-bearing basalt blocks within the Late Cretaceous Central Sakarya Ophiolitic Melange, Ankara, NW Anatolia: Geological constraints. In *Jeo 2000 Proceedings*, pp. 54–61.
- Göncüoğlu, M. C., Turhan, N., Sentürk, K., Özcan, A., Uysal, S., & Yaliniz, M. K. (2000). A geotraverse across NW Turkey: Tectonic units of the Central Sakarya region and their tectonic evolution. In E. Bozkurt, J. A. Winchester, & J. D. A. Piper (Eds.), *Tectonics and magmatism in Turkey and the surrounding area Geological Society, Special Publications* (Vol. 173, pp. 139–161). London, England: Geological Society.
- Göncüoğlu, M. C., Turhan, N., & Tekin, U. K. (2003). Evidence for the Triassic rifting and opening of the Neotethyan Izmir-Ankara ocean and discussion on the presence of Cimmerian events at the northern edge of the Tauride-Anatolide platform, Turkey. *Bollettino della Societa Geologica Italiana, Special Volume*, 2, 203–212.
- Görür, N., Sengör, A. M. C., Akkök, R., & Yılmaz, Y. (1983). Sedimentological evidence for the opening of the northern branch of Neo-Tethys in the Pontides. *Bulletin of the Geological Society of Turkey*, 26, 11–20 (in Turkish with English abstract).
- Gradstein, F. M., Ogg, J. G., Schmitz, M. D., & Ogg, G. M. (Eds.). (2012). *The geological time scale 2012*. Amsterdam, The Netherlands: Elsevier, 2 vols.
- Groves, J. R., & Boardman, D. R. (1999). Calcareous smaller foraminifers from the Lower Permian Council Grove Group near Hooser, Kansas. *Journal of Foraminiferal Research*, 29, 243–262.
- Groves, J. R., Kulagine, E. I., & Villa, E. (2007). Diachronous appearances of the fusulinid *Profusulinella* in Eurasia and North America. *Journal of Paleontology*, 81, 227–237.
- Groves, J. R., & Wahlman, G. P. (1997). Biostratigraphy and evolution of late Carboniferous and early Permian smaller foraminifers from the Barents Sea (offshore Arctic Norway). *Journal of Paleontology*, 71, 758–779.
- Hoernle, K., Hauff, F., Kokfelt, T. F., Haase, K., Garbe-Schönberg, D., & Werner, R. (2011). On and off-axis chemical heterogeneities along the South Atlantic Mid-Ocean-Ridge (5–11° S): Shallow or deep recycling of ocean crust and/or intraplate volcanism? *Earth and Planetary Science Letters*, 306, 86–97.
- Humphris, S. E., & Thompson, G. (1978). Trace element mobility during hydrothermal alteration of oceanic basalts. *Geochimica et Cosmochimica Acta*, 42, 127–136.
- Ishiga, H. (1986). Late Carboniferous and Permian radiolarian biostratigraphy of Southwest Japan. *Journal of Geosciences, Osaka City University*, 29, 89–100.
- Ishiga, H. (1990). Paleozoic radiolarians. In K. Ichikawa, S. Mizutani, I. Hara, S. Hada, & A. Yao (Eds.), *Pre-cretaceous terranes of Japon* (pp. 285–295). Osaka, Japan: Nippon Insatsu, Shuppan.
- Ishiga, H., & Imoto, N. (1980). Some Permian radiolarian in the Tamba District, southwest Japan. *Earth Science (Chikyu Kagaku)*, 34, 333–345.
- Ishiga, H., Kito, T., & Imoto, N. (1982). Permian radiolarian biostratigraphy. *News of Osaka Micropaleontologists, Special Volume*, 5, 17–26.
- Isozaki, Y., Kawahata, H., & Minoshima, K. (2007). The Capitanian (Permian) Kamura Cooling Event: The beginning of the Paleozoic–Mesozoic transition. *Palaeoworld*, 16, 16–30.
- Isozaki, Y., Kawahata, H., & Ota, A. (2007). A unique carbon isotope record across the Guadalupian-Lopingian (Middle-Upper Permian) boundary in mid-oceanic paleoatoll carbonates: The high-productivity “Kamura Event” and its collapse in Panthalassa. *Global and Planetary Change*, 55, 21–38.
- Ito, T., Feng, Q., & Matsuoka, A. (2013). Radiolarian faunal change in the Middle Permian Gufeng Formation in the Lihuang section, Chaohu, South China. *Science Reports of Niigata University (Geology)*, 28, 39–49.
- Ito, T., Feng, Q., & Matsuoka, A. (2015). Taxonomic significance of short forms of middle Permian *Pseudoalbaillella* Holdsworth and Jones, 1980 (Follicucullidae, Radiolaria). *Revue de Micropaleontologie*, 58, 3–12.
- Ito, T., & Matsuoka, A. (2015). Imbricate structure of the Permian Yoshii Group in the Otakeyama area, Okayama Prefecture, southwest Japan. *Frontiers of Earth Science*, 9, 152–163.
- Janney, P. E., Le Roex, A. P., Carlson, R. W., & Viljoen, K. S. (2002). A chemical and multi-isotope study of the Western Cape Olivine Melilitite Province, South Africa: Implications for the sources of Kimberlites and the origin of the HIMU signature in Africa. *Journal of Petrology*, 43, 2339–2370.

- Jasin, B., & Harun, Z. (2011). Radiolarian biostratigraphy of Peninsular Malaysia-An update. *Bulletin of the Geological Society of Malaysia*, 57, 27–38.
- Jasin, B., Harun, Z., Said, U., & Saad, S. (2005). Permian radiolarian biostratigraphy of the Semanggol Formation, south Kedah, Peninsular Malaysia. *Bulletin of the Geological Society of Malaysia*, 51, 19–30.
- Jasin, B., Said, U., & Rahman, R. A. (1995). Late Middle Permian Radiolaria from the Jengka area, central Pahang, Malaysia. *Journal of Southeast Asian Earth Sciences*, 12, 79–83.
- Jin, Y. G., Shang, Q. H., & Wang, X. D. (2003). Permian biostratigraphy of China. In P. J. Chen, A. R. Palmer, & W. T. Zhang (Eds.), *Biostratigraphy of China* (pp. 331–378). Amsterdam: Elsevier.
- Jin, Y. G., Shen, S. Z., Henderson, C. M., Wang, X. D., Wang, W., Wang, Y., ... Shang, Q. H. (2006). The Global Stratotype Section and Point (GSSP) for the boundary between the Capitanian and Wuchiapingian stage (Permian). *Episodes*, 29, 253–262.
- Johnson, K. T. M. (1998). Experimental determination of partition coefficients for rare earth and high-field-strength elements between clinopyroxene, garnet, and basaltic melt at high pressures. *Contributions to Mineralogy and Petrology*, 133, 60–68.
- Jost, A. B., Mundil, R., He, B., Brown, S. T., Altiner, D., Sun, Y., ... Payne, J. L. (2014). Constraining the cause of the end-Guadalupian extinction with coupled records of carbon and calcium isotopes. *Earth and Planetary Science Letters*, 396, 201–212.
- Kaiho, K., Chen, Z.-Q., Ohashi, T., Arinobu, T., Sawada, K., & Cramer, S. C. (2005). A negative carbon isotope anomaly associated with the earliest Lopingian (Late Permian) mass extinction. *Palaeogeography, Palaeoclimatology, Palaeoecology*, 223, 172–180.
- Kobayashi, F. (1997). Upper Permian foraminifers from the Iwai-Kanyo area, west Tokyo, Japan. *Journal of Foraminiferal Research*, 27, 186–195.
- Kobayashi, F. (2006a). Middle Permian foraminifers of the Izuru and Nabeyama formations in the Kuzu area, Tochigi Prefecture, Japan, part 1. Schwagerinid, Neoschwagerinid and verbeekinid fusulinoideans. *Paleontological Research*, 10, 37–59.
- Kobayashi, F. (2006b). Middle Permian foraminifers of the Izuru and Nabeyama formations in the Kuzu area, Tochigi Prefecture, Japan, part 2. Schubertellidae and ozawainellid fusulinoideans, and non-fusulinoidean foraminifers. *Paleontological Research*, 10, 61–77.
- Kobayashi, F. (2006c). Middle Permian foraminifers of Kaize, southern part of the Saku Basin, Nagano prefecture, central Japan. *Paleontological Research*, 10, 179–194.
- Kobayashi, F., & Altiner, D. (2011). Discovery of the Lower Murghabian (Middle Permian) based on neoschwagerinids and verbeekinids in the Taurides, southern Turkey. *Rivista Italiana di Paleontologia e Stratigrafia*, 117, 39–50.
- Kobayashi, F., Shiino, Y., & Suzuki, Y. (2009). Middle Permian (Midian) foraminifers of the Kamiyasse Formation in the Southern Kitakami Terrane, NE Japan. *Paleontological Research*, 13, 79–99.
- Kotlyar, G. V., Nestell, G. P., Zakharov, Y. D., & Nestell, M. K. (1999). Changhsingian of the northwestern Caucasus, southern Primorye and southeastern Pamirs. *Permophiles*, 35, 18–22.
- Kozur, H., & Mostler, H. (1989). Radiolarien und Schwamskieren aus dem unterperm Vorurals. *Geologisch-Paläontologische Mitteilungen Innsbruck*, 2, 147–275.
- Kozur, H. W., Moix, P., & Ozsvart, P. (2007a). Characteristic Nassellaria of the lower Tuvalian (Upper Triassic) *Spongortilispinus moixi* Zone of the Huglu Unit in the Mersin Mélange, southeastern Turkey. *Bulletin de la Société Vaudoise des Sciences Naturelles*, 90, 151–173.
- Kozur, H. W., Moix, P., & Ozsvart, P. (2007b). Stratigraphically important Spumellaria and Entactinaria from the lower Tuvalian (Upper Triassic) of the Huglu Unit in the Mersin Mélange, southeastern Turkey. *Bulletin de la Société Vaudoise des Sciences Naturelles*, 90, 175–195.
- Kozur, H. W., Moix, P., & Ozsvart, P. (2007c). Further new Nassellaria of the lower Tuvalian (Upper Triassic) *Spongortilispinus moixi* Zone of the Huglu Unit in the Mersin Mélange. *Bulletin de la Société Vaudoise des Sciences Naturelles*, 90, 197–215.
- Kozur, H. W., Moix, P., & Ozsvart, P. (2009). New Spumellaria (Radiolaria) from the early Tuvalian *Spongortilispinus moixi* Zone of southeastern Turkey, with some remarks on the age of this fauna. *Jahrbuch der Geologischen Bundesanstalt*, 149, 29–59.
- Kozur, H. W., & Wardlaw, B. R. (2010). The Guadalupian conodont fauna of Rustaq and Wadi Wasit, Oman and a West Texas connection. *Micro-paleontology*, 56(1), 213–233.
- Krull, E. S., & Retallack, G. J. (2000). $\delta^{13}\text{C}$ depth profiles from paleosols across the Permian-Triassic boundary: Evidence for methane release. *Geological Society of America Bulletin*, 112, 1459–1472.
- Krull, E. S., Retallack, G. J., Campbell, H. J., & Lyon, G. L. (2000). ^{13}C chemostratigraphy of the Permian-Triassic boundary in the Maitai Group, New Zealand: Evidence for high-latitude methane release. *New Zealand Journal of Geology and Geophysics*, 43, 21–32.
- Kuwahara, K. (1999). Phylogenetic lineage of Late Permian *Albaillella* (Albaillellaria: Radiolaria). *Journal of Geosciences, Osaka City University*, 42, 84–101.
- Kuwahara, K., Yao, A., & An, T. (1997). Paleozoic and Mesozoic complexes in the Yunnan area China (part 1): Preliminary report of Middle-Late Permian radiolarian assemblages. *Journal of Geosciences, Osaka City University*, 40, 37–49.
- Kuwahara, K., Yao, A., & Yamakita, S. (1998). Reexamination of Upper Permian radiolarian biostratigraphy. *Earth Science (Chikyū Kagaku)*, 52, 391–404.
- Kuwahara, K., Yao, A., Yao, J., Feng, S., Ji, Z., & Yao, H. (2007). Middle Permian radiolarian biostratigraphy on the Gufeng Formation in Songzi-Wufeng area, Hubei province, China. *Journal of Geosciences, Osaka City University*, 50, 55–66.
- Lambert, L. L., Wardlaw, B. R., Nestell, M. K., & Nestell, G. P. (2002). Latest Guadalupian (Middle Permian) conodonts and foraminifers from the West Texas. *Micro-paleontology*, 48, 343–364.
- Lapierre, H., Samper, A., Bosch, D., Maury, R. C., Bechennec, F., Cotten, J., ... Marcoux, J. (2004). The Tethyan plume: Geochemical diversity of Middle Permian basalts from the Oman rifted margin. *Lithos*, 74, 167–198.
- Le Roex, A. P., Bell, D. R., & Davis, P. (2003). Petrogenesis of Group I kimberlites from Kimberley, South Africa: Evidence from Bulk-Rock Geochemistry. *Journal of Petrology*, 44, 2261–2286.
- Leven, E. J. (1993). Main events in Permian history of the Tethys and Fusulinids. *Stratigraphy and Geological Correlation*, 1, 59–75.
- Leven, E. J. (1981). Permian Tethys stage scale and correlation of sections of the Mediterranean-Alpine Folded Belt. In S. Karamata & F. P. Sassi (Eds.), *IGCP No 5, Newsletter* (Vol. 3, pp. 100–112). Italy: University of Padova.
- Leven, E. J. (2001). On possibility of using the global Permian stage scale in the Tethyan region. *Stratigraphy and Geological Correlation*, 9, 118–131.
- Leven, E. J. (2003). The Permian stratigraphy and fusulinids of the Tethys. *Rivista Italiana di Paleontologia e Stratigrafia*, 109, 267–280.
- Leven, E. J., & Bogoslovskaya, M. F. (2006). The Roadian stage of the Permian and problems of its global correlation. *Stratigraphy and Geological Correlation*, 14, 67–78.
- Leven, E. J., & Gorgij, M. N. (2006). Upper Carboniferous–Permian stratigraphy and Fusulinids from the Anarak Region, Central Iran. *Russian Journal of Earth Sciences*, 8, 1–25.
- Leven, E. J., & Gorgij, M. N. (2011). Fusulinids and stratigraphy of the Carboniferous and Permian in Iran. *Stratigraphy and Geological Correlation*, 19, 687–776.
- Leven, E. J., & Okay, A. I. (1996). Foraminifera from the exotic Permo-Carboniferous limestone blocks in Karakaya Complex, northwestern Turkey. *Rivista Italiana di Paleontologia e Stratigrafia*, 102, 139–174.
- Leven, E. J., & Taheri, A. (2003). Carboniferous–Permian stratigraphy and Fusulinids of East Iran, Gzhelian and Asselian deposits of the Ozbak-Kuh Region. *Rivista Italiana di Paleontologia e Stratigrafia*, 109, 399–415.
- Ma, Q., Feng, Q., Caridroit, M., Danelian, T., & Zhang, N. (2016). Integrated radiolarian and conodont biostratigraphy of the Middle Permian Gufeng Formation (South China). *Comptes Rendus Palevol*, 15, 453–459.
- Mamet, B. L. (1996). Late Paleozoic small foraminifers (endothyrids) from South America (Ecuador and Bolivia). *Canadian Journal of Earth Sciences*, 33, 452–459.

- McCulloch, M. T., & Gamble, J. A. (1991). Geochemical and geodynamical constraints on subduction zone magmatism. *Earth and Planetary Science Letters*, 102, 358–374.
- McDonough, W. F., & Sun, S.-S. (1995). The composition of the Earth. *Chemical Geology*, 120, 223–253.
- McKenzie, D., & O'Nions, R. K. (1991). Partial melt distributions from inversion of rare earth element concentrations. *Journal of Petrology*, 32, 1021–1091.
- McKenzie, D., & O'Nions, R. K. (1995). The source regions of ocean island basalts. *Journal of Petrology*, 36(1), 133–159.
- Metcalfe, I. (2000). The Bentong-Raub Suture Zone. *Journal of Asian Earth Sciences*, 18, 691–712.
- Mohtat-Aghai, P., & Vachard, D. (2005). Late Permian foraminiferal assemblages from the Hambast region (Central Iran) and their extinctions. *Revista Española de Micropaleontología*, 37, 205–227.
- Moix, P., Beccalotto, L., Masset, O., Kozur, H. W., Dumitrica, P., Vachard, D., ... Stampfli, G. M. (2011). Geology and correlation of the Mersin Mélanges, southern Turkey. *Turkish Journal of Earth Sciences*, 20, 57–98.
- Moix, P., Kozur, H. W., Stampfli, G. M., & Mostler, H. (2007). New paleontological, biostratigraphic and paleogeographic results from the Triassic of the Mersin Mélange, SE Turkey. *New Mexico Museum of Natural History and Science Bulletin*, 41, 282–311.
- Nazarov, B. B., & Ormiston, A. R. (1985). Radiolaria from the Late Paleozoic of the Southern Urals, USSR and West Texas, USA. *Micropaleontology*, 31, 1–54.
- Nazarov, B. B., & Ormiston, A. R. (1993). New biostratigraphically important Palaeozoic radiolaria of Eurasia and North America. In J. Blueford & B. Murchey (Eds.), *Radiolaria of giant and subgiant fields in Asia*, Nazarov Memoir (pp. 22–59). New York: Micropaleontology Press, American Museum of Natural History.
- Nishikane, Y., Kaiho, K., Henderson, C. M., Takahashi, S., & Suzuki, N. (2014). Guadalupian–Lopingian conodont and carbon isotope stratigraphies of a deep chert sequence in Japan. *Palaeogeography, Palaeoclimatology, Palaeoecology*, 403, 16–29.
- Nishikane, Y., Kaiho, K., Takahashi, S., Henderson, C. M., Suzuki, N., & Kanno, M. (2011). The Guadalupian–Lopingian boundary (Permian) in a pelagic sequence from Panthalassa recognized by integrated conodont and radiolarian biostratigraphy. *Marine Micropaleontology*, 78, 84–95.
- Niu, Y., & Batiza, R. (1997). Trace element evidence from seamounts for recycled oceanic crust in the Eastern Pacific mantle. *Earth and Planetary Science Letters*, 148, 471–483.
- Niu, Y., Bideau, D., Hékinian, R., & Batiza, R. (2001). Mantle compositional control on the extent of mantle melting, crust production, gravity anomaly, ridge morphology, and ridge segmentation: A case study at the Mid-Atlantic Ridge 33–35N. *Earth and Planetary Science Letters*, 186(3), 383–399.
- Noble, P., Aitchison, J. C., Danelian, T., Dumitrica, P., Maletz, J., Suzuki, N., ... O'Dogherty, L. (2017). Taxonomy of Paleozoic radiolarian genera. In T. Danelian, M. Caridroit, P. Noble, & J. C. Aitchison (Eds.), *Catalogue of Paleozoic radiolarian genera Geodiversitas* (Vol. 39, pp. 419–502). Paris: Scientific Publications of the Muséum national d'Histoire naturelle.
- Ogg, J. G., Ogg, G. M., & Gradstein, F. M. (2016). *A concise geologic time scale*. Amsterdam: Elsevier.
- Özcan, A., Göncüoğlu, M. C., Turan, N., Uysal, S., Sentürk, K., & Isik, A. (1988). Late Paleozoic evolution of the Kütahya-Bolkardagi Belt. *METU Journal of Pure and Applied Sciences*, 21(1-3), 211–220.
- Özer, E., Koc, H., & Özsayar, T. Y. (2004). Stratigraphical evidence for the depression of the northern margin of the Menderes-Tauride Block (Turkey) during the Upper Cretaceous. *Journal of Asian Earth Sciences*, 22, 401–412.
- Özgül, N. (1976). Some geological aspects of the Taurus orogenic belt (Turkey). *Bulletin of the Geological Society of Turkey*, 19, 65–78 (in Turkish with English abstract).
- Özgül, N. (1984). Stratigraphy and tectonic evolution of the central Taurides. In O. Tekeli & M. C. Göncüoğlu (Eds.), *Geology of the taurus belt* (pp. 77–90). Ankara: Publication of General Directorate of Mineral Research and Exploration.
- Özgül, N. (1997). Stratigraphy of the tectono-stratigraphic units in the region Bozkir-Hadim-Taskent (northern central Taurides). *Bulletin of the Mineral Research and Exploration*, 119, 113–174 (in Turkish).
- Ozsvart, P., Dumitrica, P., Hungerbühler, A., & Moix, P. (2017). Mono- and dicyrtid Nassellaria (Radiolaria) from the Upper Carnian of the Sorgun Ophiolitic Mélange, Southern Turkey and Kopria Mélange, Rhodes, Greece. *Revue de Micropaleontologie*, 60, 137–160.
- Ozsvart, P., Dumitrica, P., & Moix, P. (2017). New early Tuvalian (Carnian, Triassic) radiolarians from the Huglu-Pindos succession in the sorgun ophiolitic Melange, southern Turkey. *Ofioliti*, 42, 55–67.
- Ozsvart, P., Moix, P., & Kozur, H. (2015). New Carnian (Upper Triassic) radiolarians from the Sorgun Ophiolitic Mélange, southern Turkey. *Neues Jahrbuch für Geologie und Paläontologie, Abhandlungen*, 277, 337–352.
- Pampal, S. (1984). Geology of the Arslanköy-Tepeköy region. *Bulletin of Science, Faculty of Sciences-Arts, University of Selcuk*, 3, 247–258 (in Turkish with English Abstract).
- Parlak, O., & Robertson, A. H. F. (2004). The ophiolite-related Mersin Mélange, southern Turkey: Its role in the tectonic-sedimentary setting of Tethys in the Eastern Mediterranean region. *Geological Magazine*, 141, 257–286.
- Pearce, J. A., & Peate, D. W. (1995). Tectonic implications of the composition of volcanic arc magmas. *Annual Review of Earth and Planetary Sciences*, 23, 251–285.
- Pessagno, E. A., Jr., & Newport, R. L. (1972). A new technique for extracting Radiolaria from radiolarian cherts. *Micropaleontology*, 18, 231–234.
- Peters-Kottig, W., Strauss, H., & Kerp, H. (2006). The land plant $\delta^{13}\text{C}$ record and plant evolution in the Late Palaeozoic. *Palaeogeography, Palaeoclimatology, Palaeoecology*, 240, 237–252.
- Pinard, S., & Mamet, B. L. (1998). Taxonomie des petits foraminifères du Carbonifère supérieur-Permien inférieur du bassin de Sevrdrup, Arctique Canadien. *Palaeontographica Canadiana*, 15, 1–253.
- Raymond, L. A. (1984). Classification of mélanges. In L. A. Raymond (Ed.), *Mélanges: Their nature, origin, and significance*, Geological Society of America, Special Paper (Vol. 198, pp. 7–20). Boulder, Colorado: Geological Society of America.
- Retallack, G. J., & Jahren, A. H. (2008). Methane outbursts from igneous intrusion of coal at the Permian–Triassic boundary. *Journal of Geology*, 116, 1–20.
- Retallack, G. J., Metzger, C. A., Greaver, T., Jahren, A. H., Smith, R. M. H., & Sheldon, N. D. (2006). Middle–Late Permian mass extinction on land. *Bulletin of the Geological Society of America*, 118, 1398–1411.
- Robertson, A. H. F., & Dixon, J. E. (1984). Introduction: Aspects of the geological evolution of the Eastern Mediterranean. In J. E. Dixon & A. H. F. Robertson (Eds.), *The geological evolution of the Eastern Mediterranean*, Geological Society, Special Publications (Vol. 17, pp. 1–74). London, England: Geological Society.
- Robertson, A. H. F., & Ustaömer, T. (2009). Formation of the Late Palaeozoic Konya Complex and comparable units in southern Turkey by subduction–accretion processes: Implications for the tectonic development of Tethys in the Eastern Mediterranean region. *Tectonophysics*, 473, 113–148.
- Rojay, B., Altiner, D., Altiner, S. Ö., Önen, A. P., James, S., & Thirlwall, M. F. (2004). Geodynamic significance of the Cretaceous pillow basalts from North Anatolian Ophiolitic Mélange Belt (Central Anatolia, Turkey): Geochemical and paleontological constraints. *Geodinamica Acta*, 17(5), 349–361.
- Rojay, B., Yaliniz, K., & Altiner, D. (2001). Age and origin of some pillow basalts from Ankara Melange and their tectonic implications to the evolution of Northern Branch of Neotethys, central Anatolia. *Turkish Journal of Earth Sciences*, 10, 93–102.
- Salteras, V. J. M., Longhi, J. E., & Bizimis, M. (2002). Near mantle solidus trace element partitioning at pressures up to 3.4 GPa. *Geochemistry, Geophysics, Geosystems*, 3, 1–23. <https://doi.org/10.1029/2001GC000148>
- Sashida, K., & Salyapongse, S. (2002). Permian radiolarian faunas from Thailand and their paleogeographic significance. *Journal of Asian Earth Sciences*, 20, 691–701.
- Sayit, K., Bedi, Y., Tekin, U. K., Göncüoğlu, M. C., & Okuyucu, C. (2017). Middle Triassic back-arc basalts from the blocks in the Mersin Mélange, southern Turkey: Implications for the geodynamic evolution of the Northern Neotethys. *Lithos*, 268–271, 102–113.
- Sayit, K., Göncüoğlu, M. C., & Tekin, U. K. (2015). Middle Carnian arc-type basalts from the Lycian Nappes, southwestern Anatolia: Early Late

- Triassic subduction in the Northern Branch of Neotethys. *The Journal of Geology*, 123, 561–579.
- Senel, M. (2002). *1/500.000 scale Turkish geological maps, Adana Quadrangle*. Ankara: Publication of General Directorate of Mineral Research and Exploration.
- Sengör, A. M. C. (1979). Mid-Mesozoic closure of Permo-Triassic Tethys and its implications. *Nature*, 279, 590–593.
- Sengör, A. M. C., Altiner, D., Cin, A., Ustaomer, T., & Hsu, K. J. (1988). Origin and assembly of the Tethyside orogenic collage at the expense of Gondwanaland. In M. G. Audley-Charles & A. Hallam (Eds.), *Gondwana and Tethys*, Geological Society of London, Special Publications (Vol. 37, pp. 119–181). London: Geological Society of London.
- Sengör, A. M. C., & Yilmaz, Y. (1981). Tethyan evolution of Turkey: A plate tectonics approach. *Tectonophysics*, 75, 181–241.
- Sengör, A. M. C., Yilmaz, Y., & Sungurlu, O. (1984). Tectonics of the Mediterranean Cimmerides: Nature and evolution of the western termination of Palaeo-Tethys. In E. Dixon & A. H. F. Robertson (Eds.), *The geological evolution of the Eastern Mediterranean*, Geological Society of London Special Publication (Vol. 17, pp. 77–112). London: Geological Society of London.
- Shang, C., Caridroit, M., & Wang, Y. (2001). Radiolarians from the uppermost Permian Changhsingian of southern Guangxi. *Acta Micropalaeontologica Sinica*, 18, 229–240.
- Shen, S. Z., Cao, C. Q., Zhang, H., Bowring, S. A., Henderson, C. M., Payne, J. L., ... Wang, W. (2013). High-resolution $d^{13}C_{carb}$ chemostratigraphy from latest Guadalupian through earliest Triassic in south China and Iran. *Earth and Planetary Science Letters*, 375, 156–165.
- Shimakawa, M., & Yao, A. (2006). Lower-Middle Permian radiolarian biostratigraphy in the Qinzhou area, south China. *Journal of Geosciences, Osaka City University*, 49, 31–47.
- Simoneit, B. R. T., Rogge, W. F., Mazurek, M. A., Standley, L. J., Hildemann, L. M., & Cass, G. R. (1993). Lignin pyrolysis products, lignans and resin acids as specific tracers of plant classes in emissions from biomass combustion. *Environmental Science and Technology*, 27, 2533–2541.
- Spandel, E. (1901). Die foraminiferen des Permo-Carbon von Hooser, Kansas, Nord Amerika. *Festschrift, Saecular-Freier der Naturhistorischen Gesellschaft in Nürnberg, 1801-1901*, 177–194.
- Spiker, E. C., & Hatcher, P. G. (1984). Carbon isotope fractionation of sapropellic organic matter during early diagenesis. *Organic Geochemistry*, 5, 283–290.
- Spiller, F. C. P. (2002). Radiolarian biostratigraphy of Peninsular Malaysia and implications for regional paleotectonics and paleogeography. *Palaeontographica A*, 266, 1–91.
- Stampfli, G. M., & Borel, G. D. (2002). A plate tectonic model for the Paleozoic and Mesozoic constrained by dynamic plate boundaries and restored synthetic oceanic isochrons. *Earth and Planetary Science Letters*, 196, 17–33.
- Staudigel, H., Plank, T., White, B. & Schmincke, H-U. (1996). *Geochemical fluxes during seafloor alteration of the basaltic upper oceanic crust: DSDP sites 417 and 418*. Washington DC, USA: AGU Geophysical Monographs, 96.
- Sun, D., & Xia, W. (2006). Identification of the Guadalupian–Lopingian boundary in the Permian in a bedded chert sequence, South China. *Palaeogeography, Palaeoclimatology, Palaeoecology*, 236, 272–289.
- Sun, S. S., & McDonough, W. F. (1989). Chemical and isotopic systematics of oceanic basalts: Implications for mantle composition and processes. In A. D. Saunders & M. J. Norry (Eds.), *Magmatism in the ocean basins*, Geological Society of London, Special Publications (Vol. 42, pp. 313–345). Oxford, England: Geological Society of London.
- Tekin, U. K., Bedi, Y., Okuyucu, C., Göncüoğlu, M. C., & Sayit, K. (2016). Radiolarian biochronology of upper Anisian to upper Ladinian (Middle Triassic) blocks and tectonic slices of volcano-sedimentary successions in the Mersin Mélange, southern Turkey: New insights for the evolution of Neotethys. *Journal of African Earth Sciences*, 124, 409–426.
- Tekin, U. K., Bedi, Y., Okuyucu, C., Göncüoğlu, M. C., Sayit, K., Krystyn, L., ..., Uzuncimen-Keceli, S. (2016). Dating of sedimentary units of the Mersin Mélange (Central Taurides, Southern Turkey) using radiolarian and other faunas (Conodont, Ammonite and Foraminifera) and geochemistry/petrography of its volcanic/volcanosedimentary units. Turkish Scientific Council. Project No: 112Y370 (Final Report). 645 p. (unpublished, in Turkish with English abstract).
- Tekin, U. K., & Göncüoğlu, M. C. (2002). Middle Carnian radiolarians from the intra-pillow limestones of the Turunç Unit within the Gülbahar Nappe (Lycien Nappes, Marmaris, southern Turkey): Geodynamic implications. In *First International Symposium of the Faculty of Mines (ITU) on Earth Science and Engineering, Special Session-C: Regional Geology and Geophysics: The Evolution of Orogenic Belts and Surroundings*, Istanbul, Abstracts, p. 84.
- Tekin, U. K., & Göncüoğlu, M. C. (2007). Discovery of oldest (late Ladinian to middle Carnian) radiolarian assemblages from the Bornova Flysch Zone in western Turkey: Implications for the evolution of the Neotethyan Izmir-Ankara Ocean. *Ofioliti*, 32, 131–150.
- Tekin, U. K., Göncüoğlu, M. C., & Turhan, N. (2002). First evidence of Late Carnian radiolarians from the Izmir-Ankara suture complex, central Sakarya, Turkey: Implications for the opening age of the Izmir-Ankara branch of Neo-Tethys. *Geobios*, 35, 127–135.
- Topuz, G., Celik, Ö. F., Sengör, A. M. C., Altintas, I. E., Zack, T., Rolland, Y., & Barth, M. (2013). Jurassic ophiolite formation and emplacement as backstop to a subduction-accretion complex in north-east Turkey, the Refahiye ophiolite, and relation to the Balkan ophiolites. *American Journal of Science*, 313, 1054–1087.
- Turhan, N., Okuyucu, C., & Göncüoğlu, M. C. (2004). Autochthonous Upper Permian (Midian) carbonates in the western Sakarya Composite Terrane, Geyve Area, Turkey: Preliminary data. *Turkish Journal of Earth Sciences*, 13, 215–229.
- Tyson, R. V. (1995). *Sedimentary organic matter: Organic facies and palynofacies*. London, England: Chapman and Hall.
- Ueno, K. (1989). Carboniferous and Lower Permian foraminiferal biostratigraphy in the Akiyoshi Limestone Group—studies of the Upper Paleozoic foraminifers in the Akiyoshi Limestone Group, southwest Japan, part 1. *Bulletin of the Akiyoshi-dai Museum of Natural History*, 24, 1–39. (in Japanese with English abstract).
- Vachard, D., Oviedo, A., Flores, D. E., Dios, A., Malpica, R., Brunner, P., ... Buitron, B. E. (1993). Barrancad d'Olinala (Guerrero): une coupe de reference pour le Permien du Mexique central; etude preliminaire. *Annales de la Societe geologique du Nord (2eme serie)*, 2, 153–160.
- Vaziri, S. H., Yao, A., & Kuwahara, Y. (2005). Lithofacies and microfacies (foraminifers and radiolarians) of the Permian sequence in the Shalazar area, Central Alborz, North Iran. *Journal of Geosciences, Osaka City University*, 48, 39–69.
- Walsh, J. J. (1983). Death in the sea: Enigmatic phytoplankton losses. *Progress in Oceanography*, 12, 1–86.
- Wang, E. (1982). Carboniferous and Permian foraminifera of Xizang. In *Palaeontology of Xizang, The series of scientific expeditions to the Qinghai-Xizang Plateau* (pp. 1–32). Beijing: Nanjing Institute of Geology and Paleontology, Academia Sinica, Book, IV.
- Wang, W., Cao, C., & Wang, Y. (2004). The carbon isotope excursion on GSSP candidate section of Lopingian-Guadalupian boundary. *Earth and Planetary Science Letters*, 220, 57–67.
- Wang, Y. J., Cheng, Y., & Yang, Q. (1994). Biostratigraphy and systematics of Permian Radiolarians in China. In J. Yügan, J. Uting, & B. L. Worldlow (Eds.), *Permian stratigraphy, environments and resources 1, paleontology and stratigraphy Paleoworld* (Vol. 4, pp. 172–202). Nanjing: Nanjing University Press.
- Wang, Y. J., Luo, H., & Yang, Q. (2012). *Late Paleozoic radiolarians in the Qinfang Area, Southeast Guangxi*. Nanjing: University of Science and Technology of China, Publishing.
- Wang, Y. J., & Yang, Q. (2011). Biostratigraphy, phylogeny and paleobiogeography of Carboniferous–Permian radiolarians in South China. *Palaeoworld*, 2, 134–145.
- Wang, Y. J., Yang, Q., Cheng, Y. N., & Li, J. X. (2006). Lopingian (Upper Permian) radiolarian biostratigraphy of South China. *Palaeoworld*, 15, 31–53.
- Wei, H., Baima, Q., Qiu, Z., & Dai, C. (2018). Carbon isotope perturbations and faunal changeovers during the Guadalupian mass extinction in the middle Yangtze Platform, South China. *Geological Magazine*, 155, 1667–1683.
- Wei, H., Chen, D., Yu, H., & Wang, J. (2012). End-Guadalupian mass extinction and negative carbon isotope excursion at Xiaojiaba, Guangyuan, Sichuan. *Science China Earth Sciences*, 55, 1480–1488.

- Werner, R. A., Bruch, B. A., & Brand, W. A. (1999). ConFlo III- an interface for high precision delta C-13 and delta N-15 analysis with an extended dynamic range. *Rapid Communications in Mass Spectrometry*, 13, 1237–1241.
- Wignall, P. B., Kershaw, S., Collin, P.-Y., & Crasquin-Soleau, S. (2009). Erosional truncation of uppermost Permian shallow marine carbonates and implications for Permian-Triassic boundary events: Comment. *Geological Society of America Bulletin*, 121, 954–956.
- Winchester, J. A., & Floyd, P. A. (1977). Geochemical discrimination of different magma series and their differentiation products using immobile elements. *Chemical Geology*, 20, 325–343.
- Workman, R. K., & Hart, S. R. (2005). Major and trace element composition of the depleted MORB mantle (DMM). *Earth and Planetary Science Letters*, 231, 53–72.
- Xia, W. C., Ning, Z., Kakuwa, Y., & Lil, Z. (2005). Radiolarian and conodont biozonation in the pelagic Guadalupian–Lopingian boundary interval at Dachongling, Guangxi, South China, and mid-upper Permian global correlation. *Stratigraphy*, 2, 217–238.
- Xia, W. C., Zhang, N., Wang, G. Q., & Kakuwa, Y. (2004). Pelagic radiolarian and conodont biozonation in the Permian–Triassic boundary interval and correlation to the Meishan GSSP. *Micropaleontology*, 50, 27–44.
- Yamamuro, M., & Kayanne, H. (1995). Rapid direct determination of organic carbon and nitrogen in carbonate-bearing sediments with a Yanaco MT-5 CHN analyzer. *Limnology and Oceanography*, 40, 1001–1005.
- Yao, A., & Kuwahara, K. (2004). Radiolarian fossils from the Permian-Triassic of China. *News of Osaka Micropaleontologists*, Special Volume, 13, 29–45 (in Japanese with English abstract).
- Yao, A., Kuwahara, K., Ezaki, Y., Liu, J., & Hao, W. (2004). Permian radiolarians from the Qinfang Terrane, South China and its geological significance. *Journal of Geosciences, Osaka City University*, 47, 71–83.
- Yao, J., Yao, A., & Kuwahara, K. (2001). Upper Permian biostratigraphic correlation between conodont and radiolarian zones in the Tamba-Mino Terrane, Southwest Japan. *Journal of Geosciences, Osaka City University*, 44, 97–119.
- Zhang, L., Ito, T., Feng, Q., Caridroit, M., & Danelian, T. (2014). Phylogenetic model of *Follicucullus* lineages (Albaillellaria, Radiolaria) based on high-resolution biostratigraphy of the Permian Bancheng Formation, Guangxi, South China. *Journal of Micropalaeontology*, 33, 179–192.
- Zhang, N., Henderson, C. M., Xia, W., Wang, G., & Shang, H. (2010). Conodonts and radiolarians through the Cisuralian–Guadalupian boundary from the Pingxiang and Dachongling sections, Guangxi region, South China. *Alcheringa*, 34, 135–160.
- Zindler, A., Staudigel, H., & Batiza, R. (1984). Isotope and trace element geochemistry of young Pacific seamounts: Implications for the scale of upper mantle heterogeneity. *Earth and Planetary Science Letters*, 70, 175–195.

SUPPORTING INFORMATION

Additional supporting information may be found online in the Supporting Information section at the end of the article.

How to cite this article: Tekin UK, Okuyucu C, Sayit K, et al. Integrated Radiolaria, benthic foraminifera and conodont biochronology of the pelagic Permian blocks/tectonic slices and geochemistry of associated volcanic rocks from the Mersin Mélange, southern Turkey: Implications for the Permian evolution of the northern Neotethys. *Island Arc*. 2019;28:e12286. <https://doi.org/10.1111/iar.12286>